AD657791

University of Utah

Department of Chemical Engineering

Salt Lake City, Utah

UNIVERSITY OF UTAH

DEPARTMENT OF CHEMICAL ENGINEERING

Technical Report

on

IGNITION AND COMBUSTION OF SOLID PROPELLANTS

Under Air Force Grant AFOSR 40-66

October 1, 1965, to September 30, 1966

Report prepared by:

Robert G. Mantyla
Jih-tien Cheng
Larry S. Bouck
John A. Keller
Alva D. Baer
Norman W. Ryan

Report approved by:

Norman W. Ryan, Principal Investigator

TABLE OF CONTENTS

SUMMARY

A model for the ignition response of solid propellants is presented, which predicts ignition behavior with respect to pressure and surface heat flux in qualitative agreement with experimental measurements. Surface regression is treated, and a steady-state burning model is employed which assumes equilibrium vaporization at the surface and a regression rate limited by the feedback flux. The model predicts ignition response in agreement with earlier thermal ignition theories for low igniter fluxes and at high pressures. Longer ignition times are predicted at high fluxes and low pressures than those of the thermal theories, and this increase in ignition time is found to be the time required to add sufficient energy to the solid to permit termination of the igniter flux while maintaining a finite regression rate.

The net heat of gasification, q, is as important a parameter in theories of extinguishment and L* instability as in the regression-ignition model. It is shown that this parameter is a simple function of the ratio of initial to final pressure for that instantaneous pressure drop which just produces extinguishment. A technique which employs a rarefaction tube has been developed to measure this pressure ratio. From results obtained by use of this method, q values from 15 to 100 cal/(g) have been calculated for composite propellants; because of limitations of the rarefaction tube, extinguishment cannot be achieved if the value of q for the propellant is greater than about 100 cal/g.

Brief summaries of results from two studies which are to be discussed in detail in subsequent technical reports are presented. The analysis of the extensive data on the thermal effects of reactions of a PBAA binder and of mixtures of PBAA and fine AP in nitrogen and oxygen has been completed. The reaction between undecomposed PBAA and AP or its decomposition products appears to be of critical importance in ignition. A technique has been developed and employed to measure the surface temperature of composite propellants while heating by high convective heat fluxes. Measured surface-temperature histories during the ignition time for opaque propellants with smooth, blackened surfaces are in agreement with thermal theory predictions.

iii

I. INTRODUCTION

As part of a continuing research effort, experimental and analytical studies have been made relating to the combustion transients of composite solid propellants. The work was supported by the Air Force Office of Scientific Research under Air Force Grant AF-AFOSR 40-67.

This report is segregated into a series of separate progress reports, and each contains an introduction and a conclusion. These sections describe an extension of the thermal theory of ignition, ignition studies employing high convective heat fluxes, the measurement of thermal effects of propellant component reactions, and the studies of the extinguishment of burning propellant by rapid depressurization. For the sake of completeness, a brief review of special techniques is presented for each of the projects already discussed in earlier publications. Figures, tables and equations are numbered consecutively throughout the report. Common tables of nomenclature and references, as well as tables summarizing the chemical and thermal properties of all propellants discussed (Tables 3 and 4) are presented at the end of the full report. Because of the relatively large number of tables and figures in this report, all are grouped together in the appendix.

II. IGNITION THEORY

Simplified models are proposed for quantitatively describing the ignition response of a solid propellant. In terms of the context of the discussion, a model is a hypothetical physical system equivalent in known essential respects to a real propellant undergoing ignition. The model has been simplified to the degree that it is analytically tractable. Its behavior is represented by equations, themselves sometimes referred to as the model, whose solution in terms of process variables describes the behavior of the real physical system. The equations are said to simulate the real process, and the parameters are taken as the defined relevant properties of the real system. The value of the model is that it enables one to use experimental data in computing the parameters, which have other uses; also to infer aspects of ignition not yet observed (perhaps unobservable) experimentally that will guide one to means of improving ignitibility or the character of the ignition stimulus.

1. HOMOGENEOUS MODEL WITH REGRESSION

This description of the ignition process considers a solid propellant to be a semi-infinite, homogeneous solid. The surface regression rate is determined by the surface temperature and/or the heat flux impinging on the exposed solid surface. Reactions which involve significant energy release rates occur only on this exposed surface. The factors of primary interest are the time-temperature history of the solid, surface heat fluxes from external sources or generated by reactions at or near to the surface, and the regression rate of the solid.

Formulation of the Model

Equation (1) is the form of the one-dimensional, transient heat conduction equation which is assumed to describe the temperature history in the solid.

$$\frac{\partial U}{\partial T} - R_{ex} \frac{\partial U}{\partial X} = \frac{\partial^2 U}{\partial X^2} \tag{1}$$

At $T = 0$, $U = Y$; the solid surface is fixed at $X = 0$. Eq. (1) is in terms of dimensionless variables defined as:

  U = the temperature in the solid;

  T = time;

  X = the distance into the solid;

  R_{ex} = the velocity of the solid (regression rate); and

  Y = the initial temperature.

Appendix C defines these dimensionless variables in terms of the propellant properties. Reactions in the solid involving significant energy rates are not considered directly. Previous calculations have shown that inclusion of condensed-phase endothermic reactions leads to erroneous predictions concerning ignition behavior at low fluxes [1]. Endothermic reactions are thus to be neglected. In the case of composite propellants which are of greatest interest here, it appears likely that the important exothermic reactions occur between decomposition products at or near the surface, and at low temperatures at least, the rate of these reactions is determined by the "surface temperature." In this model, the initial exothermic reaction is assumed to be an exponential function of surface temperature.

A **Pre-ignition** formulation is assumed for the period during which the initially uniform temperature solid is heated by an external (ignition) heat flux. The boundary conditions for Equation (1) are for $T>0$

$$X \to \infty, \; U = Y; \text{ and } X = 0, \frac{\partial U}{\partial X} = F_e + F_r$$

here F_e and F_r are heat fluxes respectively from the external source and from reaction. The regression rate, R_{ex}, is assumed proportional to F_r. F_r is given as

$$\frac{1}{F_r} = \exp \frac{1}{[-1/U_2]} + \frac{1}{G_{aa} P^n} \tag{2}$$

where U_2 is the surface temperature and $G_{aa} P^n$ is the feedback heat flux to the solid during steady-state regression. P is the ratio of the total pressure to a reference pressure, taken as 1 atm, n the burning rate exponent and G_{aa} the dimensionless heat flux at one atmosphere. The term

exp $[-1/U_2]$ is the exponentially temperature-dependent reaction flux. At low values of surface temperature, this term is small compared to $G_{aa}P^n$ and F_r approaches exp $[-1/U_2]$. At high surface temperatures, the relative magnitude of these two terms is reversed and F_r approaches $G_{aa}P^n$. Thus, the selected form of Eq. (2) approximates the likely process of the rate of the exothermic reaction, being limited by the rate of generation of reactive species at low temperatures and then being limited by possibly diffusional processes to a constant, pressure-dependent value at high surface temperatures. Additional parameters are not introduced and runaway exothermic reactions are avoided by use of this approxima' on. Also, for this model, calculated ignition times are not strongly dependent on the form selected for F_r as long as the limiting values are the same.

The pre-ignition boundary conditions are assumed to apply until, at low igniter fluxes, F_r becomes much greater than F_e, or else at high igniter fluxes, the surface temperature reaches an assumed equilibrium vaporization temperature for the solid. In either case, a transition to a steady-state regression must be considered.

The steady-state regression rate is formulated as a function of pressure by assuming that the steady-state feedback flux is proportional to P^n and that a constant "net heat of gasification" is required to vaporize the solid at the equilibrium vaporization temperature. An energy balance at the surface gives, in dimensionless form,

$$G_a P^n = G_m + R_{ex} (R_{nd}) \qquad (3)$$

here, G_a is the flux at 1 atms, U_{sb} the vaporization temperature, G_m the heat flux in the solid surface, and R_{nd} the net heat of gasification. When the surface temperature, calculated by the pre-ignition model, reaches U_{sb}, the boudary conditions on Eq. (1) become

$$X \to \infty, \ U = Y; \ \text{and} \ X = 0, \ \frac{\partial U}{\partial X} = G_m = F_e + G_a P^n - R_{ex} (R_{nd})$$

With the surface temperature fixed at U_{sb}, the regression rate is determined by the energy balance at the surface. During steady-state regression, $G_m = R_{ex} (U_{sb} - Y)$.

The _regression rate_ during the ignition transient is calculated as

$$R_{ex} = C_b F_r \tag{4}$$

when U_2 is less than U_{sb}. When U_2 is equal to U_{sb},

$$R_{ex} = (G_a P^n \cdot F_e - G_m)/R_{nd} \tag{5}$$

Since the method for calculation of R_{ex} changes as U_2 becomes equal to U_{sb}, a discontinuous and physically unrealistic change in R_{ex} would occur at this time if a poor choice is made for the parameter C_b. Prior calculations [1] have shown that calculated ignition times are little affected by the magnitude of C_b as long as this parameter has a physically reasonable value, and it was found that if C_b is approximated as

$$C_b = 34 \ P^{1/8}$$

as essentially smooth transition of the regression rate as U_2 became equal to U_{sb} was obtained. The value of the parameter G_a in Eqs. (3) and (5) is somewhat different from the value of G_{aa} in Eq. (2). As used, the value of G_{aa} must be corrected for the net heat of gasification, R_{nd}, if calculated regression rates are to be consistent with those calculated by Eq. (5). G_{aa} is related to G_a by the relationship

$$G_{aa} = (U_{sb} - Y) \ G_a/(R_{nd} + U_{sb} - Y).$$

Numerical values are required for the parameters Y, U_{sb}, R_{nd}, G_a and n to describe a simulated propellant, and, in general, values were selected for study based upon the best available estimates for propellant properties. In this study, the initial dimensionless temperature was taken to be .02, which corresponds to the assumption of an activation energy for the critical reaction of 15,000°K for an initial temperature of 300°K. The equilibrium vaporization temperature (steady-state surface temperature) as a function of pressure was normally assumed equal to the values for vaporization

of AP as determined either by Rosser, Inami and Wise [2] or by the early
work of Powling and Smith [3]. Values of the dimensionless heat of gasi-
fication, R_{nd}, were calculated by the considerations that the actual net
heat of gasification would be somewhat less than the heat of vaporization
of AP (about 1000 cal/cm^3). The values of G_a were chosen to give real
steady-state regression rates on the range of .05 to 0.4 cm/sec. at one
atmosphere. Normally, the dimensionalizing parameter for flux, b, was
calculated from earlier ignition data [4] and was assumed equal to
5×10^{10} cal/(sec)(cm^2), thus, F_e or G_a times b, yeilds the real flux
values in cal/(sec)(cm^2). The burning rate exponent, n, was taken to be
0.5. Typical thermal properties of composite propellants were used.
Table 1 summarizes the values of the various parameters for the several
cases considered.

Numerical solutions to Eq. (1) are obtained for the indicated initial
and boundary conditions by use of the conventional, explicit Schmidt
method. Because non-linear terms occur only in the boundary conditions,
it is possible to guarantee stability of the solution by setting the
ratio of the dimensionless time increment to the square of the dimension-
less spatial increment equal to 1/2. Scaling of the numerical solution
is set to realize the ignition condition after about 100 time increments;
the maximum accuracy is thus about 1 percent for ignition times. Test
scaled to terminate after fewer and greater numbers of increments show
that the accuracy of the compilations was roughly inversly proportional
to the number of time increments.

Because, near the end of the pre-ignition period, the surface heat
flux changes rapidly with time, a predictive relationship is used to
obtain an average flux between the Nth and N + 1st time st . After the
surface temperature reaches the equilibrium vaporization value, the re-
gression rate is determined by an energy balance on the surface; and by
use of an iterative procedure, a regression rate averaged between the Nth
and N + 1st step is used for the numerical calculations.

Ignition is defined in terms of an essentially go-no-go criterion.
Once the vaporization temperature is reached, the effect of terminating
the igniter flux is determined. Normally, if, while maintaining the surface

at the vaporization temperature, the igniter flux can be reduced to zero without also reducing the calculated regression rate to zero, ignition is assumed to have been achieved. The igniter flux is maintained until this condition can be realized. At low igniter flux levels, it is found that the igniter flux can be terminated before reaching the vaporization temperature if the reaction flux greatly exceeds the igniter flux; this is, in fact, essentially the ignition criterion of earlier theories.

A set of parameters for a representative simulated propellant was found useful as the basis of a parametric study. This particular set of parameters was designated as Case III. In terms of real parameters, the simulated steady-state regression rate is 0.15 cm/sec at 1 atms, the equilibrium vaporization temperature is 545°C at 1 atms, and the net heat of gasification is about 400 cal/cm^3 (see Table 1). Details of the simulated response of this case are discussed here, and other cases normally represent changes of a single parameter of Case III.

Figure 1 shows a plot of calculated ignition times as a function of the igniter flux at various total pressures. The qualitative aspects of Fig. 1 are similar to typical arc-image furnace results, the similarity being one condition for the validity of the model.

At low fluxes, all ignition times approach the line labeled "simple thermal ignition" which was determined on the basis of a non-regression ignition model [4], [5]. The low flux asymptotes for the lines in Fig. 1 are displaced away from the simple thermal ignition line in the direction of longer ignition times as a result of regression during the pre-ignition period. The magnitude of this displacement is a function of the parameter C_b [1].

Calculated ignition times become significantly longer than the calculated "simple thermal ignition" times when the igniter flux is greater than the steady-state feedback flux ($G_a p^n$). Also for a given pressure, ignition cannot be realized above a certain value of igniter flux. This ignition-limiting flux corresponds to development of steady-state regression of the solid subjected to the sum of the igniter flux and steady-state feedback flux with the heat flux just below the regressing surface equal to the steady-state feedback flux. Without the igniter flux, the feedback flux can just maintain the slowly changing temperature gradient in the

solid, and no excess energy is available for vaporizing the solid. The regression rate would drop to zero with cut-off of the igniter flux. The limiting igniter flux is given as

$$F_{lim} = \frac{(R_{nd})(G_a P^n)}{U_{sb} - Y} \qquad (6)$$

Figures 2 and 3 are useful in illustrating the characteristics of this ignition model. Fig. 2 shows the calculated variations in surface temperature, regression rate and heat flux below the solid surface, G_m, as a function of time for the case of an ignition flux less than the steady-state feedback flux. The igniter flux is cut off before U_2 reaches U_{sb}, although the regression rate is above the steady-state value. After cut-off, the surface temperature quickly rises to U_{sb} and the regression rate and internal flux quickly assume the steady-state values.

Figure 3 illustrates the situation when the igniter flux is greater than the feedback flux. During the pre-ignition preiod, as the surface temperature rises to U_{sb}, the regression rate starts at zero and rises, and the internal flux starts above the feedback flux and increases. When the surface temperature is fixed at U_{sb}, the regression rate continues to rise and the internal flux decreases. At the time the internal flux drops to the value of the feedback flux, the igniter flux is terminated and the regression rate drops to essentially zero. After cut-off, the internal flux continues to drop and the regression rate rises; both then approach the steady-state regression values. Since the time that the surface temperature reaches U_{sb} is quite close to the "simple thermal ignition" time, the increase of calculated ignitions times is about to be equal to the time required to drop the internal flux to a critical value. During this period, energy is being stored in the propellant and the steady-state thermal wave in the solid is being established.

In the following paragraphs, changes in the calculated ignition response produced by variation of the parameters in the model are discussed. Only the most interesting or significant effects noted are discussed here. Table 1 summarizes all the various cases considered.

Case II is a modification of Case III, in which the equilibrium surface temperature is assumed to be 500°C rather than 545°C. Fig. 4 illustrated calculated ignition times for this case as a function of igniter flux and pressure. A comparison of these results to those for Case III (for example, the dash line for 1 atm in Fig. 4) shows that the effect of reducing the surface temperature is to decrease the ignition time at high flux levels and to increase in the limiting igniter flux level. The qualitative nature of the calculated response is not changed.

Case V is a modification of Case III, in which the real net heat of gasification was assumed to be 200 cal/cm^3 rather than 400 cal/cm^3. The parameter G_a was reduced to give essentially the same steady-state regression rate. Figure 5 summarizes the calculations obtained for this case. At low flux levels, the ignition times are essentially the same as for Case III; however, the limiting flux level is significantly reduced and the constant pressure curves in Fig. 5 break sharply from the simple thermal ignition line.

Case VI is a simple modification of Case III, in which the feedback flux, G_a, was reduced to give a steady-state regression rate equal to one half the value for Case III. Figure 6 shows the results of calculations for Case VI. Because G_a was halved, the limiting flux for ignition is also halved, and the lines in Figure 6 in constant pressure were displaced proportionally. No other effect was noted.

Case VIII was obtained by increasing both the net heat of gasification and the steady-state feedback flux by a factor of 2.5. This case represents the opposite change from Case V, and Fig. 7 shows that the observed effects are consistent with the effects noted for Case V.

Case X is identical to Case III at a pressure of one atmosphere, since the only difference is the effect of pressure on the vaporization temperature. The value for the heat of vaporization of 20 kcal g-mole rather than 28 kcal/g-mole (of gas) was assumed. Figure 8 shows that the ignition times calculated for Case X were longer at low pressure and shorter at high pressure than for Case III.

Calculations employing the parameters for Case III were made to study some of the assumptions concerning the basic model and to consider possible uses of the model.

The criterion normally employed for defining ignition must represent a limiting condition, since the regression rate can never become less than zero. However, material evolved from the surface must react to produce the feedback flux, and it is unlikely that the steady-state feedback flux can be maintained if the regression becomes very significantly less than the steady-state value. An alternative criterion was employed in which ignition was not assumed to have been achieved until the steady-state feedback flux was 20 percent greater than the internal flux in the solid. Figure 9 illustrates calculated ignition times based upon this criterion as compared to the normal criterion. Ignition times are found to be increased at high flux levels and the limiting flux is decreased for a given pressure. For Case III, the regression rate drops to about 20 percent of the steady-state regression rate after cut-off. Other requirements for cut-off are possible, but the general character of the calculated response is likely not markedly affected by such variations.

The nature of the termination of the igniter heat flux is found to have a pronounced effect on calculated ignition times at high flux levels. Normally, the flux was assumed to terminate abruptly; if, however, the evolution of material from the surface is assumed to attenuate the igniter flux before the solid surface is reached, the heat flux seen by the surface is gradually reduced. Fig. 10 shows calculated ignition times as a function of incident igniter flux pressure if the flux reaching the surface, F_i, is given as $F_i = F_e e^{-m\ell}$ where m is a constant and ℓ the total surface regression. For Fig. 10, regression of 10 microns produces a 37.1 percent reduction in F_i. No limiting flux for ignition is observed, and the plot strongly resembles many plots of experiment arc-image furnace data. Fig. 11 shows the regression rate and internal flux as a function of time for a condition of a high igniter flux which is attenuated by evolved material for the conditions of Fig. 10.

If attenuation is assumed to occur as a result of gasified material during the pre-ignition period, it is found that it is difficult to produce ignition at low heat fluxes, but calculated ignition response equivalent to that shown in Fig. 10 is obtained if a reasonable mechanism is introduced for removal of evolved material as by diffusion or by sweeping of the surface by an inert gas.

Although some attenuation of the incident heat flux would occur as a result of regression and defocusing at the secondary focus of an image furnace, it can be shown that, for the magnitudes of regression encountered, the depth of focus of a typical image furnace is great enough to make such attenuation of minor import.

A trapezoidal igniter heat flux-time relationship is typical of arc-image furnaces which employ rotating disc shutters. Figure 12 compares the calculated ignition response for Case III parameters of a sharply initiated and terminated igniter heat flux to that of a simulated trapezoidal flux-time input. The trapezoidal wave form is a linear rise to a maxiumum value during the first 1/5 of the total period followed by 3/5 of the period at the maximum flux level and a linear decrease to zero during the last 1/5 of the exposure period. If, when the igniter flux becomes zero, the calculated regression rate was non-negative, ignition of the solid is assumed to have occured. Fig. 12 is a plot of the total energy input, Q, by the energy pulses as a function of the maximum igniter flux at two different pressures. The form of this plot would be typical for data from a rotating-disc-shuttered arc-image furnace, since ignition time has no precise meaning for such systems. Experimentally, the total energy output, Q, would be measured in terms of the total temperature rise of a calorimeter during exposure, and the maximum flux would be determined by the rate of rise of the calorimeter temperature. At low maximum flux levels, more energy is required of the trapezoid pulse form to produce ignition. Since ignition never occurs during the decreasing flux period, the energy input during the decreasing flux period is not utilized. In contrast, at high maximum flux levels, less energy is required for the trapezoidal pulse form, and the limiting flux level for ignition is greatly increased. This effect again illustrates the importance of the rate of flux termination at high igniter flux levels. It should be noted that the comparison shown in Fig. 12 is

somewhat arbitrary, for example, an average rather than the maximum flux level might be employed; however, the conclusion that the trapezoidal pulse is more efficient at high flux levels remains valid.

The ignition reaction flux, F_r, which is defined by Eq. (2) represents the feedback flux during the pre-ignition period. An alternate to the normal assumption that at the vaporization surface temperature the feedback flux equals $G_a P^n$ is to assume that the ignition reaction heat flux (with G_a replacing G_{aa}) is the feedback flux. Fig. 13 is a plot of ignition times calculated by use of this assumption as a function of the igniter heat flux. A comparison of these results to previous calculations shows that at high pressures, the results are essentially identical. For the parameters employed, at high pressures F_r equals $G_a P^n$ since the exponential term is very large. At low pressure, use of the ignition-reaction flux results in longer ignition periods and a lowering of the limiting flux for ignition.

Fig. 14 shows a comparison of calculated regression rates as a function of pressure for feedback fluxes equal to $G_a P^n$ and to the ignition-reaction flux. At high pressures, the two results become equal with regression rate exponents equal to 1/2 while at low pressures the effective regression exponent for the ignition-reaction flux case increases. Under these conditions, the surface heat flux is found to be almost an exponential function of temperature or pressure. Continuation of such a trend to lower pressure could lead to instability and to the prediction of a low pressure deflagration limit.

Summary

The ignition model presented here is not proposed as an exact representation of any propellant. Although the parameters in the model have some physical significance, they represent only the gross features of very complex processes; only qualitative agreement between prediction and experiment is possible at present. The accuracy

of experimental ignition results must be improved considerably before quantitative agreement is an attainable goal.

Calculations employing the model have shown that it is possible to simulate the total ignition transient. Coupling of the ignition processes to a steady-state burning model was achieved. Predicted processes occuring during the transient are intuitively anticipated and are reasonable. For example, the regression rate is found to exceed the steady-state regression rate during part of the transient; however, the calculated rate seldom exceeds the steady-state value by more than a factor of two. Effects of igniter flux level and of pressure are noted and explained in terms of the heat flow in the solid. The effects of gas phase processes are treated by assuming a value for the feedback flux equal to the steady-state value at a given pressure; it is not necessary to consider transients in the gas phase processes. The studies of the various parameters and assumptions of the model show that the most critical aspects are the assumed value of the net heat of gasification of the propellant and the manner in which the igniter flux is terminated.

Many alternative forms or changes in assumptions concerning the basic model are possible and should be considered. The assumed nature of the steady-state regression model introduces the critical parameter of the net heat of gasification, whose magnitude should be experimentally determined. The assumption of a feedback flux which is dependent only on pressure is justified in part by the equilibrium vaporization conditions for the surface regression; very near the surface, the concentration and temperature of reactive species would be a function only of pressure. Possibly the best test of this assumption will come the results of extinguishment tests on burning propellants.

The weight of experimental evidence [6] seems to indicate that the major component of composite propellants, ammonium perchlorate, burns as a result of a kinetically limited rather than flux limited mechanism. The surface temperature is thus not fixed at an equilibrium vaporization temperature, and the regression rate of composite propellants is likely approximated as an exponential function of the surface temperature. Thus,

an alternative formulation for this ignition model would assume that
the regression rate of the propellant is a distinct, exponential
function of surface temperature both during the pre-ignition period
and during the transition to steady-state regression. During the
later part of this grant period, such a model was formulated and a
detailed analysis of this formulation is being continued under the
continuing grant.

2. SIMPLIFIED NON-HOMOGENEOUS MODEL

A second ignition model treated describes the composite solid
propellant in terms of a simplified physical configuration of alter-
nating laminae of ammonium perchlorate and a fuel binder. Fig. 15
illustrates the details of this two-lamina model. When subjected to
a surface heat flux, heat flow in this solid was assumed to be de-
scribable by the transient heat conduction equation in two dimensions
with non-linear terms included to account for energy generation or
absorption in the two solids, at the surface of each solid, or along
the two-solid interface. The non-linear terms were of the form
$\pm b_i$ exp $[E_i/Rv]$ where the dimensions of the pre-experimental factor
were cal/(sec)(cm^2) for a surface flux or cal/(sec)(cm^3) for a con-
densed phase term, E_i/R the activation energy for a reaction, and v
the local surface or condensed phase temperature. Details of the
mathematical formulation can be found in references [1] or [7]. Igni-
tion times were calculated from numerical solutions of the two-dimensional
differential equations and ignition was assumed to occur when the rate
of temperature rise of any point on the heated surface became very great.

Selection of Parameters

The formulation of the two-lamina model was made to permit the con-
sideration of a great many possible ignition processes. Flexibility was
achieved at the expense of simplicity, and the values of a large number
of parameters, which arise from processes only vaguely understood, were
required. The manner in which the various parameters were selected is
discussed below; however, it is recognized that other schemes might be

used. It is likely that information from experimental measurements will
result not only in changes in the value of certain parameters but may
also suggest changes in the treatment of the various processes assumed
to be describably by the model.

The measured room temperature values for the thermal properties of
AP and the PBAA fuel-binder were assumed to be applicable to the two
solids under all conditions. Consideration of experimental evidence
[4], [5], suggested the assumption that the surface decomposition of
the AP was the critical process. An exothermic reaction at the AP surface
was assumed. The activation energy (30 kcal/gm mole) and pre-exponential
factor (4-5 × 10^{10} cal/(sec)(cm^2) of this reaction were determined from
values suggested by Keller [8] for AP composite propellants. The acti-
vation energies of all reactions was also assumed to be about 30 kcal
since experimental values were not available. A condition imposed on
a set of values of the parameters (a case) was that the calculated ig-
nition response be in agreement with experimentally determined charac-
teristics. Specifically, the ignition times, t_i, should be given as

$$t_i = 29/(f)^{1.84} \qquad (7)$$

Here t_i is in sec. and the surface flux, f, is in cal/(sec)(cm^2). Eq.
(7) is presented by Keller [8] and represents the experimental ignition-
time-heat-flux relationship for catalyzed AP propellants at high pressures.

Preliminary calculations showed that it was necessary to assume an
endothermic reaction at the surface of the fuel-binder if calculated
ignition times in agreement with Eq. (7) were to be obtained. The value
of the pre-exponential factor for the binder reaction was selected to
produce this agreement. The value of the pre-exponential factors for
the two condensed phase reactions was adjusted to make the effect of
these reactions of minor import. However, these factors were not zeroed
because a demonstration of the applicability of the numerical technique
to this non-linear aspect of the problem was desired.

It was necessary to suppress the effect of an exothermic interface
reaction by use of small values for the pre-exponential factor. Because
the depth of energy penetration is large for low flux ignition, and thus,
the effective area for interface reactions was large, the interface

reaction dominated the process at low fluxes. However, at high fluxes, the surface reaction produced the major fraction of the chemical energy for ignition, and the experimental flux-time relationship could not be obtained.

Table 2 summarizes the parameter values for the several cases considered. Other values of the parameters were used; however, for these cases, calculated ignition times did not agree with Eq. (7), over a range of fluxes. Some effect was noted when varying the ratio of AP to fuel-binder widths; and for AP width of 45 microns, fuel-binder widths of from 5-30 microns were considered. At a fuel-binder width of 15 microns, which corresponds to a typical AP volumetric loading of 75 percent, satisfactory results were obtained.

Typical Results

Fig. 16 shows the results of a typical calculation for case F-1 in a plot of the three surface temperatures of greatest interest as a function of time. The "runaway" surface temperature occurred at the AP-fuel-binder interface, which was always the case. At the ignition time, the three surface temperatures tend to become equal; and this effect was always noted for those cases which produced ignition-time-flux relationships in agreement with Eq. (7).

Fig. 17 is a plot of the isotherms in the two-lamina solid after exposure to a high surface heat flux for a condition in which all reaction terms were eliminated (linear heating). Although the fuel-binder surface temperature is much greater than the surface temperature of the AP, at some depth, the AP temperature is actually higher. Near the surface, energy flow parallel to the surface is from the fuel-binder to the AP while in depth the fuel binder is heated by the AP. This effect is mainly the result of the higher thermal conductivity of AP. Fig. 18 is similar to Fig. 17; however, in this case, the F-4 parameters were used. This plot is for the time increment just prior to ignition, and the essentially constant surface temperature is in marked contrast to the situation shown in Fig. 17. By inclusion of the kinetic parameters, the AP surface temperature is increased as the result of an exothermic reaction and the

fuel-binder temperature is decreased as a result of the endothermic reaction. In spite of the difference in thermal properties of the two laminae, the solid appears almost as a thermally homogeneous material.

Conclusions

Aside from the result that the numerical technique was found to be suitable for solution of the problem, conclusions from this study are, in part, determined by the manner of selection of the parameters. The ignition response of such two-lamina solids can be made to agree with that of a homogeneous body, and in fact, the major result of this work would seem to be a confirmation of assumptions concerning the validity of the homogeneous models. Although the two-lamina model could be useful as a tool to discriminate between proposed mechanisms, the present knowledge concerning the basic processes is so poor that there are too many possibilities, and effective use cannot be made of this model. It appears unlikely that both surface and interfacial reactions can be of importance for a given situation since the interface reaction would dominate at low fluxes and the surface reaction would be the significant energy source at high fluxes. The simple, experimentally observed ignition-time-igniter-flux relationship could be obtained only for very special values of the parameters of these two reactions.

3. TWO-DIMENSIONAL HOMOGENEOUS MODEL

The two-lamina model can be simply converted into a homogeneous model suitable for the study of certain two-dimensional problems associated with the ignition process. An analysis can be made for ignition of a surface subjected to a spacially non-uniform heat flux. Such non-uniformity is characteristic of the flux distributions from an arc-image furnace, and the motivation for making a short study was based upon the comparison of low flux arc-image furnace data to the results of radiation furnace tests in the same heat flux range. Normally, a plot of experimental arc-image data in the form of $\log t_i^{1/2}$ versus $\log f$ shows

a slope of -1 in the low flux range. There is some question concerning the significance of this slope because of the poor precision of normal arc-image data. The experimental data from radiation furnace tests, for which the precision is very good, is about -0.9; and if it is assumed that the difference in slope is significant, an explanation of the difference would be useful. It was postulated that this difference was possibly the result of the non-uniform heat flux employed by the imaging furnaces. Presumabley, in the radiation furnace, the essentially black-body radiation is uniform across the sample surface.

The two-dimensional model was formulated in terms of cylindrical coordinates, and ignition times were calculated for the case of average propellant thermal properties, a surface reaction with activation energy (E/R) of 15,500°K and a pre-exponential factor of $4.45 \times 10^{10} cal/(sec)(cm^2)$ [8]. Fig. 19 illustrates the spatial heat-flux distribution assumed at all flux levels. This distribution would be typical for a carbon-arc imaging furnace. Fig. 20 compares calculated ignition times for the assumed non-uniform distribution to those calculated for a uniform flux, as functions of the maximum flux. As would be anticipated, essentially the same ignition times are calculated at high flux levels. Somewhat longer times are obtained for the non-uniform flux case at low flux levels; however, only a small difference in slope of the two lines is predicted. If the slope of such a plot of arc-image data differs from the value obtained from radiation furnace data, the difference cannot be explained in terms of the spatial heat flux distribution.

III. HIGH-CONVECTIVE HEAT-FLUX STUDIES

All of the studies discussed in this section employed the shock
tube as a source of high-pressure, high-temperature gas for convective
heating. The first three topics, which are concerned with ignition
catalysts, surface roughness effects and pressed propellant ignition,
represent extensions of previously reported work, and the purpose of
these tests was to investigate conclusions suggested by prior results.
The last item presented, the measurement of propellant surface tempera-
tures during the ignition transient, describes work intended to inves-
tigate predictions of the thermal ignition theories. A detailed tech-
nical report of this work is being prepared and the discussion presented
here is intended only as a brief summary of the work.

1. IGNITION CATALYST STUDY

In earlier studies on ignition of propellants by convective heating,
reported in References [1], [8] and [4], most of the data on ignition
were obtained on propellants catalyzed with copper chromite (Harshaw
CuO_2O_2P). In the work reported here, a study of the effect of cata-
lysts was made, in which five propellants were tested. One of the pro-
pellants in this study, Propellant AH, was uncatalyzed. The other four
propellants, Propellants AJ, AK, AL and UA, were catalyzed with ammonium
dichromate, n-butyl ferrocene, cobalt oxide and copper chromite, respec-
tively. These propellants were all processed with only 15-micron AP to
facilitate the preparation of smooth surfaces on samples to be tested.
Data on all propellant compositions are given in Table 3 and their thermo-
physical properties are listed in Table 4.

The shock-tube apparatus used for convective heating of samples was
the same one used in earlier studies. Fig. 2 is a drawing of the shock-
tube driven end, showing the location of the test section used for igni-
tion studies. It was found in these studies that, when using the test
section with a bell-mouthed entrance to the flow channel as shown in Fig.
21, uncatalyzed propellants could not be ignited by convective heating in
the shock-tube apparatus. Test times in the shock-tube were not suffi-
ciently long to bring uncatalyzed AP propellants to their ignition temperature.

20

For some of the work reported here, the test section was modified by the addition of a sharp-edged orifice at the entrance to the flow channel (see Fig. 30). The sharp-edged orifice, with a cross-sectional area slightly smaller than that of the flow channel, modified flow conditions to give a higher rate of heat transfer to the test position than was obtainable with the bell-mouthed entrance. The results from a heat-transfer study on the modified test section were correlated to permit calculation of heat-transfer coefficients during an ignition test.

Ignition data in the form of mean externally applied heat flux to the propellant surface, $\overline{F}_s$, versus square root of ignition time for the uncatalyzed Propellant AH are graphed in Fig. 22. Ignition data used for preparing this graph are given in Table 5. These data are for tests with three different flow-control orifices at the downstream end of the test-section flow channel. The symbol M_{ts} used in Fig. 22 is the gas Mach number that corresponds to the bulk velocity of the test gas flowing through the flow channel. The actual gas velocities that correspond to the Mach numbers are in the range of 50 to 110 m/sec.

Ignition data for Propellant AH, plotted in the form $\ell n(\overline{F}_s)$ versus $\ell n(t_i)^{1/2}$ from convective heating experiments are compared in Fig. 23 with data for the uncatalyzed G propellant from radiation furnace experiments at low heat fluxes. Except for the particle size of the AP (a 50/50 blend of 200-micron and 15-micron), the G propellant is similar to the AH propellant. The ignition data for Propellant G, obtained in the radiation furnace at low heat fluxes, have been discussed previously in References [5] and [8]. Previous results indicate that the low flux ignition times of the AH and G propellants should be identical. It is seen from the graph of Fig. 23 that a single line of slope -0.92 passes through the data for these two uncatalyzed propellants. Some of the data for the AH propellant obtained at lower gas velocities (see Fig. 22) lie below the line extrapolated from data on Propellant G at low-radiant heat fluxes. This result suggests that gas velocity has a small effect on the ignitibility of Propellant AH for the test conditions used in this study. Because of test-time limitations in the shock tube, it was not possible to ignite Propellant AH over a wider range of test conditions for each of the flow-control orifices used.

Ignition data for Propellant UA, catalyzed with two percent copper chromite, are graphed in Fig. 24; detailed data are given in Table 6. These data, obtained in tests with the modified test section, are in good agreement with results obtained from earlier studies on this propellant and for other AP propellants catalyzed with copper chromite [4], [8]. The UA propellant data for all gas velocities are closely grouped, indicating little, if any, effect of gas velocity on ignition. The two lines in Fig. 24, representing ignition data for Propellant UA and AH, show the catalytic effect of copper chromite on the ignition process for AP-PBAA propellants.

The ignition data for Propellant AJ, catalyzed with two percent of ammonium dichromate, are graphed in Fig. 25, complete data are given in Table 7. Although these data were obtained at rather high gas velocities across the propellant surface, they are quite well represented by the straight line that defines the ignition data for Propellant UA. The two catalysts, ammonium dichromate and copper chromite, appear to have about the same effect on ignition.

Ignition data for Propellant AL, which contained four percent cobalt oxide, are shown in Fig. 26. Data for Propellant AL are listed in Table 8. Cobalt oxide was reported by Hermoni and Salmon [10] to be an effective catalyst for promoting the low-temperature decomposition of AP. The large amount of scatter among the data for this propellant was caused by surface roughness. The cobalt-oxide powder contained a few large crystals, some as large as 50 microns in diameter, which prevented the preparation of smooth surfaces on all samples of propellant. It appears likely that only the data which lie near the line for Propellant AH represent simple thermal ignition of Propellant AL. Surface roughness effects are postulated to have reduced the ignition times for the other samples. Thus, the catalytic effect of cobalt oxide is not confirmed, but neither, on the basis of these results, can it be denied.

The most effective ignition catalyst of those tested was n-butyl ferrocene. All catalysts previously considered were about equally effective. Ignition data for Propellant AK containing this material are graphed in Fig. 27 and tabulated in Table 9. Although data for Propellant AK show

more scatter than data obtained on some of the other propellants, the
data are still well defined by a straight line with a slope of -0.92.
The effectiveness of the n-butyl ferrocene may be the result of the
excellent dispersion obtained since the catalyst is added to the mix-
ture in liquid form.

The data obtained from this catalyst study show that some mater-
ials are very effective in accelerating the ignition process for AP
propellants. In general, it appears that catalysts which promote com-
bustion processes are the most effective ignition catalysts. The data
for smooth-surfaced samples are in good agreement with a thermal igni-
tion model that considers the key ignition reaction be localized at
the propellant surface. Since ignition data in the form of $\ln(\overline{F}_s)$
versus $\ln(t_i)^{1/2}$ for the different propellants are quite well repre-
sented by a straight line with a slope of -0.92, it appears that all
catalysts affect the ignition process in the same general way.

2. SURFACE ROUGHNESS TESTS

In the earlier studies on ignition of AP propellants by convec-
tive heating, it was found that for low test-gas velocities, in the
range of 50 to 200 m/(sec), propellant samples with rough surfaces
ignited faster than samples with smooth surfaces for equivalent ex-
ternally applied heat fluxes. Based on observation from these studies,
it appeared that the better ignitibility of some kinds of samples was
related to imperfections at the surface. For propellants containing
coarse AP, imperfections are produced at the sample surface during the
preparation of samples for tests. In preparing samples for tests, ex-
cess propellant above the lip of the sample holder is cut away with a
new razor blade. Crystals greater than about 50 microns are fractured
or pulled from the propellant matrix. Depending on the particle size
of the AP and mechanical properties of the binder, protrusions and pits
on the sample surface may extend 20 to 30 microns above or below the
mean surface level. It might be expected that during the heating pro-
cess, prior to ignition, some of these surface imperfections would be
reduced in size by two-dimensional heating and ablative action of the
hot, convective gas. If samples of propellant with rough surfaces

were quenched just before ignition occurred, and then ignited in a subsequent test, it might be possible to detect changes in surface features by comparing ignition data from such tests with those in which the samples were not previously heated.

To check this hypothesis, a few samples of Propellant FM with surface imperfections as large as 30 microns were subjected to convective heating in the shock tube, and the heating was stopped before ignition occurred. These same samples were then immediately subjected to more severe test conditions to produce ignition. Ignition data for samples of Propellant FM for the two kinds of tests are graphed in the form of $\ln(\bar{F}_s)$ versus $\ln(t_i)^{1/2}$ in Fig. 28. Experimental ignition and heat-transfer data for these samples are given in Table 10.

In general, data obtained from the two kinds of tests are the same. Scatter among the experimental data is too large to show any specific trends. The results do not confirm the hypothesis that the surface roughness produces early ignition. However, no conclusion is possible, since serious ablation may occur too close to the ignition time to permit detection of the effect sought by this procedure.

3. IGNITION OF PRESSED PROPELLANTS

Pressed propellants are of interest because they can be made with a wide variety of fuels; also, the oxidant-to-fuel ratios can be varied over a much wider range than is possible with cast propellants. Ignition data were obtained on two pressed propellants: (1) Pressed Propellant PP-E was formed from a powder composed of 93.0; 4.5, and 2.5 percent of AP, carbon, and copper chromite respectively, and (2) Pressed Propellant PP-F, made with 95.0 percent AP and 5 percent copper chromite. See Table 3 for complete compositional data.

Propellants containing very high levels of AP are more difficult to ignite than conventional cast propellants. Ignition times for equivalent externally applied heat fluxes are longer for pressed propellants because the thermal responsivities of pressed propellants

are larger. Thus, more time is required to heat the surfaces of pressed propellants to their ignition temperatures. However, ignition temperatures, as predicted by thermal ignition theory, are about the same for all AP containing materials (compare the data in Table 6 to Table 11).

Experimental ignition and heat-transfer data for tests with Propellant PP-E and PP-F are given in Table 11. The results for these two propellants, as shown by Fig. 29, are quite similar. Propellant PP-F, which did not contain a fuel, was composed only of AP and copper chromite. The test pressure of 20 atms was above the deflagration limit of this material. That the data for these two pressed propellants are represented by a straight line with a slope of -0.92 and have the same ignition temperature as for cast propellants suggests that the key ignition reaction is a chemical reaction involving initially only the AP.

4. PROPELLANT SURFACE TEMPERATURE MEASUREMENTS

The transient measurement of propellant surface temperatures was accomplished by detection of the total radiation emitted by the heated surface. Propellant samples, mounted in the test section shown in Fig. 30, were ignited by passage of hot nitrogen generated in the shock tube through the flow channel and across the sample surface. An orifice was mounted upstream of the sample, since this configuration produced higher heat fluxes than were obtained with a bell-mouthed entry upstream, and a wider range of conditions could be studied. A 2 × 2 mm area of sample surface was viewed through an infrared transparent window, and the emitted radiation was focused on an infrared sensitive detector by the optical system illustrated in Fig. 31. The window transparency and detector sensitivity were high in the wave-length range of 1-10 microns, and useful detector output was obtained for surface temperatures from 30-600°C. The Philco GPC 201A detector has a gold-doped germanium sensitive element and is operated at the boiling point of liquid nitrogen (77°K). The one-microsecond time constant of this detector was short enough for the purposes of this study.

The system was characterized and calibrated by use of special thin-
film heat-flux gauges. The platinum-film resistance thermometer on the
surface of these pyrex gauges was first coated with a thin layer of sili-
con monoxide by vacuum deposition, and this layer was over-coated with
carbon by deposition from decomposed methyl iodide. The coated gauge
surface was opaque and very black; the effective thickness of the sili-
con oxide and carbon was found to be equivalent to a layer of about five
microns of the pyrex substrate. The temperature coefficient of the plati-
num film on the gauge was determined at temperatures to 200°C. The gauge
surface temperature could be determined, and the detector output was re-
lated to surface temperatures during a calibration test. If the gauge
surface was assumed to be totally black, the detector output, at a given
surface temperature, represented an upper limit for emission from pro-
pellant surfaces. Fig. 32 shows a line representing the relationship
between the coated-gauge surface temperature and the infrared-detector
output (IRDO) from the surface. It was found that emission from small
amounts of dust in the hot gases represented a significant fraction of
the detected emission at low surface temperatures. It was necessary to
measure the dust emission, and the low surface temperature data were cor-
rected for such emission.

Also shown in Fig. 32 are data representing the detector output as
a function of the calculated surface temperatures for the AR propellant
(see Table 3). The surface temperature of the smooth-surface propellant
was calculated by use of heat-transfer coefficients measured both during
a prior heat transfer study and while calibrating with the coated heat
flux. Until the ignition temperature is approached, the solid is treated
as chemically passive. The effective emission from the AR propellant
surface was only 60 percent of the emission from the black gauge at the
same surface temperature. Although the fuel-binder of the AR propellant
was loaded with fine carbon black, the low apparent emissivity is likely
not only the result of surface phenomena but also of partial transparency
near the surface. The apparent emissivity of a similar propellant (UA)
which contained no carbon black in the polymer was only 0.35. When the
surface of the AR propellant was coated with a thin layer of carbon black,

the detector-output-surface-temperature relationship is found to be almost indistinguishable from that of the blackened heat-flux gauge.

Fig. 33 reperesnts a typical plot of measured propellant surface temperature as a function of time for an ignition test. The surface temperatures were obtained employing the line in Fig. 32 for AR propellant (extrapolated when necessary) from the detector output. Also shown in Fig. 33 is the surface temperature time relationship calculated by use of the thermal ignition theory which considers only a surface reaction [4], [8] for the parameters of catalyzed AP propellants. The general agreement in form of the experimental and calculated results is thought to be significant. The lack of exact agreement results from normal experimental errors, and the largest error is thought to result from lack of precise reproductability of the heat transfer conditions in the shock tube apparatus.

The infrared method for surface temperature measurement is found to produce reasonable results for smooth surface propellants which are opaque and which are preferably coated with a blacking agent. The surface temperature histories are about what is anticipated from linear heating theory and from thermal ignition theory. Tests employing rough surface propellants yield data which are hard to interpret. The initial rate of surface temperature rise is much greater than calculated for smooth surfaces. However, the measured surface temperature at which a rapid rise due to exothermic reaction occurs is about the same for the rough-surface propellants as for those with smooth surfaces. The fact that the total radiation detector measures an "average" surface temperature over the irregular surface likely makes interpretation difficult.

IV. HOT-WIRE IGNITION

Although the preliminary experiments employing electrically-heated wires to ignite propellant samples indicated that this technique might be useful for establishing the heat-flux-ignition-time relationship at high pressures, subsequent tests showed that calculated linear ignition temperatures determined by use of hot wires were not in agreement with those measured by thermal radiation or convective heating of exposed surfaces [1], [11]. An additional problem with the hot-wire technique is that the calculated ignition temperatures are apparently a function of the diameter of the heated wire. Fig. 34, which shows some previously reported data for tests with 18-gauge (.103 cm diameter) and 29-gauge (.029 cm diameter) Nichrome V wire, illustrates this point. In this plot, a line is drawn representing the experimental data obtained for exposed surfaces.

A study of the 18- and 29-gauge data suggests the use of very fine wires to obtain agreement between hot-wire results and the thermal theory. The use of very fine wires has some experimental advantages, since relatively low currents, which are electronically switchable, are used. As a consequence of such considerations, tests were run on samples in which .013 cm and .0064 cm diameter wires were cast. These data are also shown in Fig. 34. The anticipated result of using fine wires was not observed; the data are again segregated according to the diameter of wire employed even for the finest wire.

The most perplexing result is that the linear ignition temperatures for the very fine wires are significantly below the temperatures measured for tests with exposed surfaces. Higher calculated ignition temperatures from hot-wire tests can perhaps be explained by postulation of an interfacial thermal resistance or the existence of a polymer-rich layer around the wire; the lower ignition temperatures calculated for the very fine wire are difficult to explain. The technique for calculation of the interface temperature, which requires numerical integration of a complex

28

relationship, has been thoroughly checked, and it is unlikely that the interface temperature calculation is in error.

At the present time, it appears unlikely that the hot-wire technique can be developed into a useful tool for ignition characterization of composite propellants.

I. THERMAL DECOMPOSITION STUDIES

The thermal effects of reactions for the PBAA-AP propellant system
have been studied by means of the thin-film technique developed during
a previous grant period. The thermal decomposition of the PBAA fuel-binder
(see Table 3) and propellant-like materials in nitrogen and also the decompo-
sition and ignition of these materials in gaseous oxygen were studied. A
complete, detailed report of this work will be issued, and the following
paragraphs briefly present only the most interesting results and conclusions.

1. THE EXPERIMENTAL METHOD

Fig. 35 illustrates the manner in which the test films were mounted
on a copper disc which formed part of a thermocouple. These films were
cut with a microtome from pieces of material blackened with carbon black.
The upper assembly shown in Fig. 35 was mounted in a shield, also shown
in Fig. 35; and when this assembly was thrust into the interior of a
thermal-radiation furnace, the surface of the film was exposed to the
uniform radiation. The measured temperature history of the copper disc
was used to detect and characterize the nature of reactions in tne test
film. The furnace was operated at temperatures of 800 to 1100°C at pres-
sures from .01 to 5 atms with nitrogen or oxygen filling the chamber.

2. EXPERIMENTAL RESULTS

Although a wide range of experimental conditions were considered,
all of the tests cited here were made at a furnace temperature of 1100°C,
at a pressure of 0.85 atms and with films 100 microns thick containing
3 percent of very finely dispersed carbon black. Total test times of
from 2-3 seconds were obtained. Except as noted, tests were in nitrogen.

Decomposition of the PBAA Polymer

Tests on a typical "pure" PBAA polymer used in propellant formu-
lations show a surface decomposition temperature, under 0.85 atm of
nitrogen, in excess of 390°C. Fig. 36 shows data for such a test.
The time-surface-temperature relationship is a tracing from a Visi-
corder record. The occurance of the first significant endotherm at
a copper-disc (interface) temperature of 290°C is easily detected.
The surface temperature is calculated from the interface temperature
by considering the temperature drop across the film and a small time
delay (about 0.1 sec) required for signal passage through the film.
The photocell signal, which apparently results from radiation from
carbon-black particles evolved from the regressing film, changes
most rapidly some time after the first endotherm. Loss in weight
measurements on samples rapidly removed from the furnace after only
partial decomposition showed that the photocell signal indicates the
point at which significant sample regression occurs. The addition of
a "copper chromite" burning-rate catalyst to the polymer reduces the
occurrence of the endotherm to the range of 330°C to 375°C surface
temperature, depending on pressure. Again, the photocell output was
shown to correspond to significant vaporization of the film.

Fig. 37 summarizes the data obtained for PBAA films and PBAA
films containing copper chromite. The plot is a conventional repre-
sentation of the reciprocal of temperature (surface temperatures at
first endotherm and at the beginning of significant regression) versus
the logarithm of total furnace pressure. If the slopes of the lines
through the data are interpreted in terms of equilibrium heats of
vaporization, it is found that apparent heats of vaporization calcu-
lated from the first-endotherm data are too high (>30 kcal/g-mole) to
be likely values. By contrast, the heats of vaporization from the
photocell signal (regression) are what would be expected (15 kcal/g-mole)
for a high-molecular-weight organic materials vaporizing at this tempera-
ture. The data shown in Fig. 37 can be explained by considering PBAA to
decompose by essentially a two-step process. In the first step, bonds are

broken at a rate independent of pressure; and light fragments are
vaporized by an equilibrium process. this step is presumably de-
tected as the first endotherm. Heavy fragments, which presumably
are the principal product of the decomposition, are later vaporized
by an equilibrium process. This step is detected by the photocell
and weight-loss tests.

Decomposition of PBAA Films Containing AP

Tests were also made in which various amounts of minus-five-
micron AP were added to the PBAA polymer. For AP levels less than
ten percent, an endothermic decomposition of the AP occurs at a sur-
face temperature of about $33 \jmath\,°C$ and is quickly followed by an exothermic
reaction. For AP levels greater than ten percent, the effect of the
endothermic reaction is masked by the strong exotherm. These processes
are referenced in Fig. 38, which is a summary of tests with the AP-PBAA
films. Ignition in this case was detected by observation of the photo-
cell signal. For AP levels greater than thirty percent, true ignition
with a flame and total consumption of the film occurred. At the low
AP levels, the photocell signal apparently detected evolution of the
carbon black used to blacken the film. These films were not consumed
when the sample was removed from the furnace.

A most significant effect is noted when comparing the data shown
in Fig. 36 (PBAA only) with those in Fig. 38 (PBAA + AP). The addition
of ten percent AP to the film reduces the temperature at which signi-
ficant regression starts from over 450°C to about 390°C. The decompo-
sition rate of the polymer is thus greatly increased in the presence of
even small quantities of AP, and loss-in-weight measurements show that a
significant loss of the polymer occurs as a result of the action of the
AP. At high heating rates, the existence of a rapid, lower temperature
PBAA-AP reaction is indicated. Since this reaction appears to occur at
temperatures significantly lower than the decomposition temperature of
the polymer, it appears likely that the PBAA is attacked by the AP
decomposition products. The PBAA-AP reaction is of prime importance,
and the decomposition reaction of the PBAA alone is of only secondary
interest. Unfortunately, this fact was not early recognized and studied

in detail. Data, analogous to those shown in Fig. 37, were not obtained.

A study was made in which the copper chromite catalyst was added to the PBAA-AP films in the ratio of one part catalyst to ten parts of AP. Except at high AP levels, where the catalyst level was also high, the data were very similar to those shown in Fig. 38. The dispersion of a small amount of catalyst in the polymer probably prevented effective AP-catalyst contact.

Reactions of Thin Films in Oxygen

Tests were performed in which thin films of the PBAA polymer decomposed and ignited in the presence of oxygen at pressures of 0.85 to 5.0 atms. Fig. 39 shows typical data from such a test. In these tests, the photocell sensitivity was set to detect only intense radiation, and ignition denotes first appearance of a flame. In the oxygen tests, it was found that a strong exothermic reaction occurred at surface temperatures about 100°C lower than the first endotherm in a neutral atmosphere. The polymer was attacked without significant prior decomposition. This exotherm temperature is a function of the oxygen pressure. The results plotted in Fig. 39 indicate a significant time lag between the exothermic reaction and the establishment of a flame indicated by the photocell. The length of this time lag was found to be decreased by increasing the furnace (oxygen) pressure and temperature; at 1100°C and 5 atms, the exotherm and photocell signals were essentially simultaneous.

Ignition tests in oxygen were also made by use of films containing fine glass beads as an inert diluent. Fig. 40 shows a plot of the surface temperature at ignition of these materials as a function of the volume fraction of beads. The reduction in the exposed polymer surface produced a significant increase in the surface temperature; at ignition, however, the exotherm temperature increased only about 10°C from the case of the unloaded polymer to the maximum loading shown in Fig. 40.

All of the characteristics mentioned here for the PBAA reaction and ignition in oxygen can be reconciled by postulating different

mechanisms and sequential occurrence of the exothermic and ignition
reactions. As the film is heated, a surface reaction between the film
and oxygen occurs; the exotherm is likely from a heterogeneous reaction.
Gaseous products of the oxygen-PBAA reaction diffuse into the gas phase
and when the proper concentration conditions are realized, gaseous igni-
tion occurs and a flame is established; the luminous ignition reaction
is a gas phase process. A more satisfactory, more quantitative discus-
sion of this mechanism is presented in the detailed report of this work.

Feedback-Heat-Flux Calculations

If, after the occurrence of an exothermic reaction, the feedback
heat flux at the surface is essentially constant, the rate of tempera-
ture rise of the copper disc may be used to estimate the magnitude of
this heat flux. A rigorous calculation of the surface heat flux is
not possible without a detailed knowledge of the surface temperature
and regression rate of the film; however, the value of the heat flux
seen by the copper disc should be nearly proportional to the surface
heat flux. The time-surface temperature relationship shown in Fig. 39
illustrates a condition for which the feedback flux from the PBAA-surface-
oxygen reaction may be estimated. A point of significant interest is
that the maximum feedback heat flux occurs before appearance of the
flame, and in fact, the heat flux seen by the copper disc decreases
near the time the photocell detects radiation. The implication is
that the energy released by reaction at the polymer surface, and not
feedback from the flame, is primarily responsible for heating the poly-
mer. Observation of the maximum in feedback heat flux before the photo-
cell signal was typical of all tests in oxygen at low pressures. The
magnitude of the net feedback heat flux (the total flux less the measure
flux before the exotherm) in oxygen was found to be approximately propor-
tional to the square root of the oxygen pressure.

Feedback-heat-flux measurements were made from tests on PBAA films
containing various amounts of AP. Fig. 41 summarizes these data which
were obtained in 0.85 atms of nitrogen. The AP density, the abscissa
on this plot, is proportional to the surface area of the AP at the film

surface, and the net feedback heat flux to the copper disc is proportional to about the 1.8 power of the AP density. Extrapolation of these results to an AP density of 1.15, which corresponds to the UA propellant value would indicate a heat flux in the solid of about 45 cal/(sec)(cm^2). For the UA propellant, which has a burning of 0.33 cm/sec at 0.85 atms, a steady-state heat flux below the surface of 78 cal/(sec)(cm^2) is calculated for an assumed surface temperature of 500°C. Since the copper disc measures the heat flux below the film surface, the relative magnitude of these fluxes is reasonable. The feedback flux for the uncatalyzed films is about two-thirds of the value for films containing catalyst. This result would be anticipated on the basis of steady-state burning rates.

Conclusion

The experimental technique employing very thin films of materials backed by a disc calorimeter yields data concerning the thermally significant reactions in the time scale of interest in propellant ignition and burning. The data from PBAA films tested indicated that decomposition occurs by a two-step process with the second step being the equilibrium vaporization of heavy residues from the initial decomposition reaction. The addition of AP to the film reduces the temperature at which significant decomposition of the film occurs by 50 to 60°C. An AP decomposition product--PBAA--polymer reaction is strongly indicated.

The reaction and ignition of PBAA films in oxygen appears to involve a nonluminous PBAA-oxygen reaction at the surface and a later gas phase reaction to produce a luminous flame. Feedback energy to the PBAA polymer film by reactions is principally from the nonluminous reaction and is, perhaps, only partially the result of flame action.

VI. PROPELLANT EXTINGUISHMENT

Two experimental methods have been employed to produce extinction of solid propellant flames by rapid depressurization. In the first case, samples of propellant were mounted inside a relatively short tube which was pressurized and fitted with a nozzle at one end. When a diaphragm which was mounted over the nozzle was burst, the pressure decay experienced by a burning sample could be approximated as $d \ln P/dt =$ constant; such a pressure decay is termed a "blowdown" decay and is illustrated in Fig. 42. The second method used is also represented in Fig. 42. Samples were mounted in the curved wall of a long, pressurized tube which was also fitted with a diaphragm-covered nozzle. Where the diaphragm was burst, the sample was subjected to the pressure decay characteristic of a rarefaction wave generated in this fashion. The most important characteristics of such waves are a constant ratio of the initial pressure to final pressure behind the wave and a decreasing time for the total pressure drop as the point of interest approaches the nozzle. The "blowdown" tests were employed to determine the value of $d \ln P/dt$ which just produces extinction. The second technique yields data which are used to calculate the net heat of gasification.

The Blowdown Extinguishment Requirement

Extinction requirements were previously reported for a series of propellants based on the system PBAA-AP, and six different variations of such propellants were tested [1]. A seventh variation, the UG propellant, was formulated by use of a polyurethane (PU) fuel binder. The low pressure deflagration limit for the PBAA propellants was less than 0.06 atms; and while this limit for the UG propellant was higher (.15 atms), in these tests, extinction was always the result of rapid depressurization, since the minimum pressure was 0.85 atms. Table 12 summarizes the extinguishment data for the total series of propellants. Also shown are various combustion constants for the propellants. The data in

36

Table 12 can be used as a critical test for proposed theories of composite propellant extinction. No present theory even qualitatively predicts the characteristics of these results.

Consideration was given to the effect of sample diameter for these blowdown extinguishment tests. Table 13 presents the results of this study in which the extinction requirements of 0.92 cm and 1.56 cm diameter samples of G propellant are compared. The extensive, previously reported tests with .92 cm diameter strands indicates an extinction requirement (-d ln P/dt) of from 40 to 60 sec^{-1} for the G propellant. Although extinction of the 1.56 cm strands occurred when employing the same nozzle as for the smaller strands, the fractional rates of decay were higher since the large strands heated the gases in the tube and produced a greater change in the properties of the chamber gases. A more severe requirement of 60-80 sec^{-1} for the larger strands is indicated. However, the data for smaller strands shown in Table 13 also indicate a 60-80 sec^{-1} requirement; unfortunately, these data are too few to be conclusive. It will be necessary to resolve the discrepency noted, and to account for the effect, if it exists, of sample size.

Measurement of the Net Heat of Gasification

It is assumed that the character of the thermal wave in the solid controls, or at least is closely coupled to, the combustion process and that the gas-phase processes are fast enough to follow faithfully changes in the imposed pressure. The steady-state energy balance for burning at pressure P may be written as

$$f_1 = r_1 \rho q + r_1 \rho c (v_s - v_o), \tag{8}$$

where f_1 is the feedback flux from the gas phase, r_1 is the linear regression rate at ρ_1, ρ is the solid-phase density, q is the net heat of gasification per unit mass, c is the heat capacity of the solid, v_s is the surface temperature, and v_o is the initial temperature of the solid.

The final term of Equation 8 represents that part of the feedback flux conducted into the solid:

$$-k \left(\frac{\partial v}{\partial x}\right)_{x = 0^+} , \tag{9}$$

where k is the thermal conductivity and x is distance measured into the solid from the surface. The instantaneous pressure dependence of the flux is assumed to be the same as that of the steady-state burning rate, or $f_1 = aP_1^n$, where a and n are constants. Equation 1 can be written

$$f_1 = aP_1^n = r_1\rho q + r_1\rho c \left(v_s - v_o\right) \tag{10}$$

We now consider a sudden drop in pressure from P_1 to P_2. If the drop is a small one, the propellant will adjust to the new conditions and continue to burn; if it is a large drop, the flame will be extinguished. If we consider the least instantaneous pressure drop that will cause extinguishment, $r_2 = 0$; but, at the instant of pressure drop, the flux into the solid will still be given by Equation (9) or the final term of Equation (10):

$$f_2 = aP_2^n = r_1\rho c \left(v_s - v_o\right) \tag{11}$$

In words, the new conditions are such that the feedback flux can supply only the energy for the thermal wave but none for gasification. If we divide and solve for q, we have

$$q = c \left(v_s - v_o\right) \left[\left(\frac{P_1}{P_2}\right)^n - 1\right] \tag{12}$$

The net heat of gasification, q, can, therefore, be determined if we know the value of v_s and the least instantaneous pressure drop that will just produce ignition.

It is not possible experimentally to produce an instantaneous drop in pressure. It is possible, however, to decrease the pressure rapidly enough to extinguish propellants and to vary both the extent of the drop

and the rate of the drop. This was accomplished by employing a rare-
faction tube with (1) various nozzle sizes to vary the extent of the
drop, and (2) the sample mounted in the curved wall at different dis-
tances from the nozzle to vary the rate of the drop. When the tube
was pressurized with air or nitrogen to the desired pressure, P_1, the
sample was ignited, and, when the sample surface was flush with the
wall, the diaphragm was broken and a rarefaction passed over the pro-
pellant, dropping the pressure from P_1 to P_2 very quickly. A photo-
cell monitored the flame from the burning surface. Disappearance of
flame radiation during passage of the first rarefaction wave was the
criterion for extinction. It was observed that if the burning was not
extinguished by the first rarefaction, it was not extinguished at all.
The duration of the flow of cold gas across the burning surface after
the passage of the first rarefaction was varied by changing the total
length of the tube; it did not have an observable influence on the re-
sults.

A set of experiments was conducted in the following way. The
sample position, a distance, L, from the nozzle, was chosen. Tests
were run at the same pressure, P_1, but with nozzles of increasing dia-
meter until a large enough pressure drop was produced to extinguish the
burning. Similar tests were performed at other values of L, which was
proportional to the characteristic time of the pressure decay. A plot
of the critical ratio vs. L can be extrapolated to L = 0 to give the
ratio for instantaneous pressure drop as required for use in Eq. (12).
The entire set of experiments was repeated for other initial pressures.
Two propellants, G and UG, were studied by use of this technique. Criti-
cal pressure ratio data were obtained for the AH and UA propellant only
at the minimum nozzle to sample position. It was not possible to extin-
guish the F propellant by use of this technique.

Figs. 43 and 44 present the experimental results for the G and UG
propellants. Pressure ratio is plotted on the ordinate, and dimensionless
characteristic pressure-decay time as the abscissa. The characteristic
time of pressure decay is given by L/a_o, where a_o is the speed of sound
in the original gas in the tube. It is divided by the characteristic
time associated with the thermal wave in the solid, α/r_1^2, where α is
the thermal diffusivity of the solid.

Data for all pressures investigated correlated together for G propellant (Fig. 43), indicating that q, determined from the pressure ratio at L = 0, is not a function of pressure. The further important inference is that q is properly a property of the propellant and that it may be used with some confidence in theoretical combustion models. For G propellant, the value of q is estimated to be 25 cal. per gram.

Similar observations may be made for UG propellant at the higher pressures studied, the estimated value of q being cal. per gram. At 4.3 atm., however, q is less. The single nozzle to sample length data for the AH, UA and F propellants are summarized in Table 12. Lower ratios, more severe extinction requirements and higher values of q are indicated for the catalyzed propellants.

Conclusions

This indirect technique developed for measurement of the net heat of gasification yields reasonable values of this parameter. The charac-teristics of the rarefaction tube limit the pressure ratio to practical values somewhat greater than 0.35, and extinction of propellants with q values greater than about 100 cal/gram cannot be achieved. However, when applicable, this technique should be quite useful for characteri-zation of propellants since the experimental apparatus and procedures are quite simple. The most critical assumption of the method, that the feedback flux is aP^n at both the initial and final pressures, would be very difficult to check directly, and investigation of this assumption is only possible by comparison of the results reported here to values obtained by techniques which do not require this assumption.

APPENDIX A.   FIGURES 1 THROUGH 44
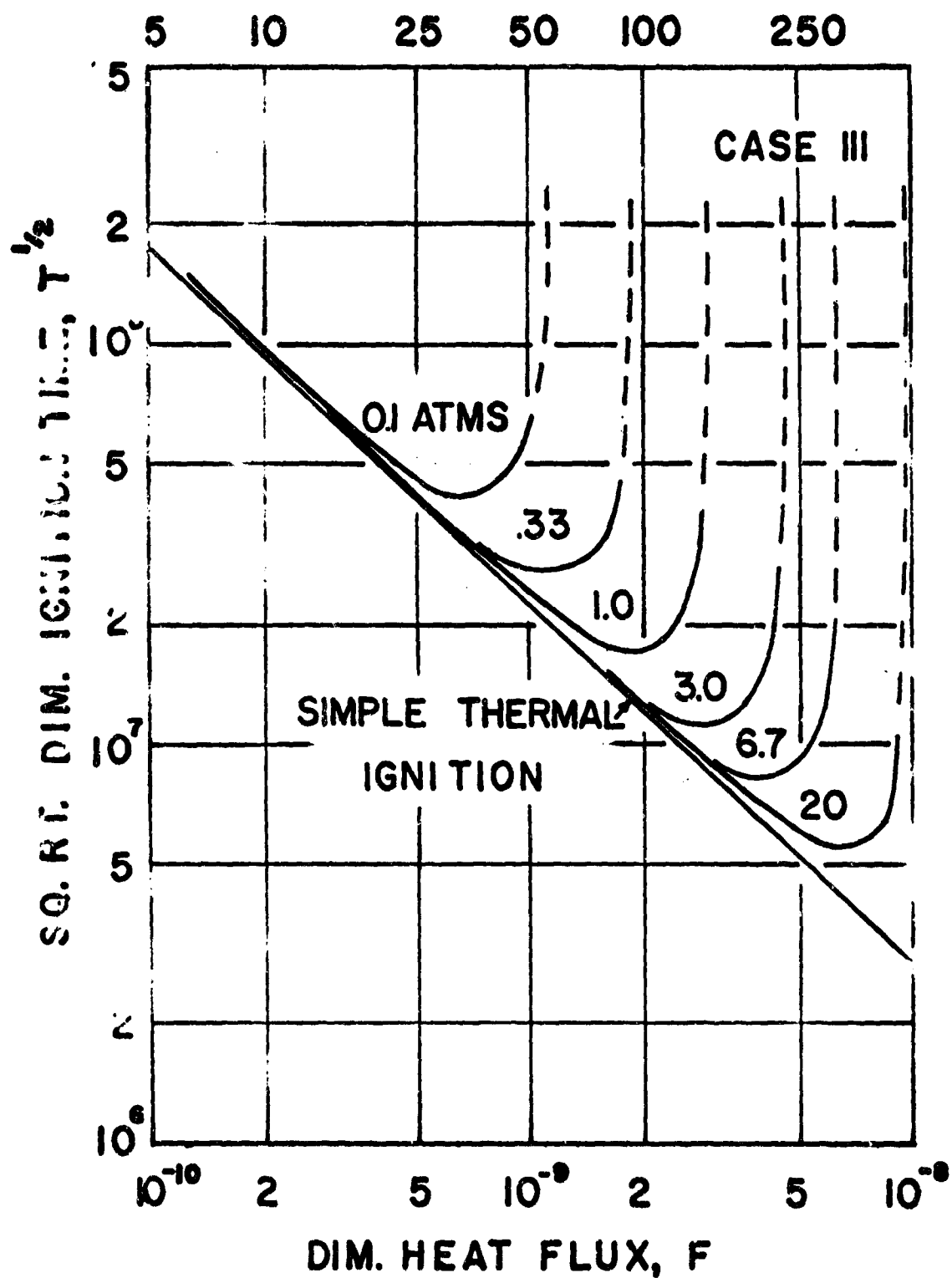
Figure 1. Calculated ignition response for the Case III parameters.
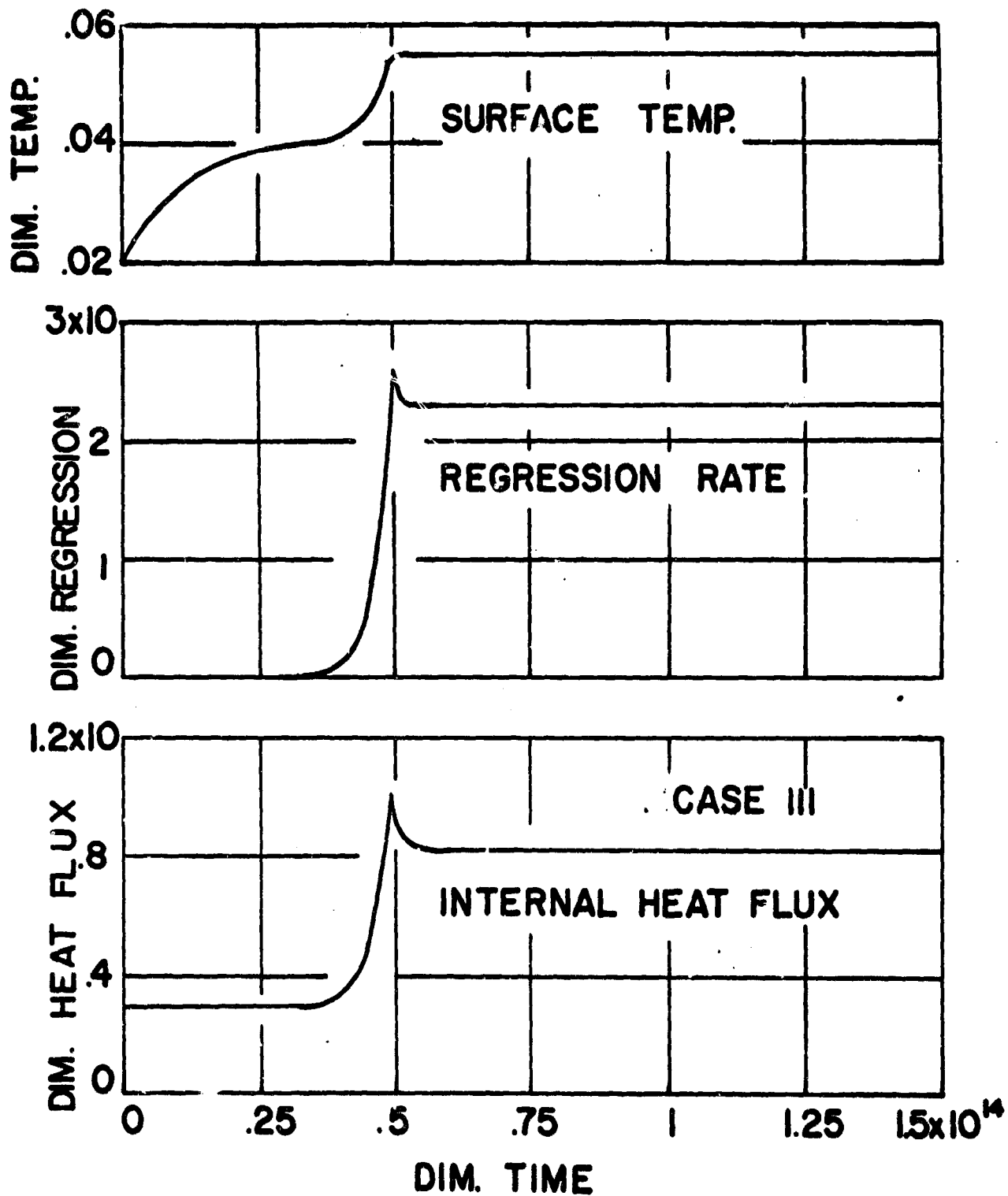
Figure 2.   Important variables as a function of time for the case of an igniter flux less than the steady-state feedback flux.
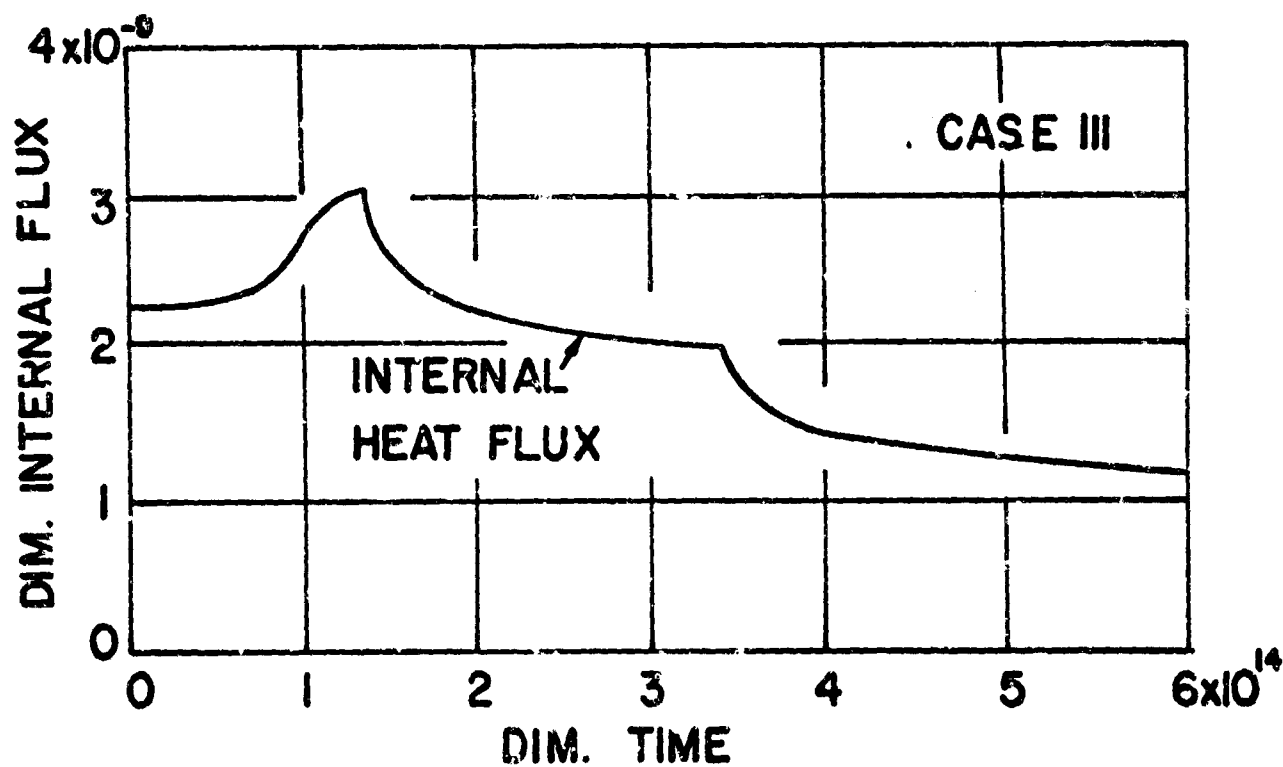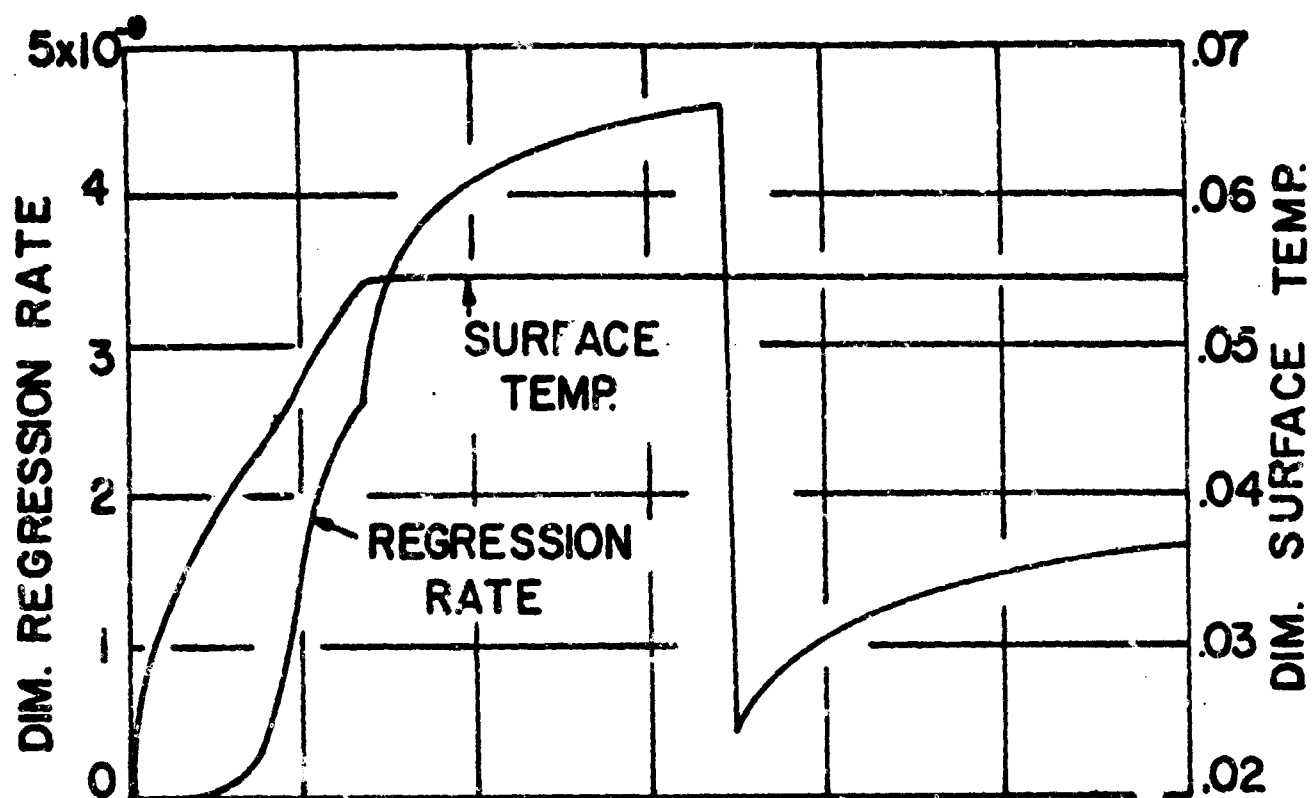
Figure 3. Important variables as a function of time for the case of an igniter flux greater than the steady-state feedback flux.
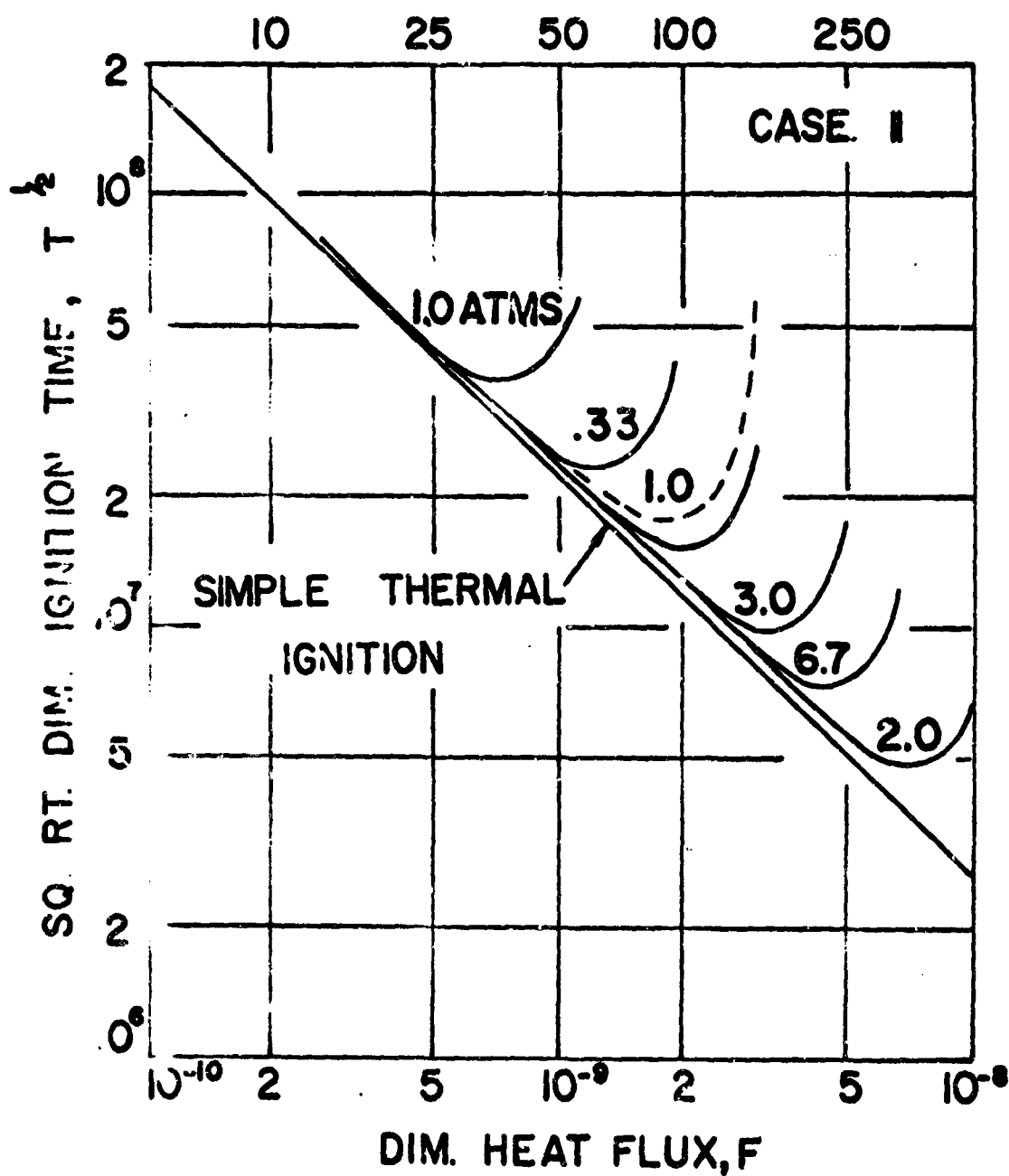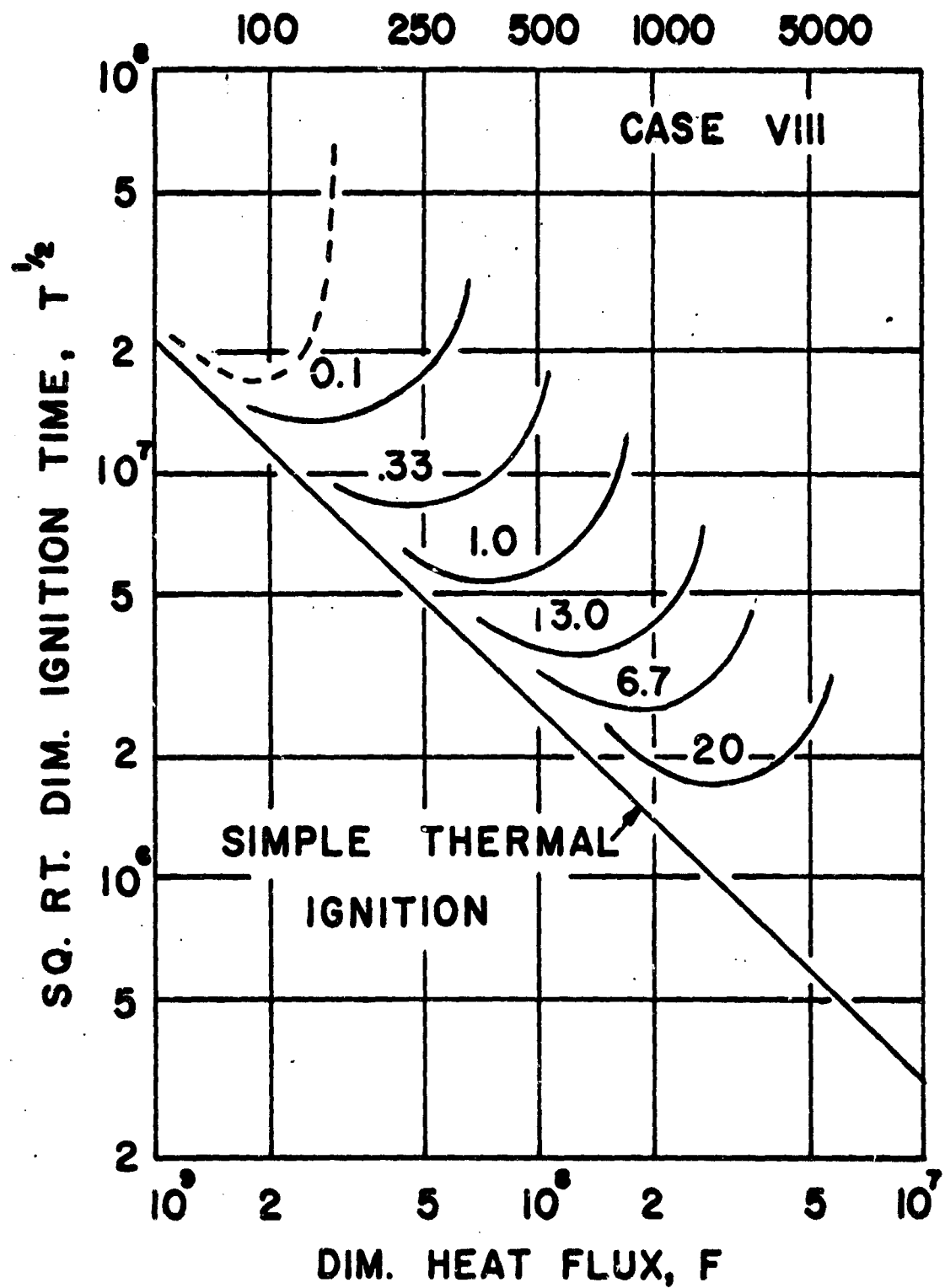
Figure 4. Calculated ignition response for the Case II parameters. The dashed line is for Case III response at 1 atms. The dimensionless regression surface temperature is .05 for Case II and .055 for Case III.
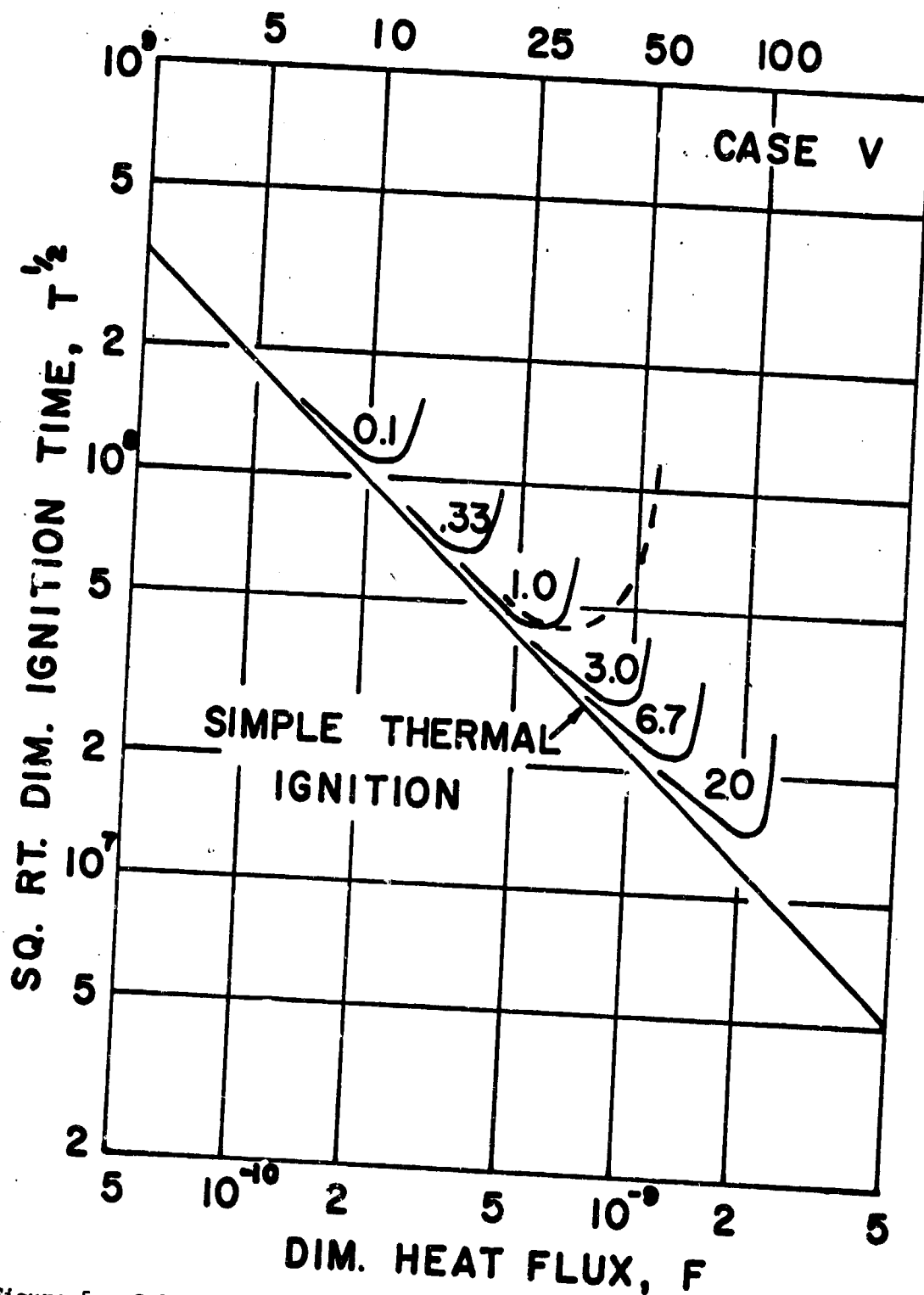
Figure 5. Calculated ignition response for the Case V parameters. The dashed line is for Case III response at 1 atms. The dimensionless net heat of gasification is .025 for Case V and .05 for Case III.
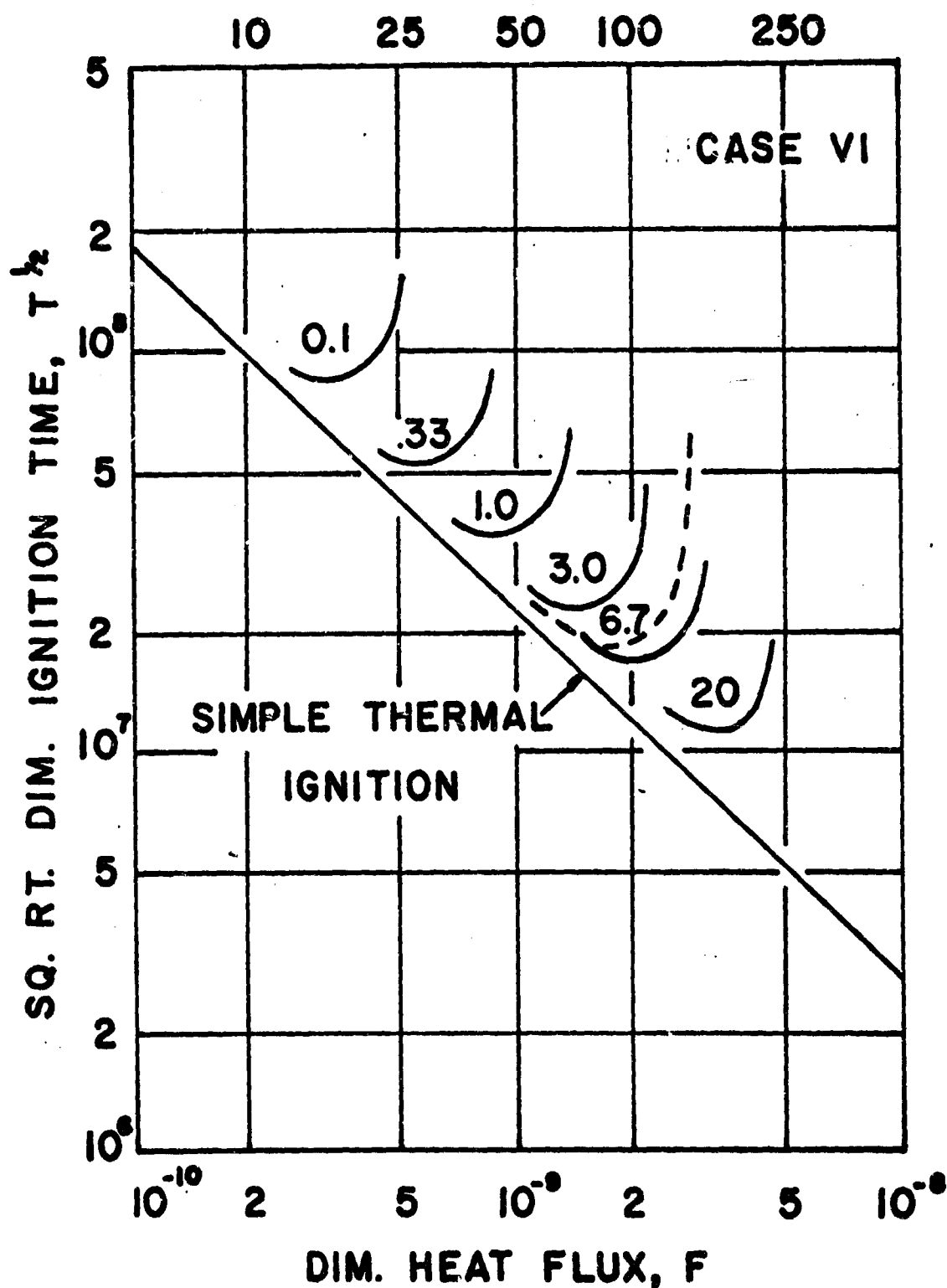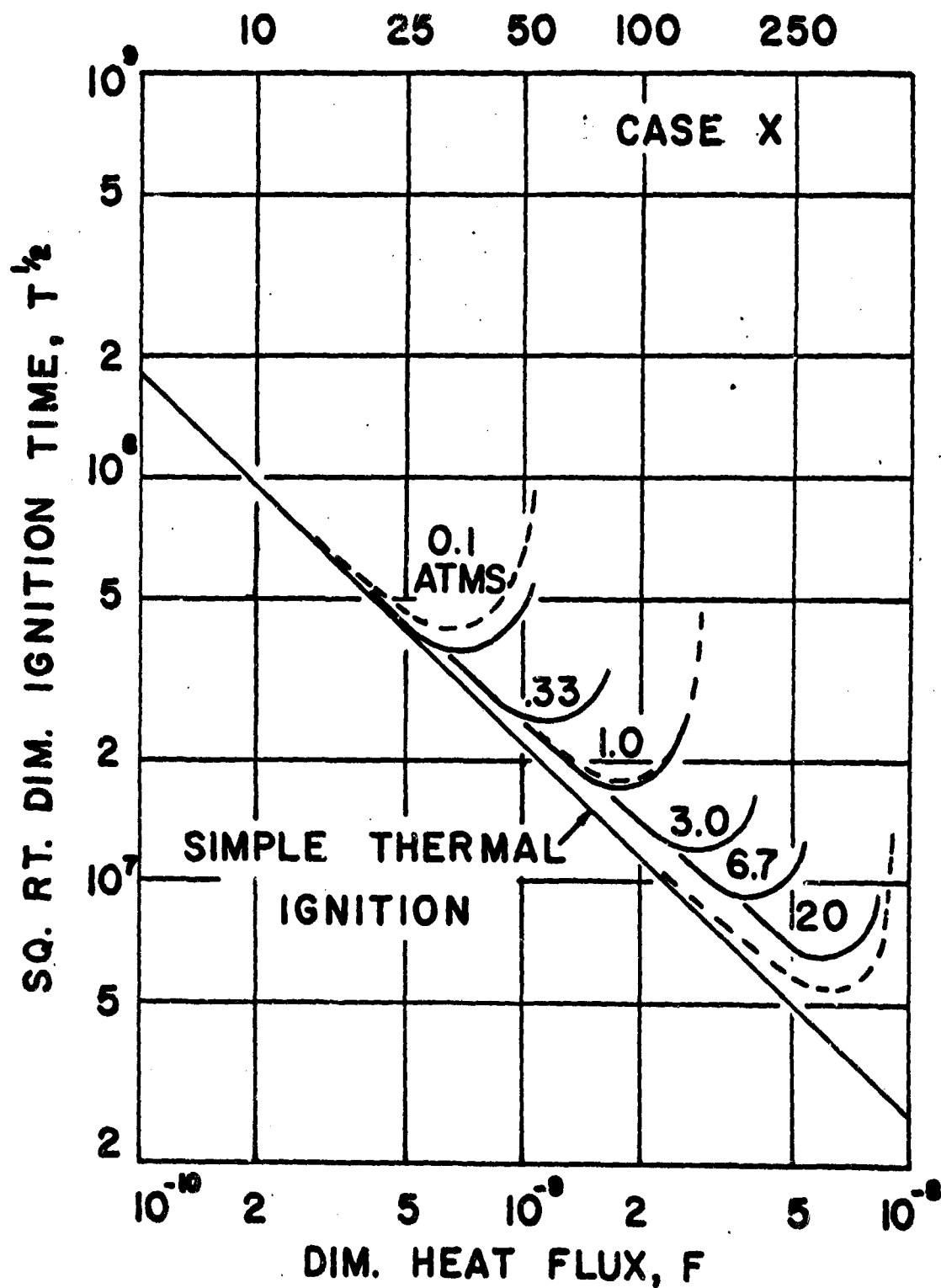
Figure 6. Calculated ignition response for the Case VI parameters. The dashed line is for Case III response at 1 atms. The dimensionless steady-state regression rate at 1 atms is 1.8 × 10⁻⁸ for Case VI and 2.37 × 10⁻⁸ for Case III.

Figure 7. Calculated ignition response for the Case VIII parameters. The dashed line is for Case III response at 1 atms. The dimensionless net heat of gasification is 0.125 for Case VIII and .05 for Case III.

Figure 8. Calculated ignition response for the Case X parameters. The dashed lines are for Case III response at 0.1, 1.0 and 20.0 atms. The equilibrium heat of vaporization per g-mole of gas is 20 kcal. for Case X and 28 kcal. for Case III.
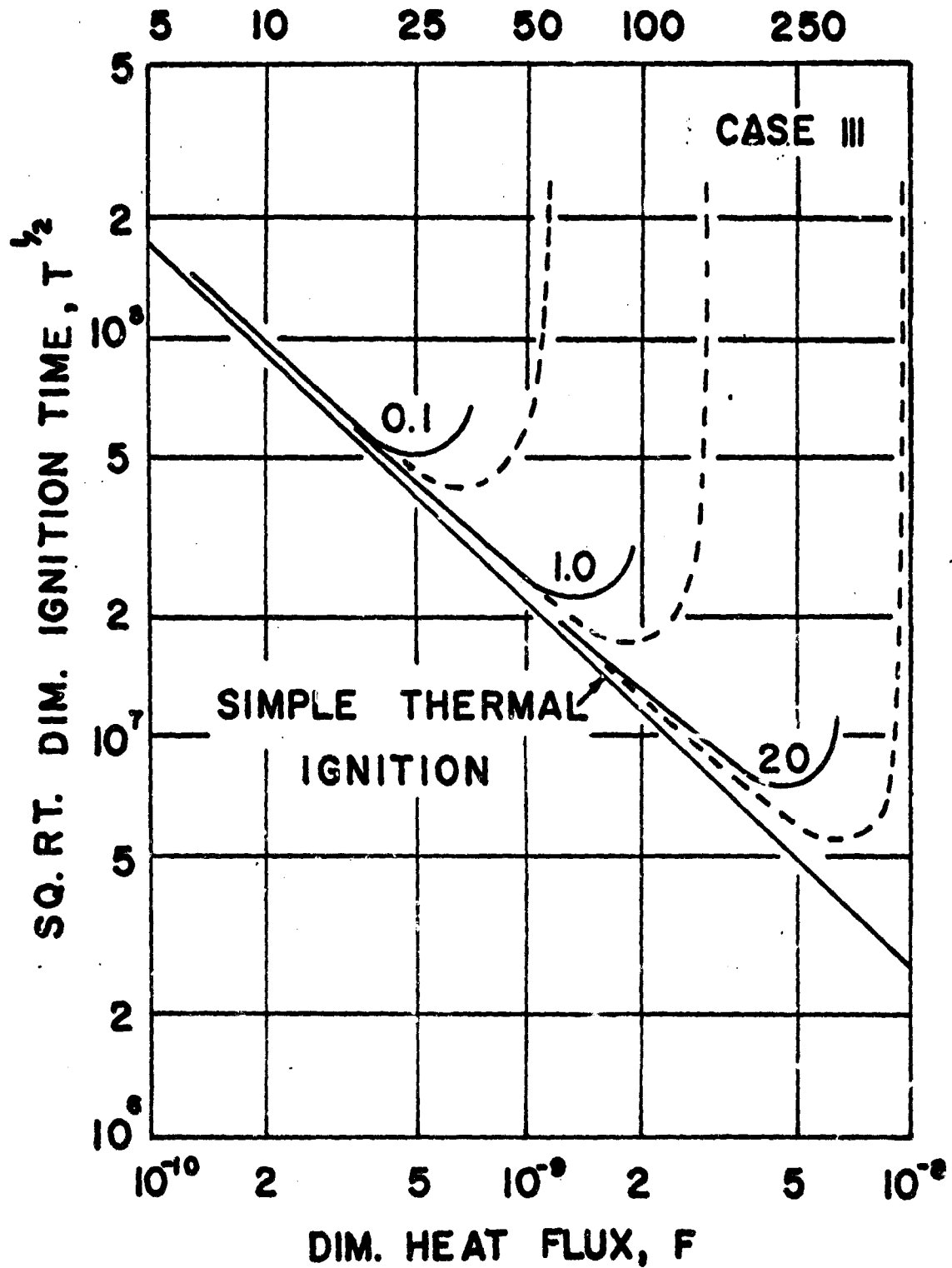
Figure 9. Modified, calculated ignition response for Case III parameters. The dashed lines correspond to assuming ignition when the heat flux in the solid just equals the steady-state feedback flux; the solid lines are for assumed ignition when this feedback flux is 20 percent greater than the heat flux at the solid surface.
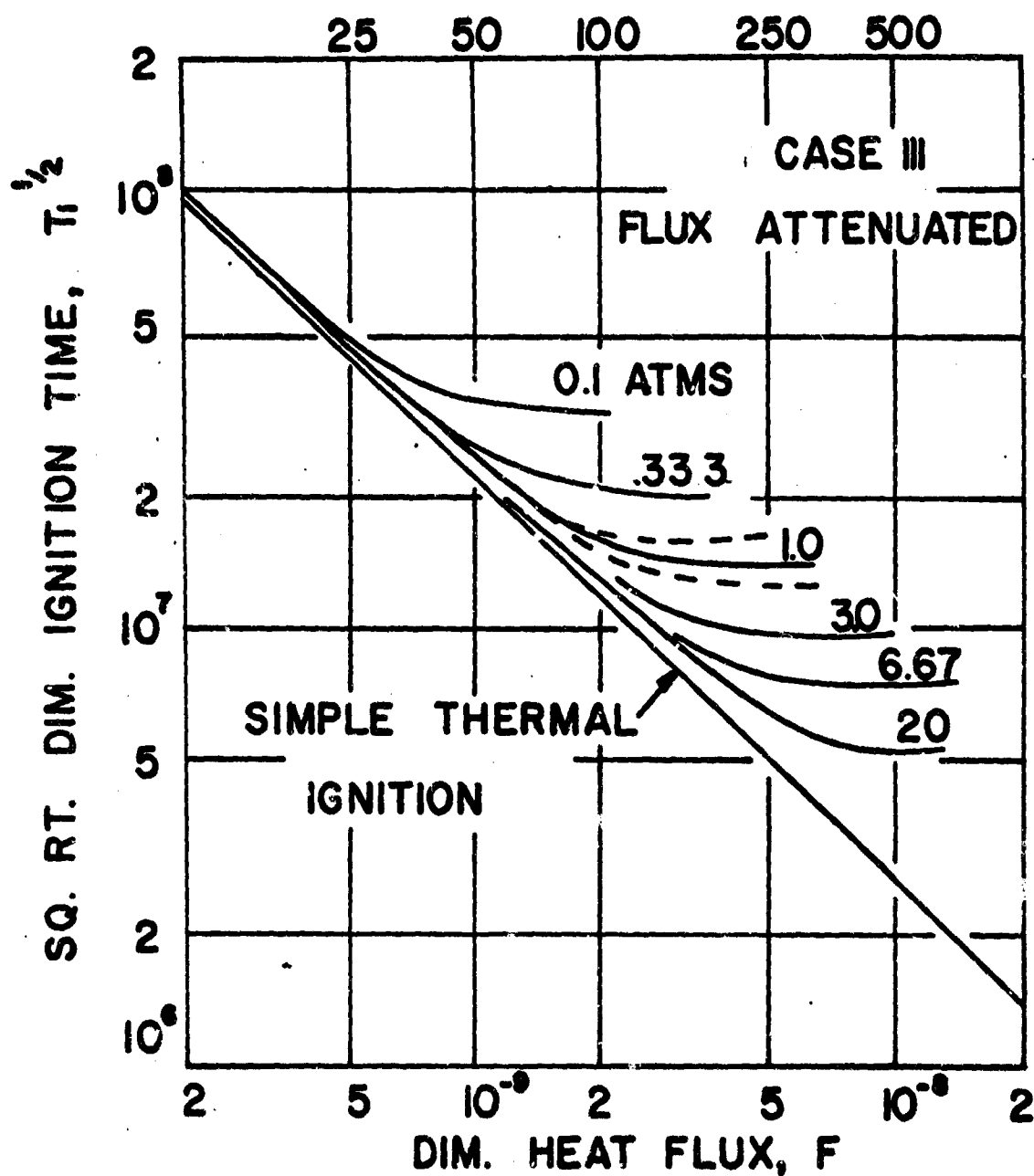
Figure 10. Calculated ignition response for igniter flux attenuation.
The Case III parameters were employed and the total heat flux impinging
on the solid surface is assumed to be attenuated by evolved material.
The solid lines are for 1/e th attenuation after 10 microns of regres-
sion. The dashed lines above and below the 1 atms line and respectively
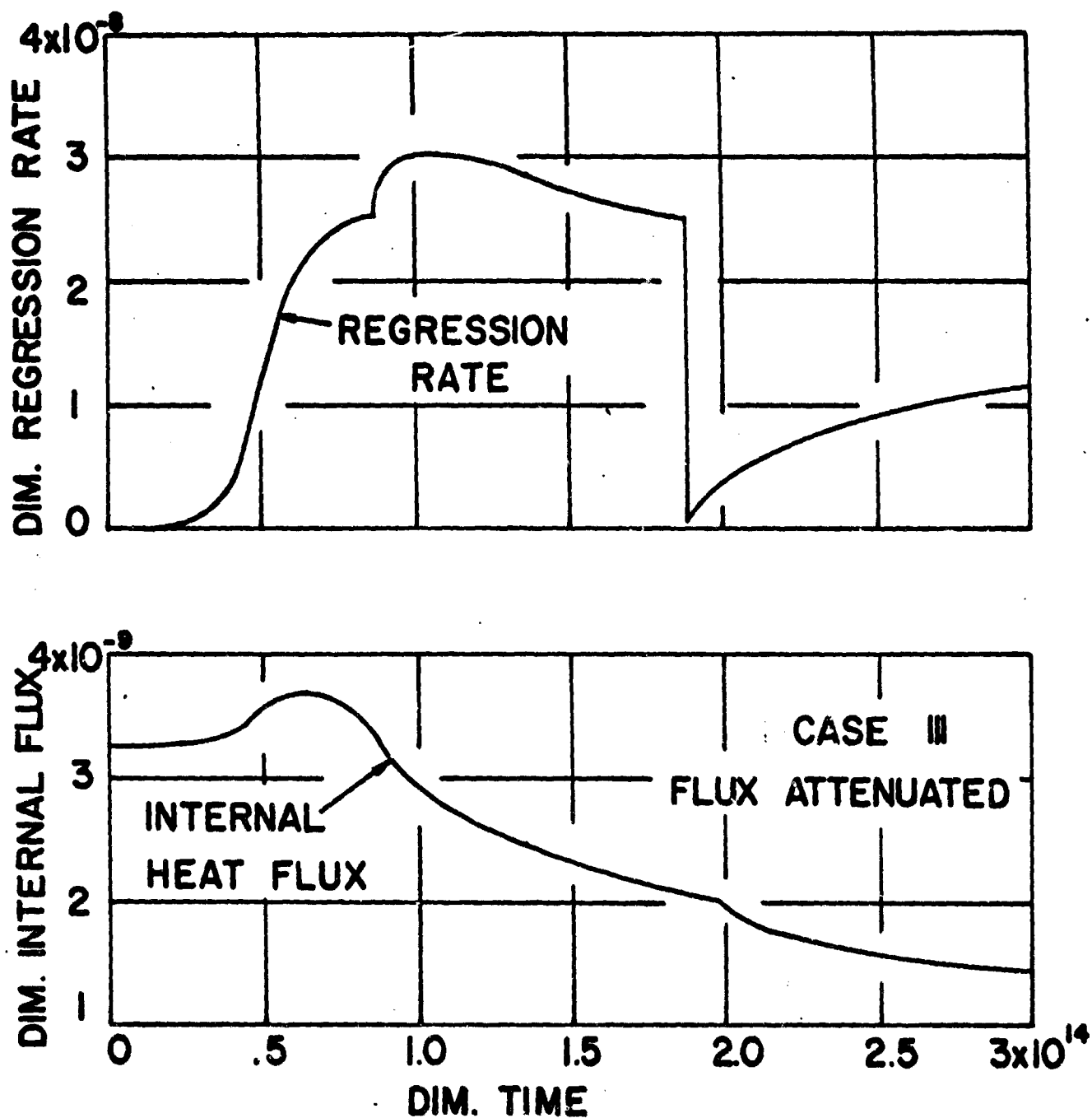for the same attenuation after 25 and 5 microns of regression.

Figure 11. Important variables as a function of time for the igniter flux attenuation corresponding to the solid lines in Fig. 10.
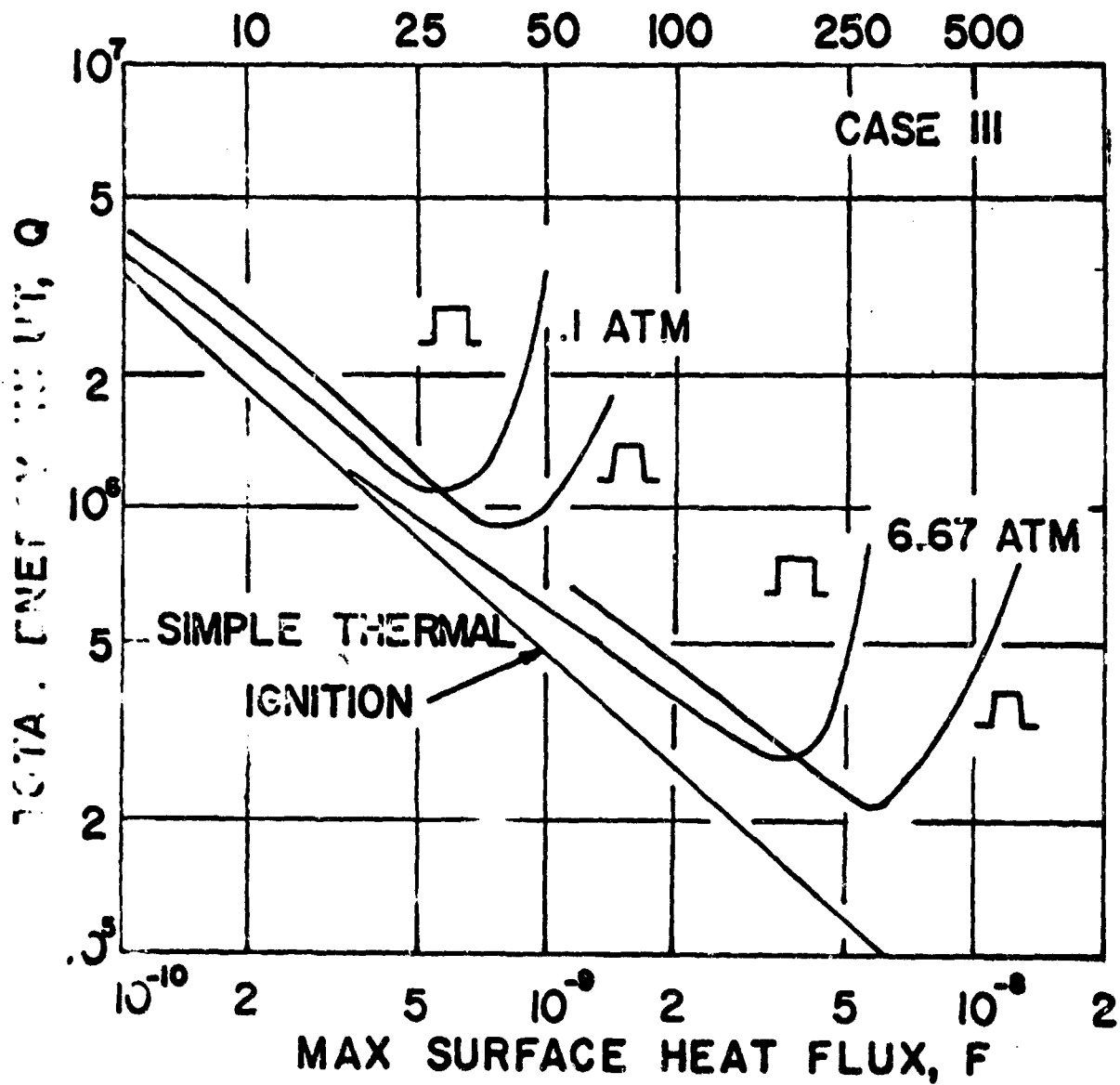
Figure 12. Total dimensionless ignition energy per unit area as a function of the maximum dimensionless igniter flux. Case III parameters are used. The comparison is of a sharply initiated and terminated igniter flux (denoted by the rectangular form) to an igniter flux which rises linearly during the first 1/5 of the time, is maximum during the next 3/5 of the time, and decreases linearly during the last 1/5 of the time (indicated by the trapezoidal form).
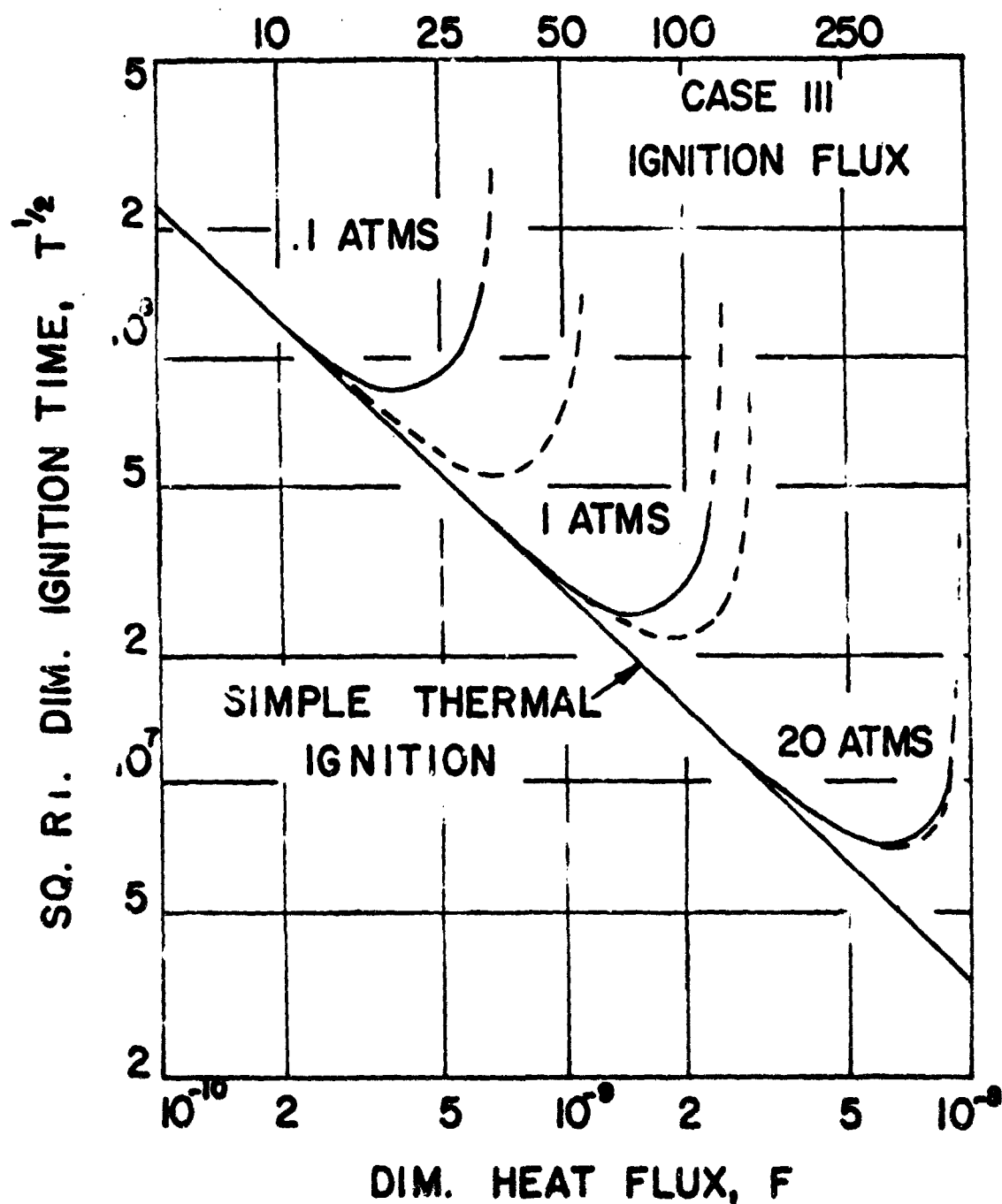
Figure 13. Calculated ignition response for the Case III parameters and the ignition feedback flux. For steady state regression condition, this feedback flux F_r is assumed to be given by Eq. (2).
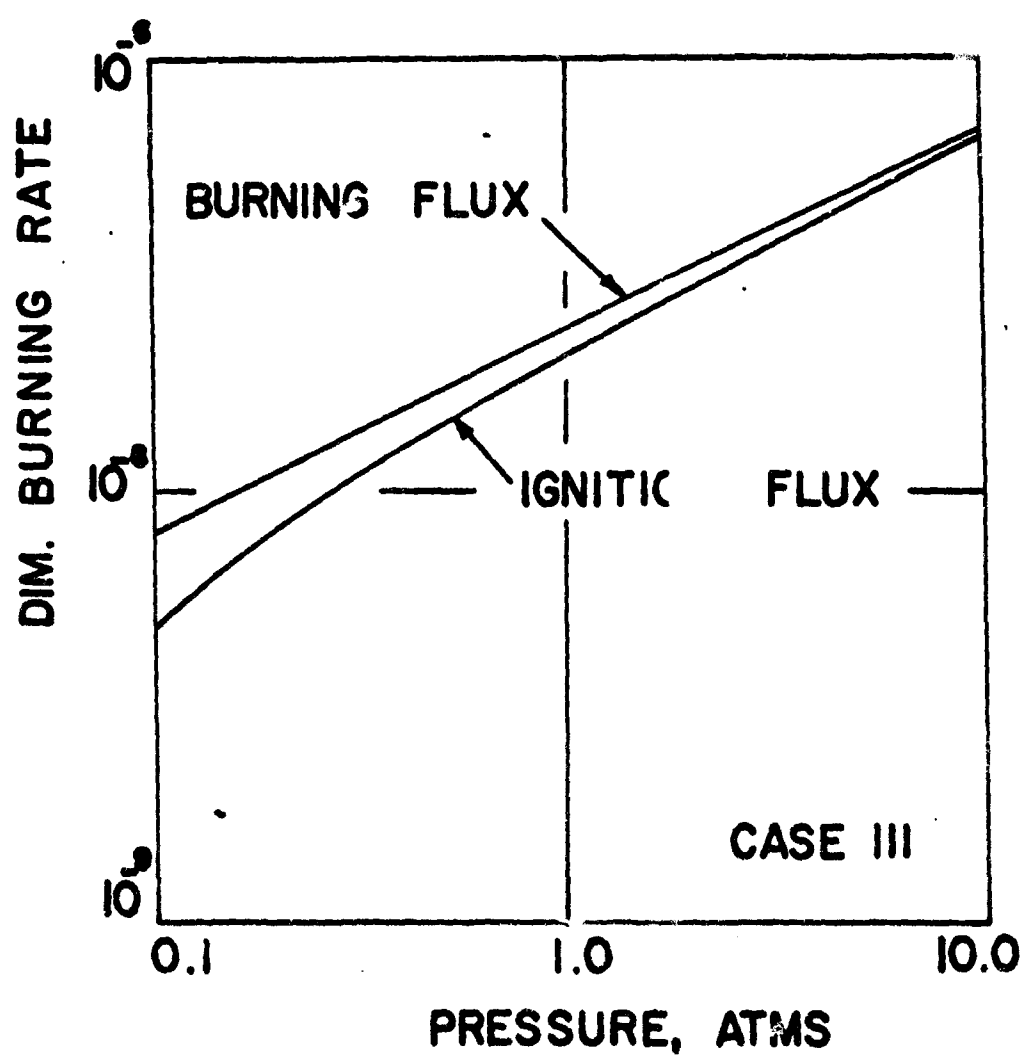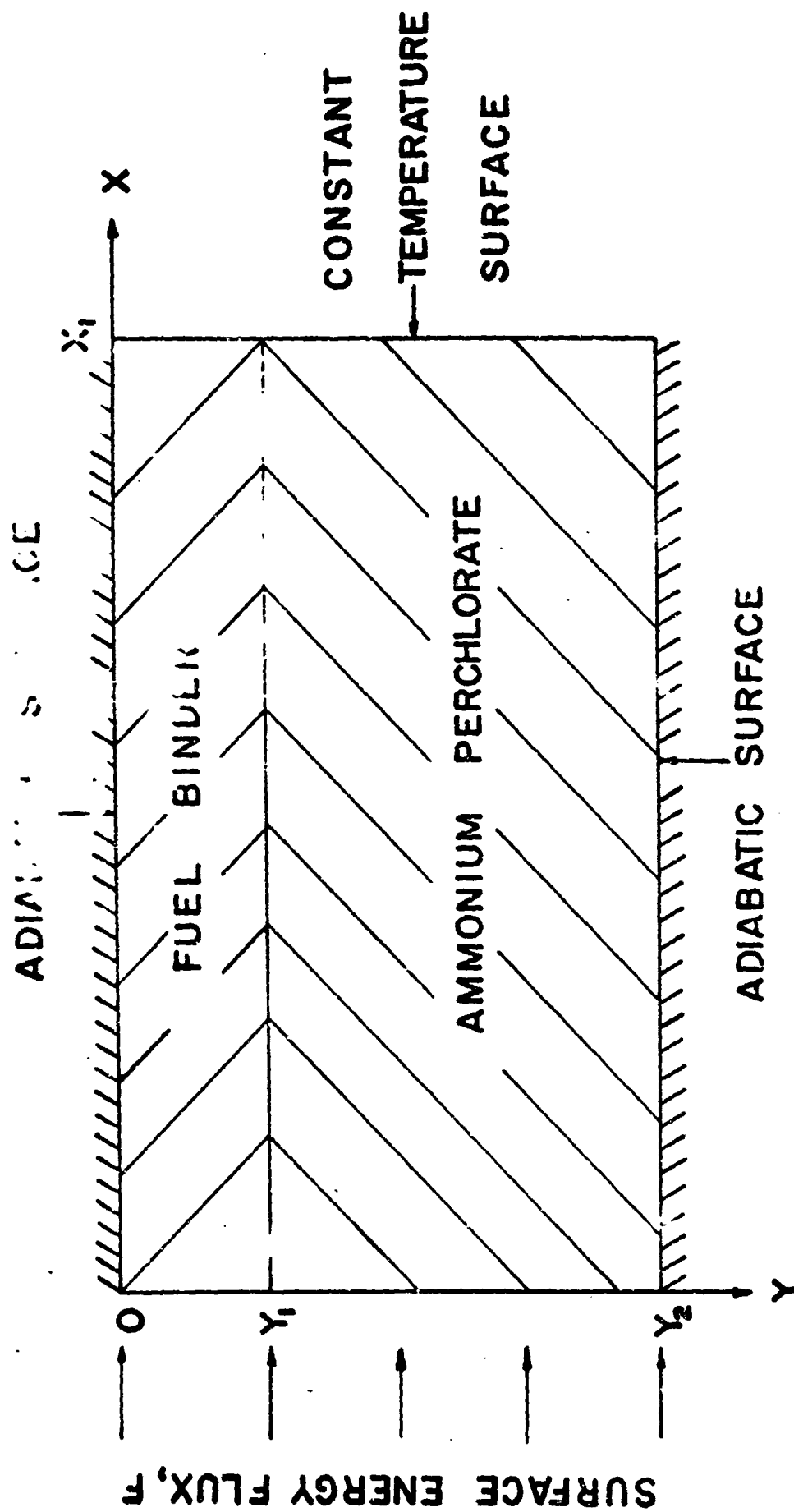
Figure 14. Steady-state dimensionless regression rates as a function of pressure for Case III parameters. The burning feedback flux is assumed equal to aP^n; the ignition feedback, F_r, flux is given by Eq. (2).

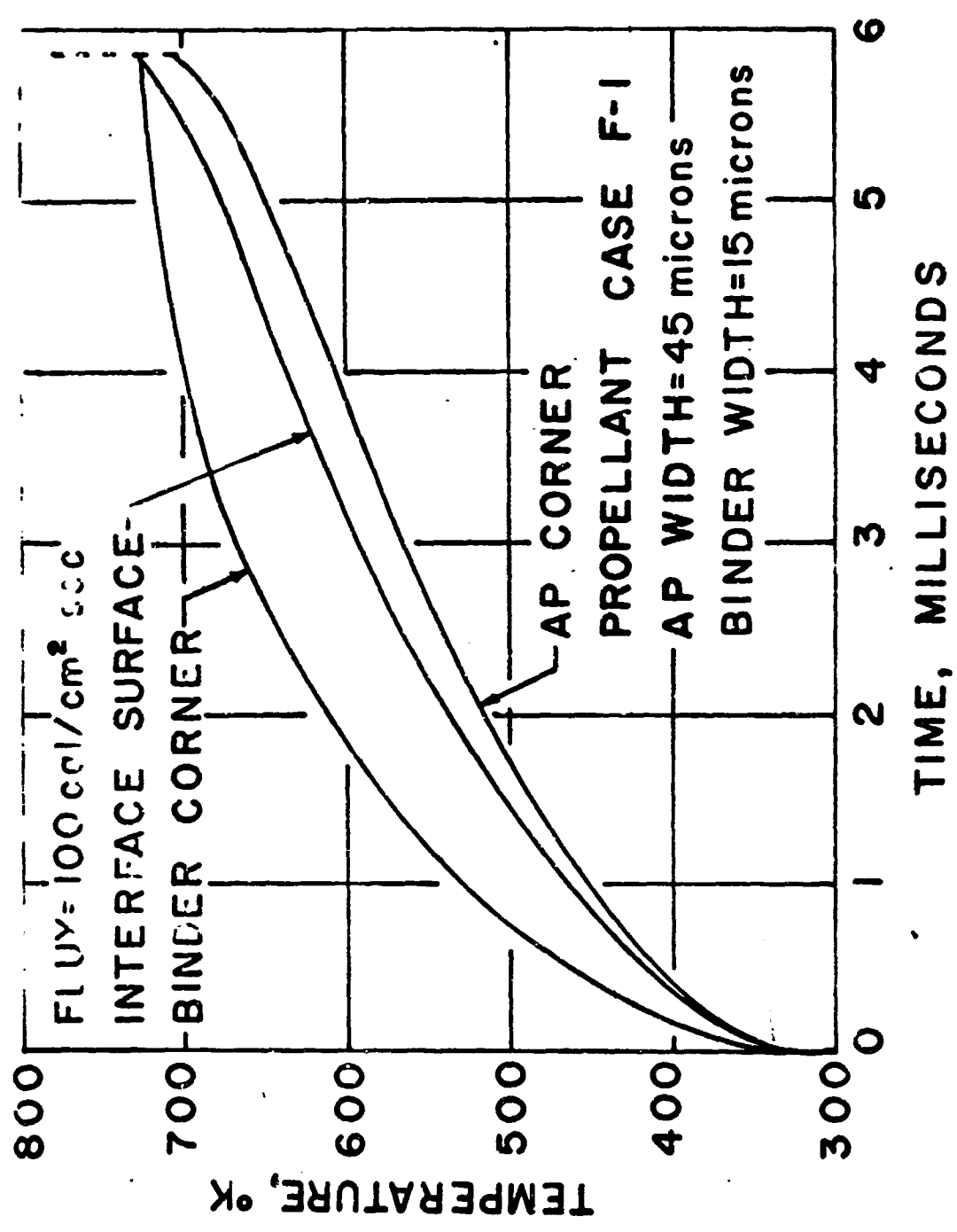Figure 15. The physical representation for the two lamina ignition model.

Figure 16. Calculated surface temperatures for the two lamina model employing the F-1 parameters.

Figure 17. Isotherms in the AP and PBAA laminas for linear heating. This condition is reached after 5.98 msec of exposure to a surface heat flux of 100 cal/(sec)(cm^2). Essentially identical results are obtained by use of the F-1 parameters.
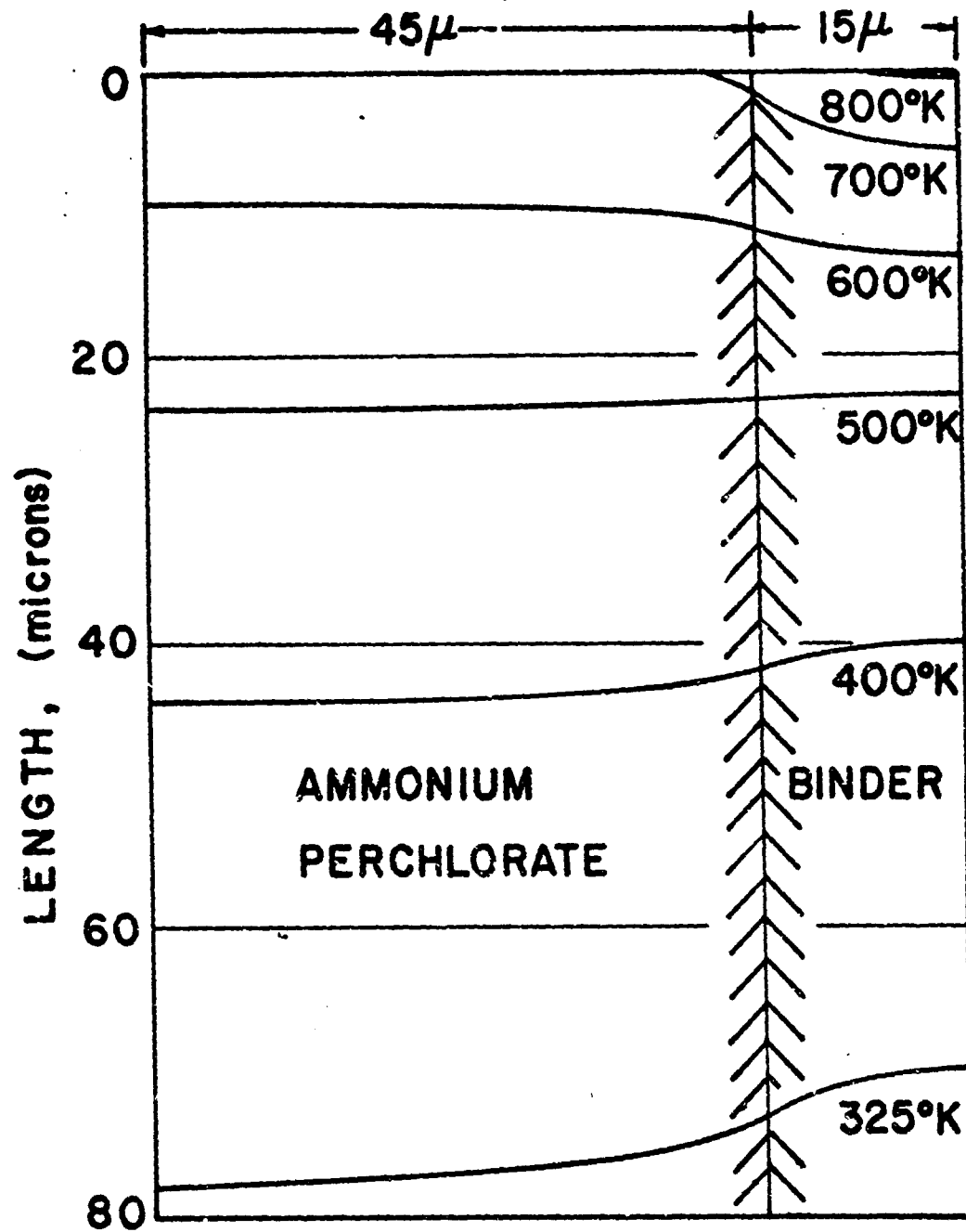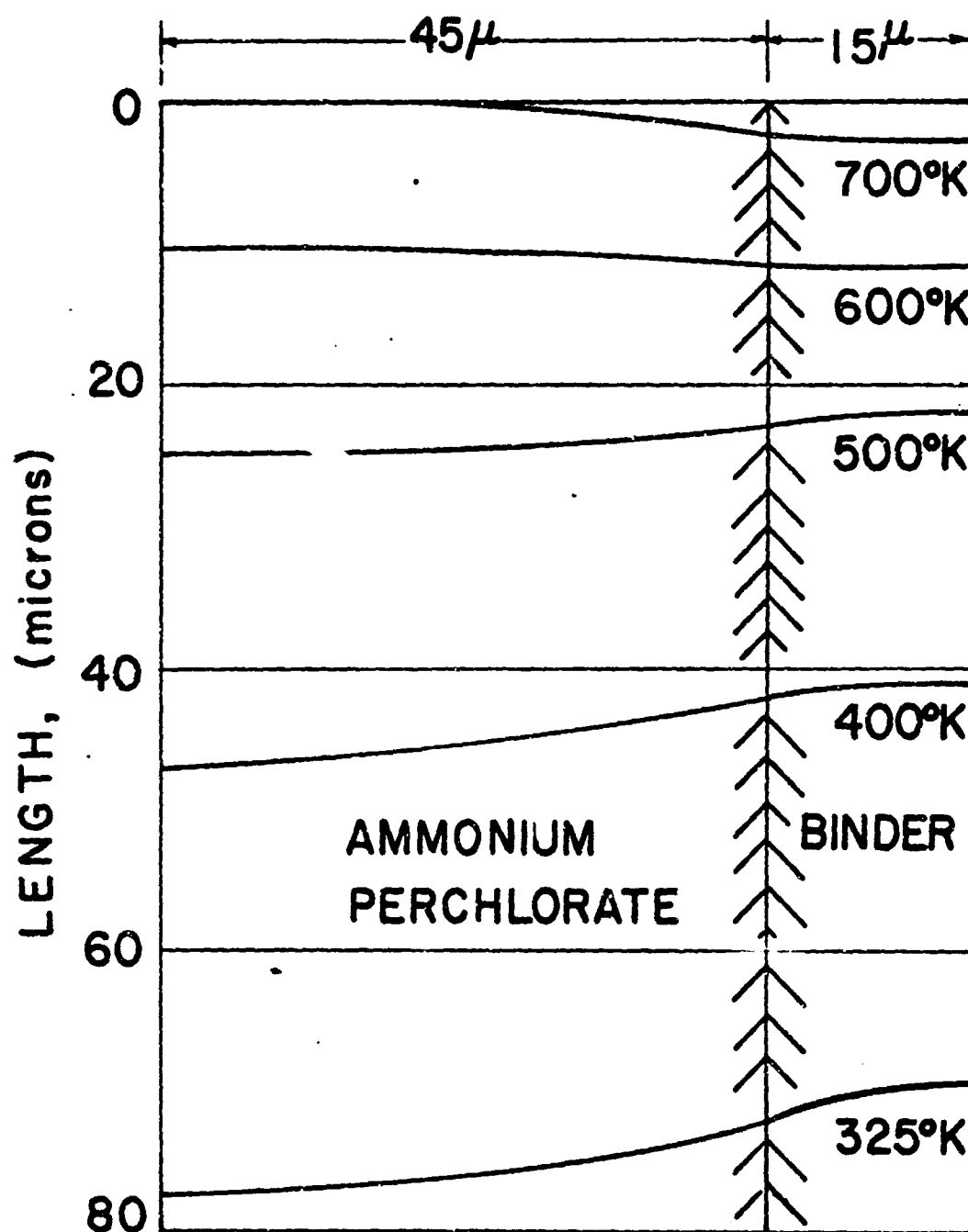
Figure 18. Isotherms in the AP and PBAA laminas for the F-4 parameters. This condition is reached after 5.98 msec of exposure to a surface heat flux of 100 cal/(sec)(cm^2). Essentially identical results are obtained by use of the F-1 parameters.
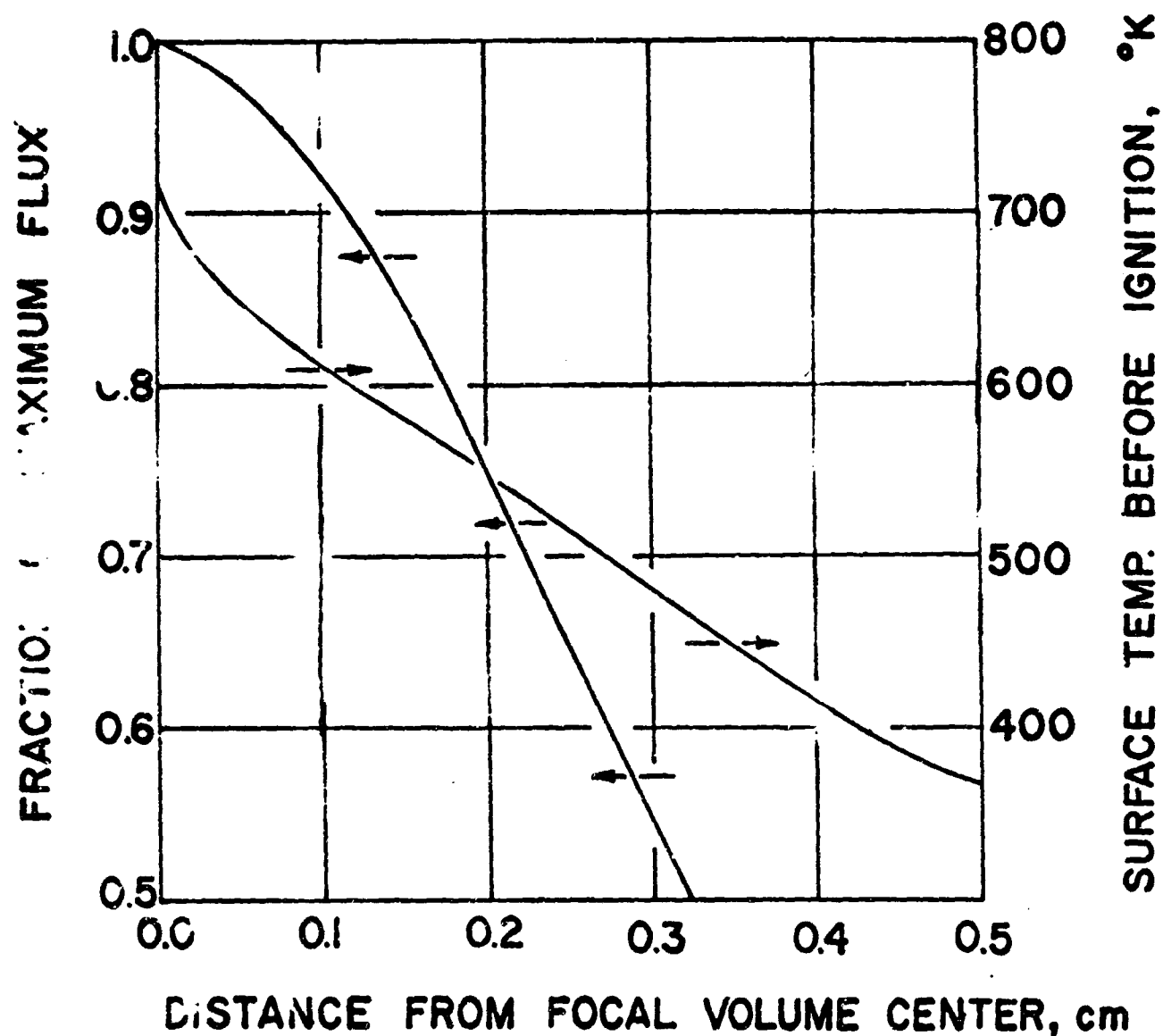
Figure 19. Spatial surface heat flux distribution and calculated surface temperature just before ignition for a non-uniform igniter flux at the surface of a homogeneous propellant.
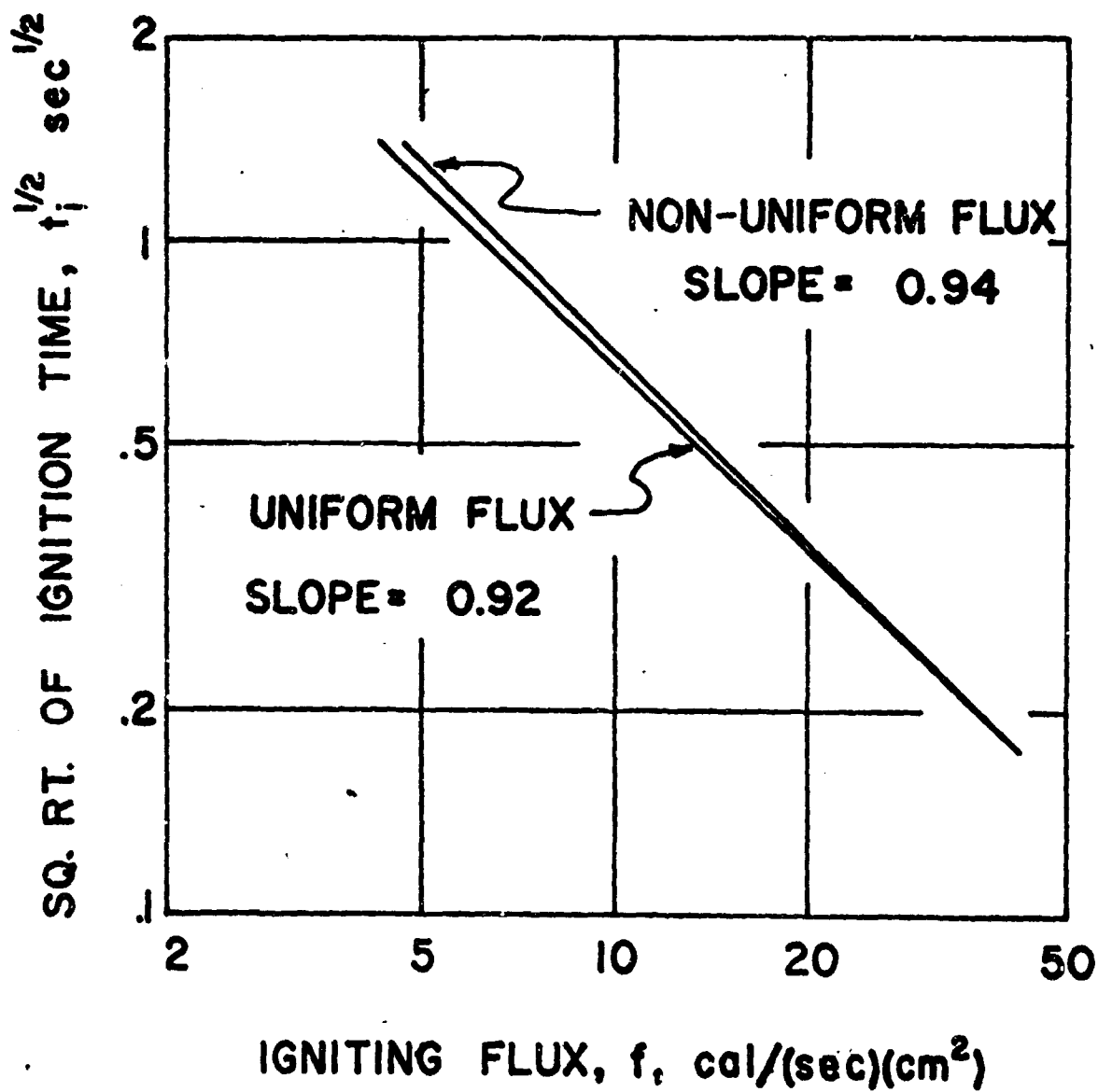
Figure 20. A comparison of calculated ignition response for uniformly distributed surface heat flux and the non-uniform distributions illustrated in Fig. 19.
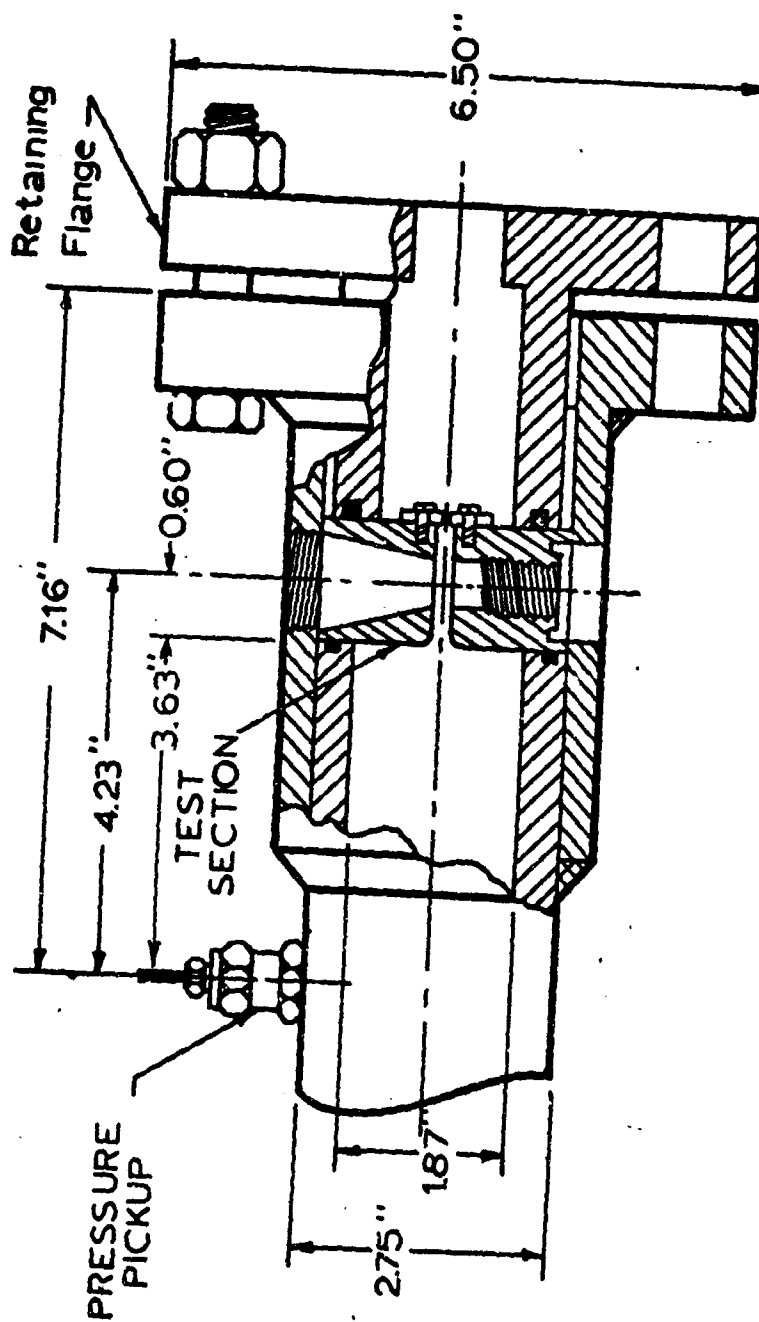
Figure 21. A cross section of the driven end of the shock tube, showing the test section. Hot, high pressure gases generated by reflection of the shock wave at the test section. the rectangular channel, flow past the sample surface (mounted in the bottom of the channel) and pass through a flow control orifice to the atmosphere. A photocell views the sample surface through the conical window to detect ignition.
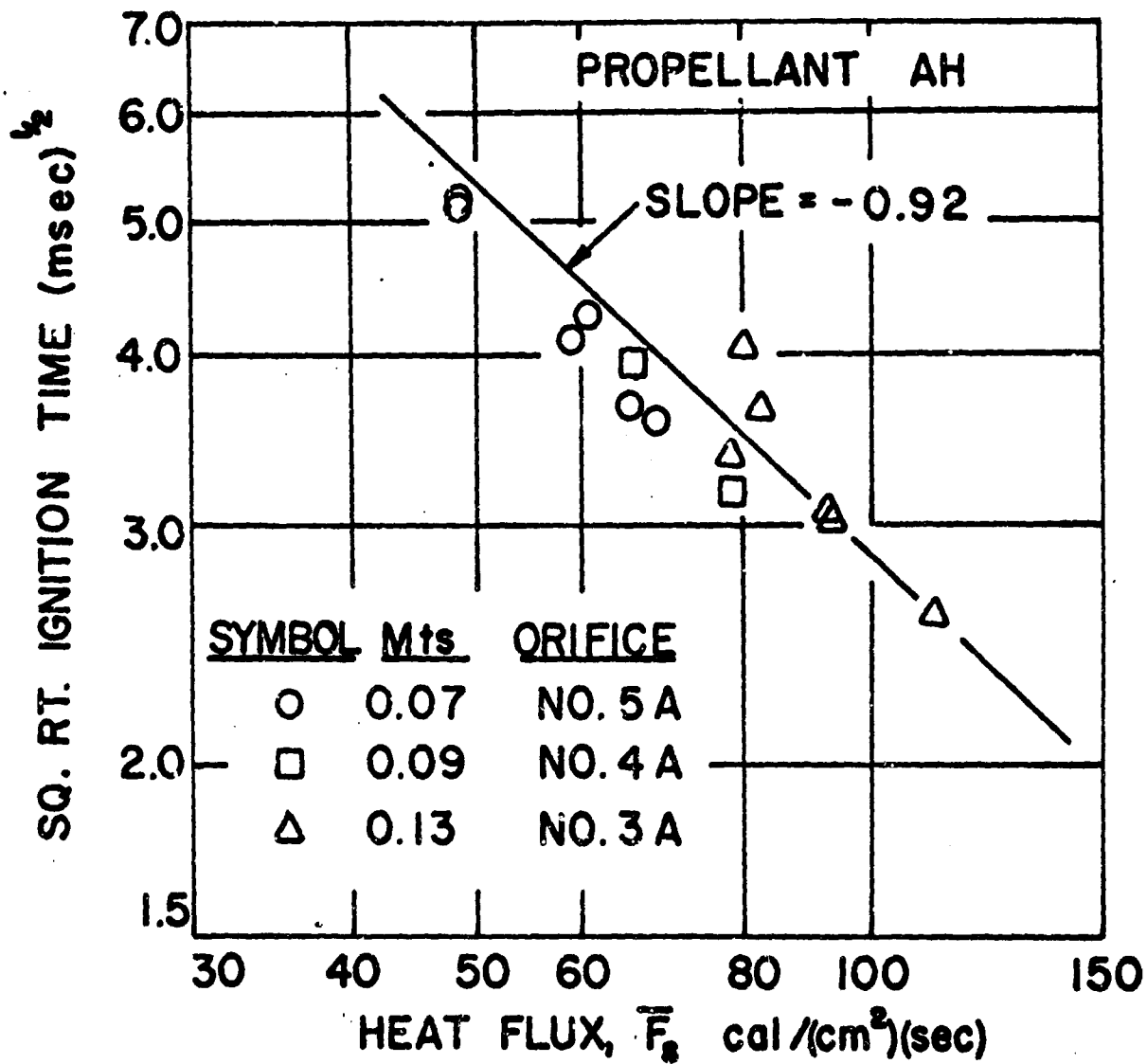
Figure 22. Experimental ignition data for the AH propellant. The gas flow Mach number at the sample surface is denoted as M_{st}.
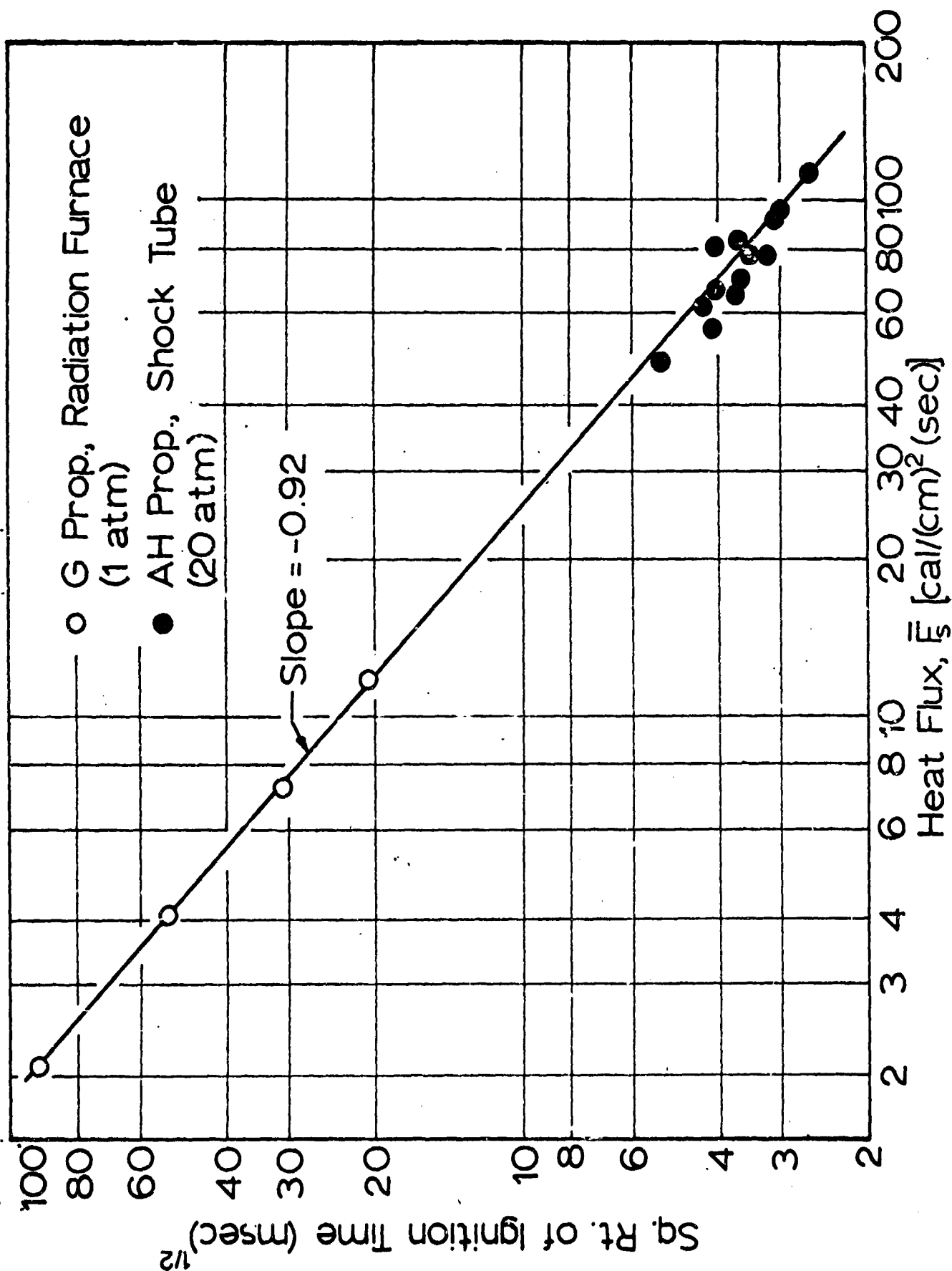
Figure 23   Experimental ignition data for a wide range of surface heat fluxes for uncatalyzed AP-PBAA
propellants   The radiation furnace data are from Ref [5].
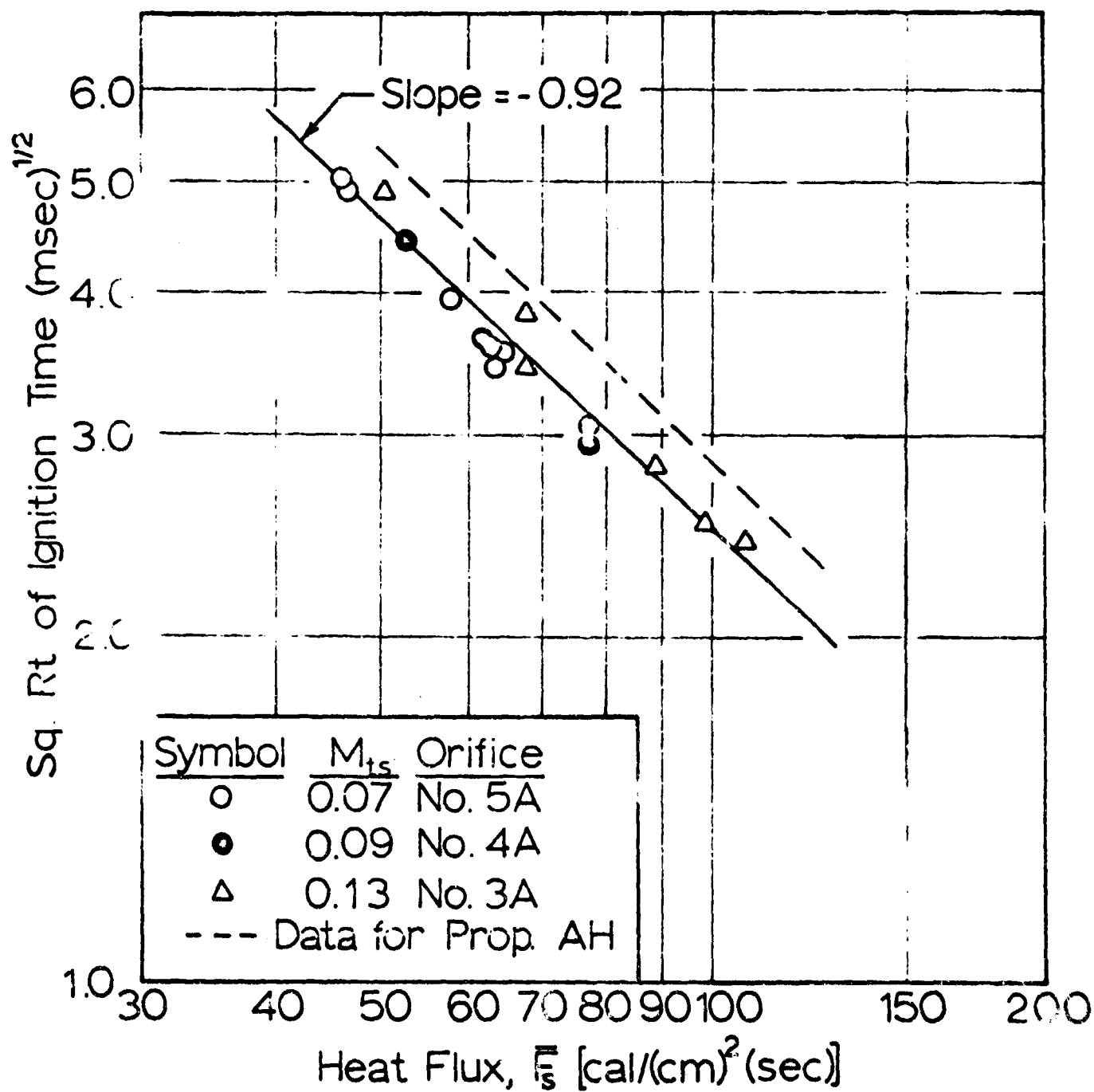
Figure 24. Experimental ignition data for the UA propellant. Here the catalyzed UA propellant is compared to the uncatalyzed AH propellant.
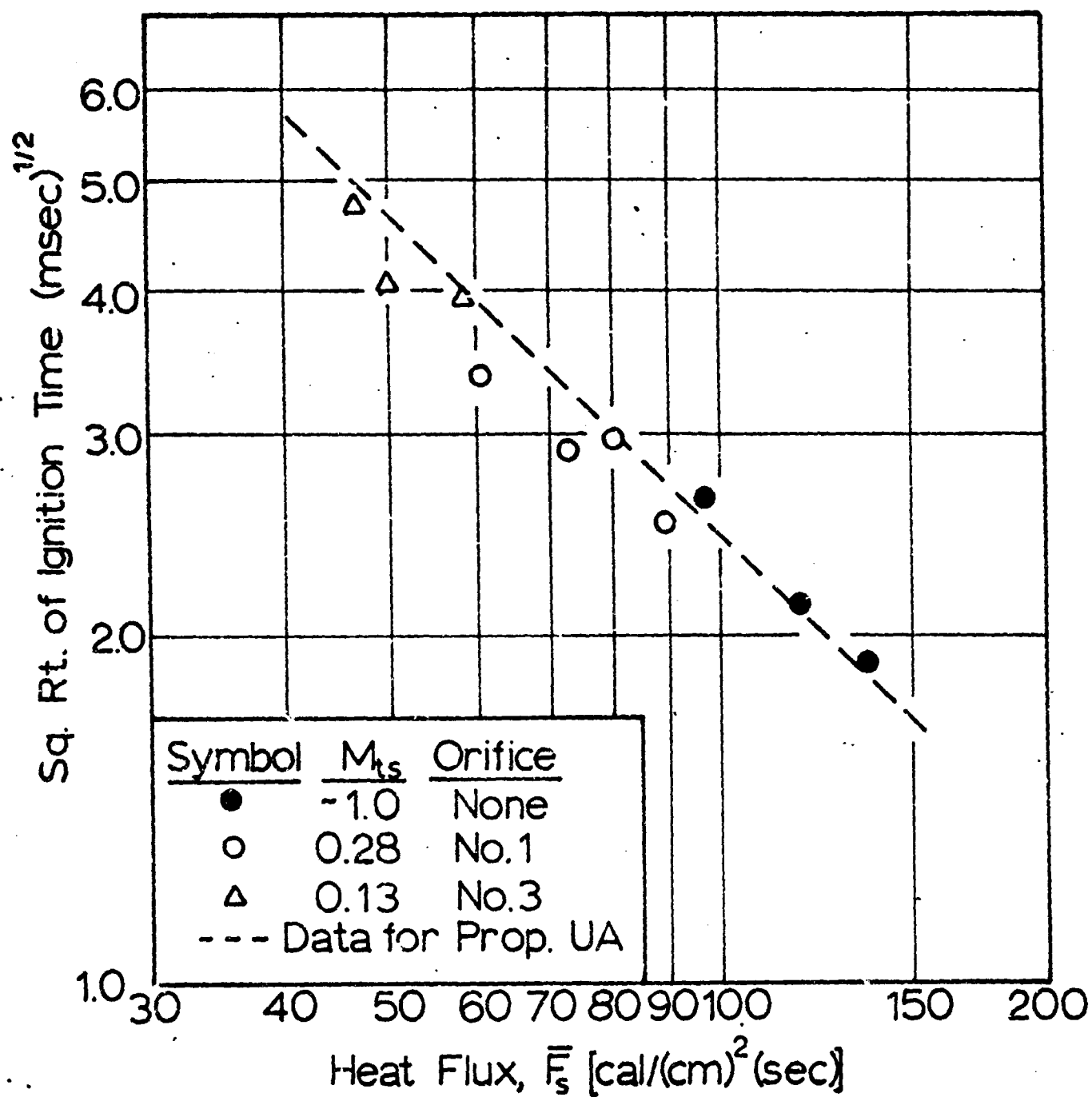
Figure 25. Experimental ignition data for the AJ propellant. Here the fine ammonium perchlorate UA propellant is compared with the AJ propellant, which contains some 200 micron AP. The gas flow Mach number at the sample surface, M_{st}, is higher for the AJ data.
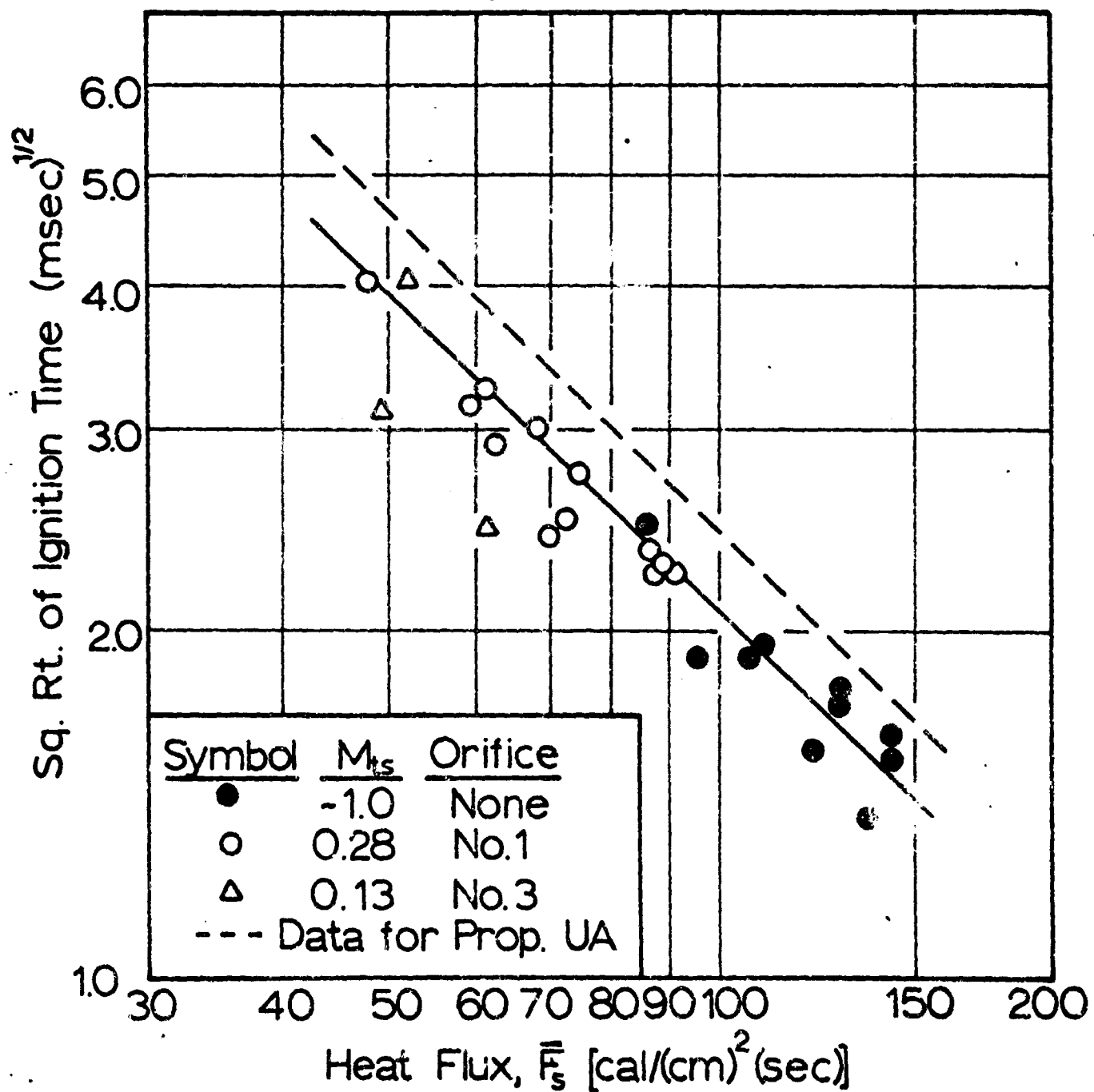
Figure 26. Experimental ignition data for the AL propellant. Here the uncatalyzed AH propellant and copper chromite catalyzed UA propellant are compared to the AL propellant which contains an AP decomposition catalyst, cobalt oxide.
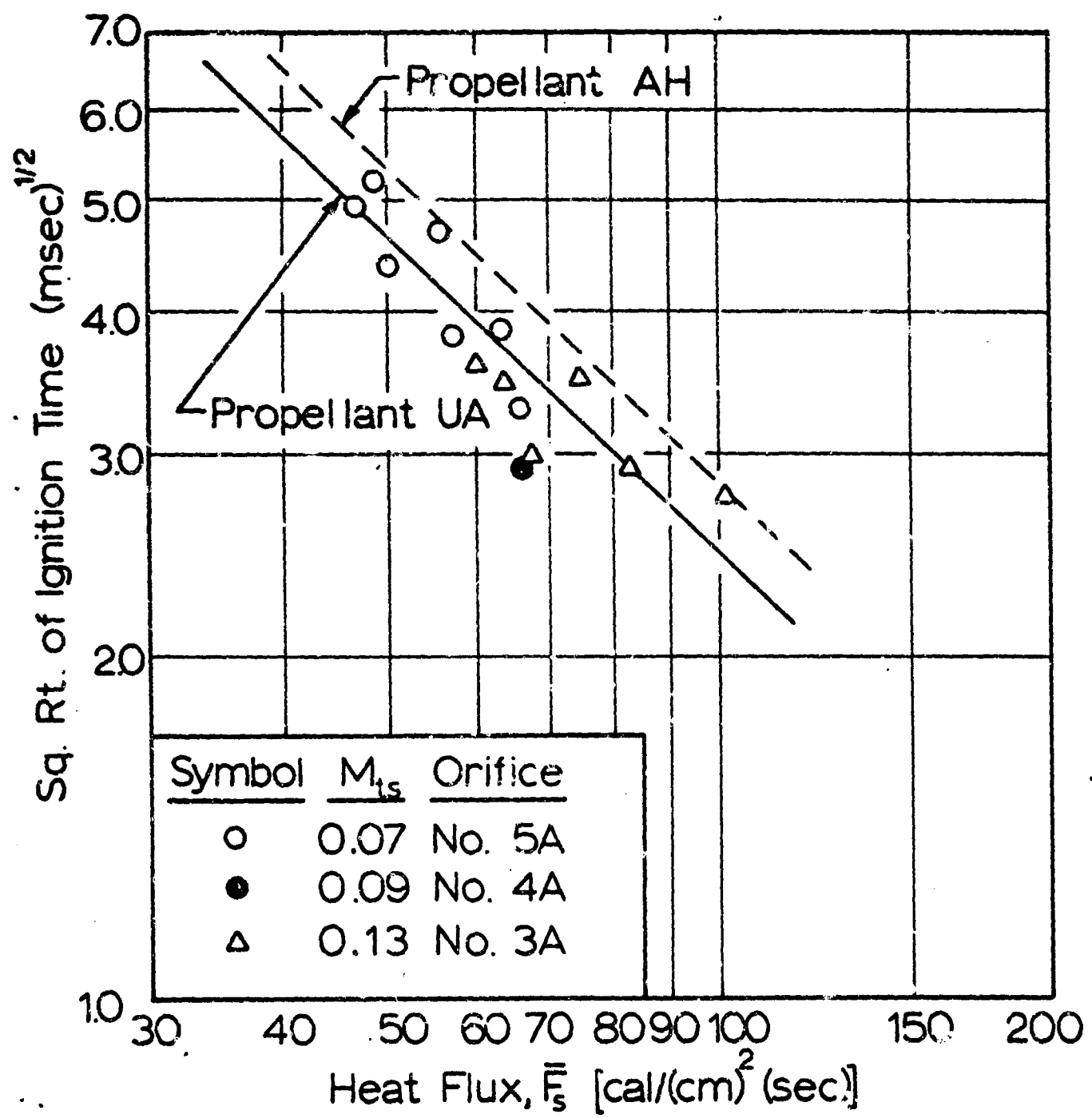
Figure 27. Experimental ignition data for the AK propellant. Here the copper chromite catalyzed UA propellant is compared to the n-buty ferrocene catalyzed AK propellant.
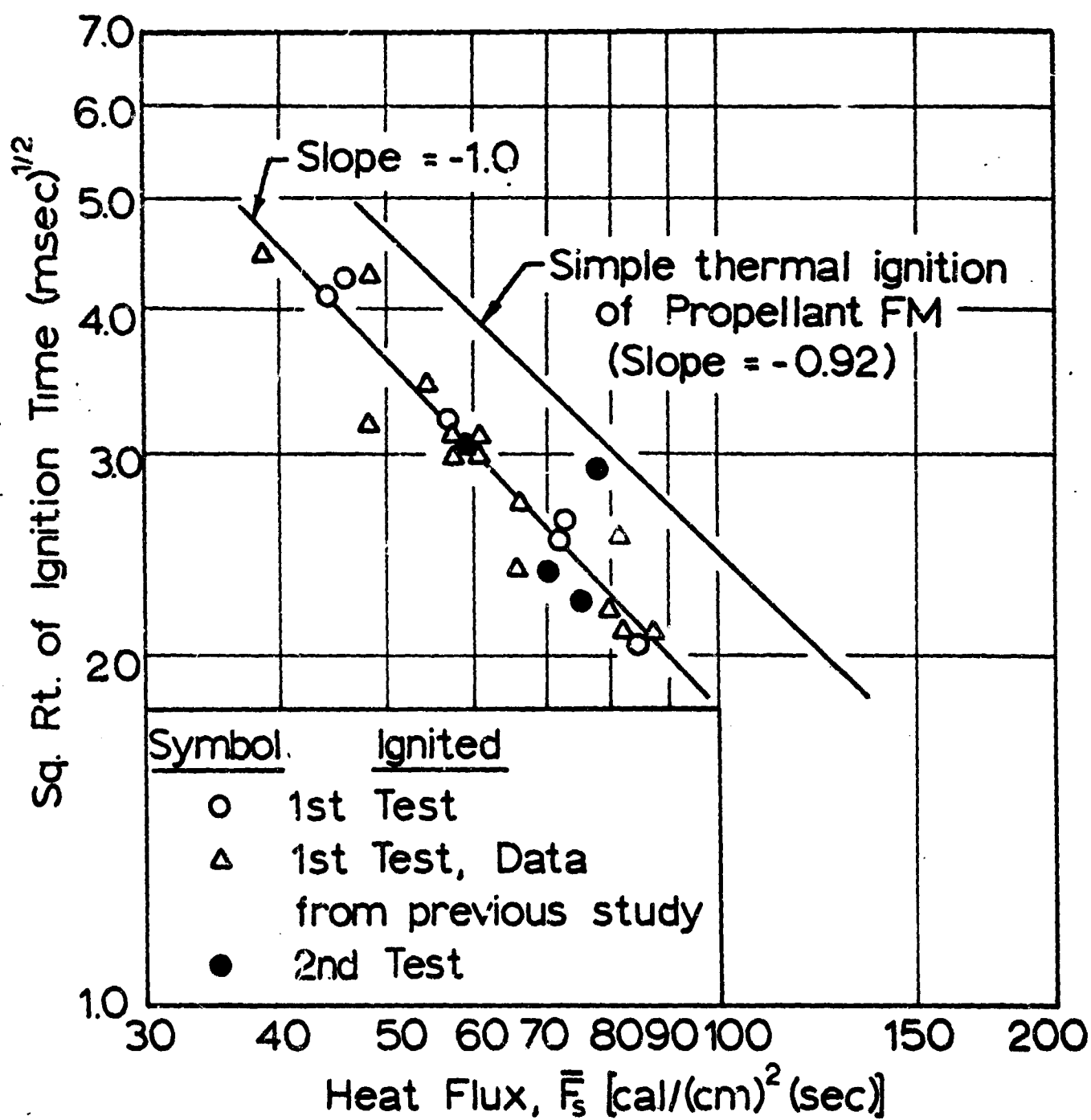
Figure 28. Experimental ignition data for the FM propellant. When cut, the surface of this propellant is not smooth. Points designated as second test were measured after first subjecting the samples to nearly ignition conditions in a prior test.
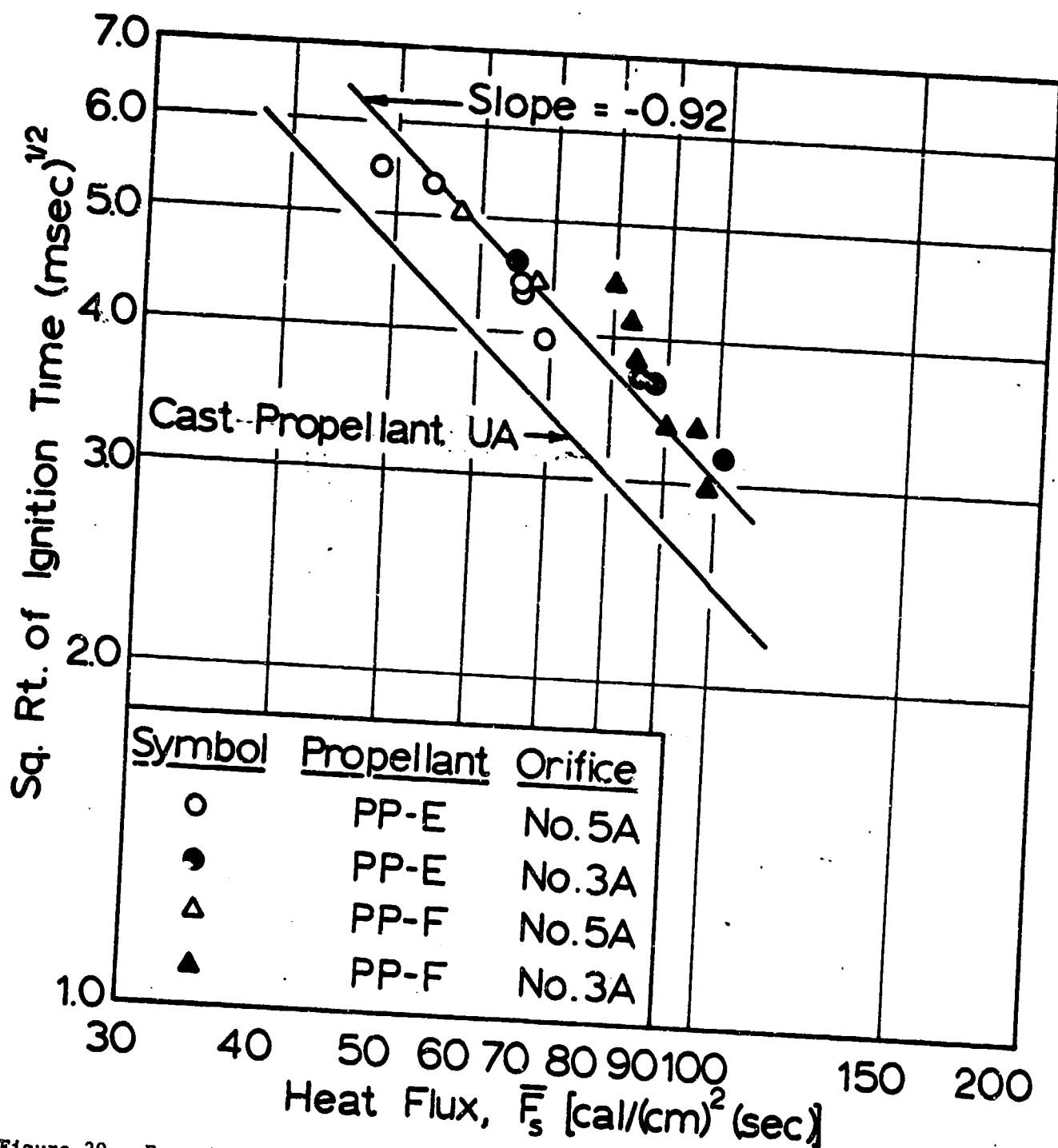
Figure 29. Experimental ignition data for two pressed materials. These samples were 95 percent AP with small amounts of carbon and catalyst added.
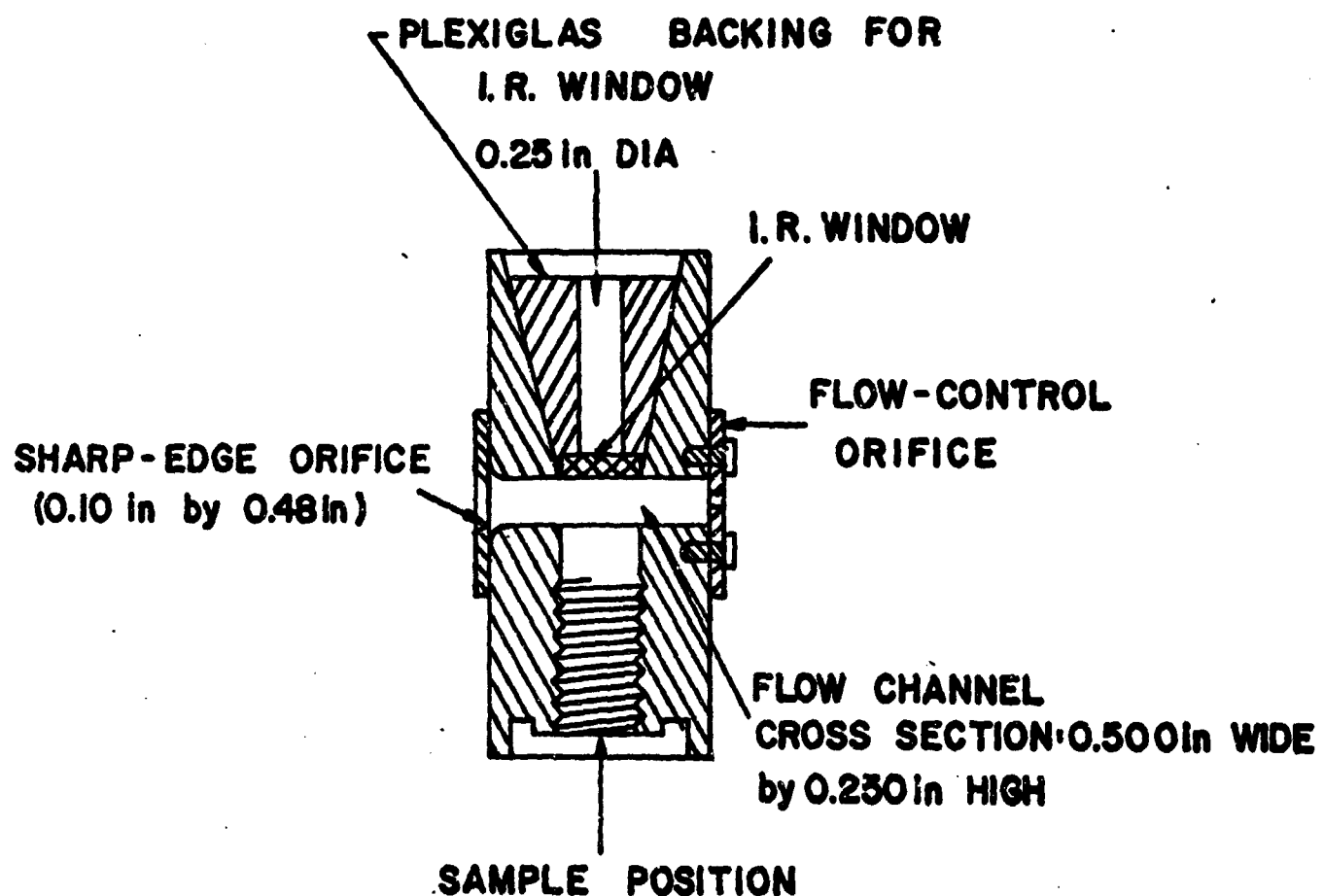
Figure 30. A cross section of the test section used for convective heating tests and surface temperature measurements. The sharp-edge orifice was used upstream of the sample to produce higher heat fluxes than were obtained with a bell-mouth entry.
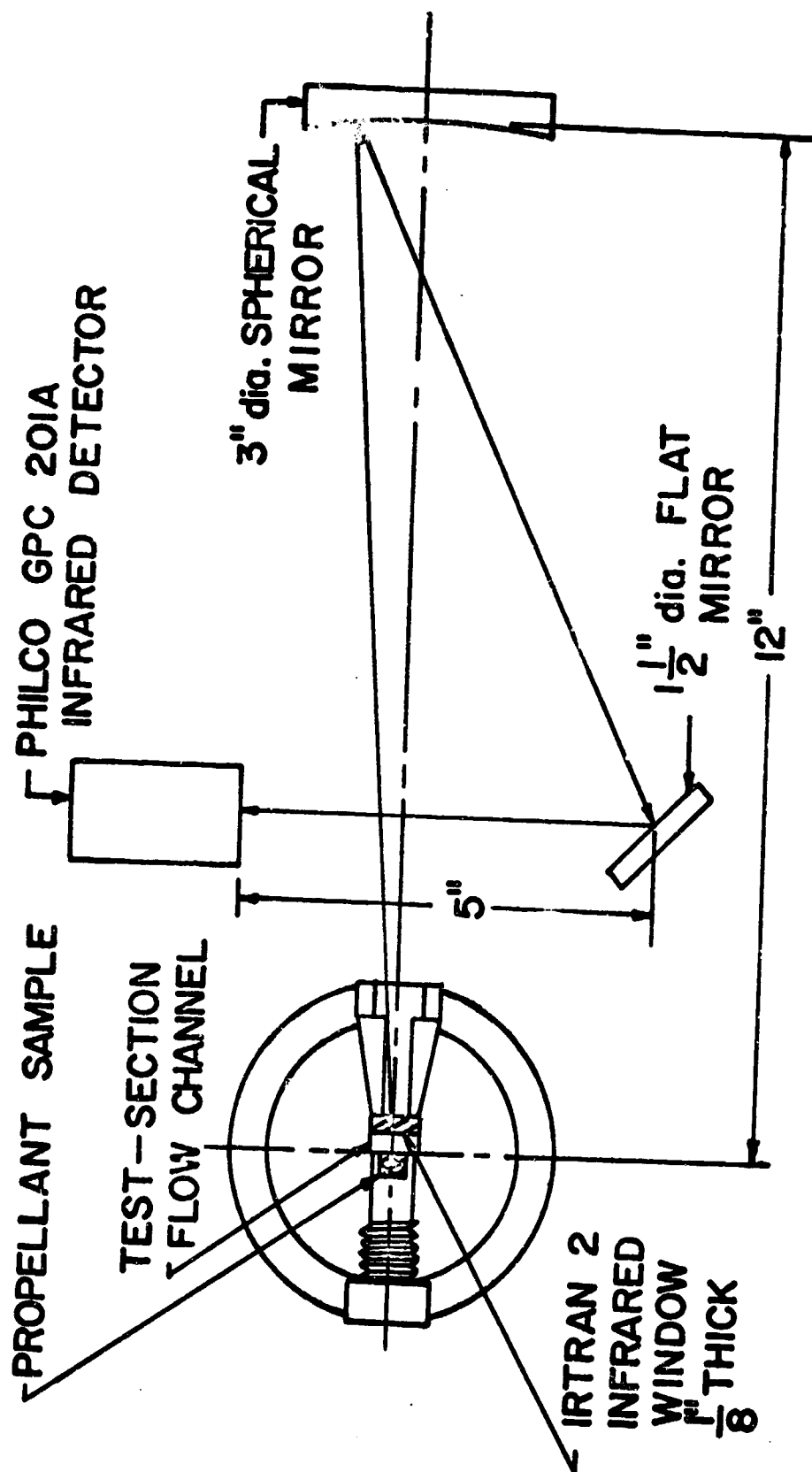
Figure 31. A schematic outline of the optical system employed when measuring propellant surface temperature. This view of the test section is at right angles to the view of Fig. 30.
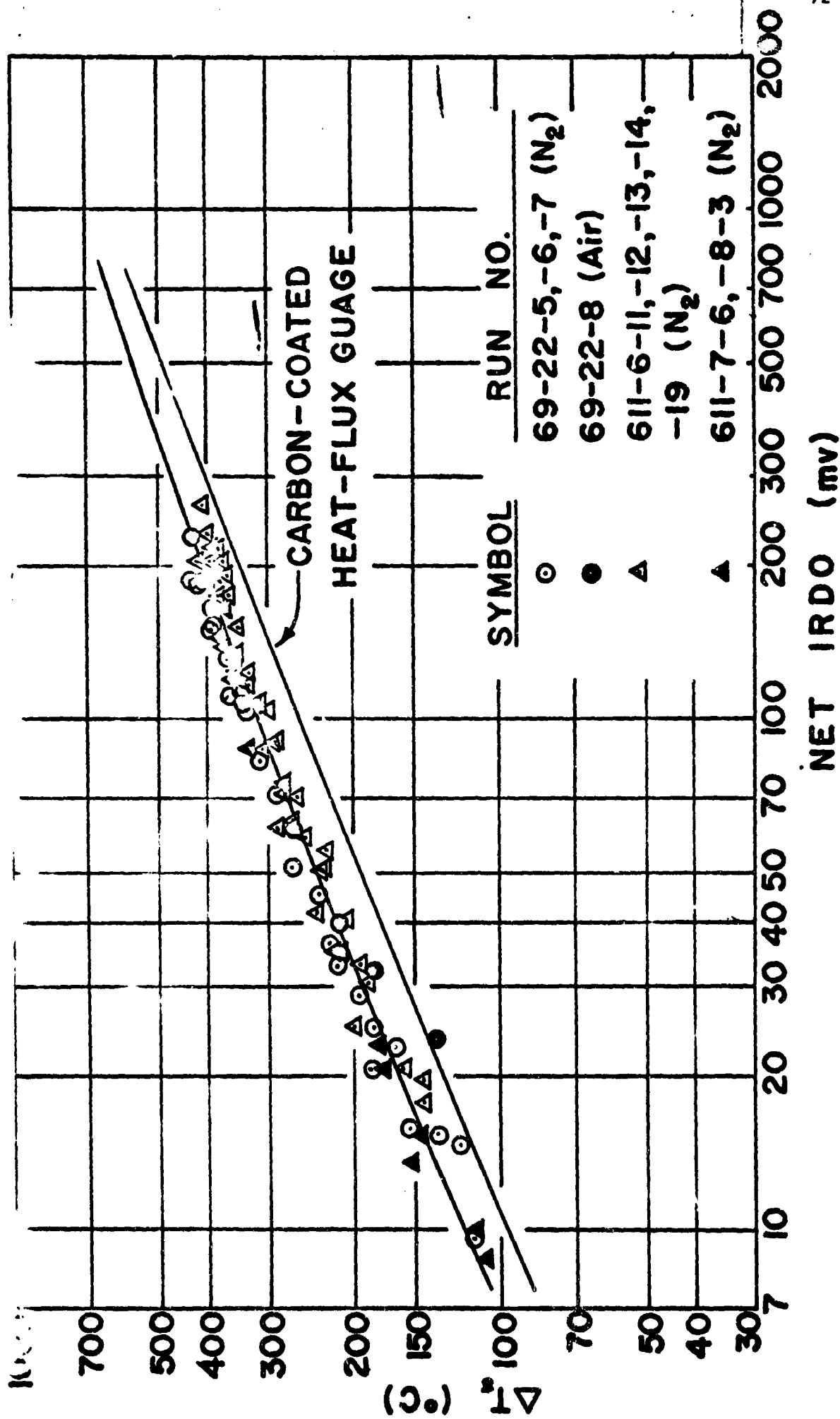
Figure 32. The infra-red detector output (IRDO) as a function of the calculate surface temperature of uncoated samples of AR propellant.

72
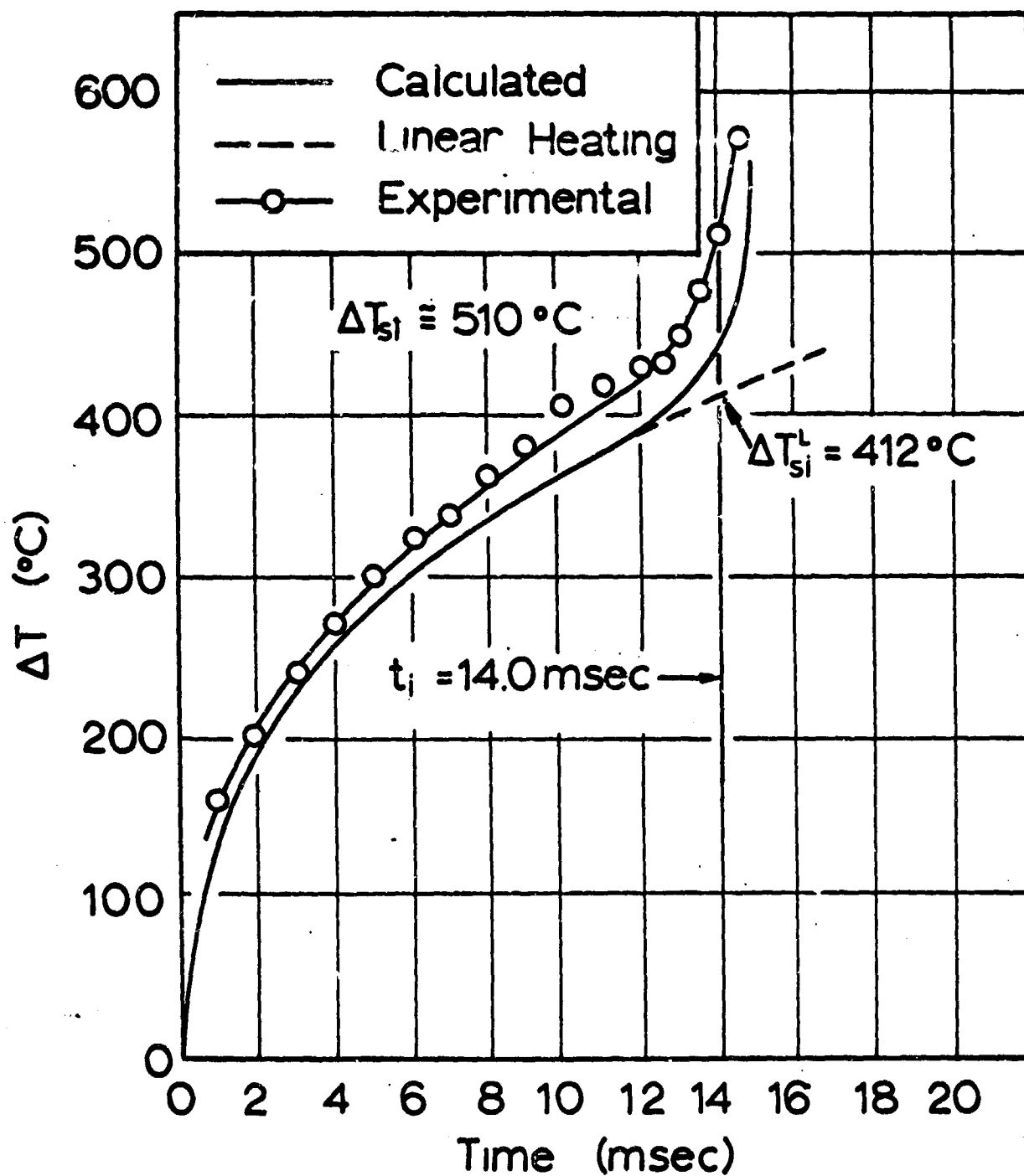
Figure 33. A comparison of the measured surface temperatures of uncoated AR propellant to surface temperatures calculated from a thermal ignition theory (5). Because of experimental variation in the heat transfer rates, exact agreement is not anticipated; however, the general qualitative agreement of these results is thought to be significant.
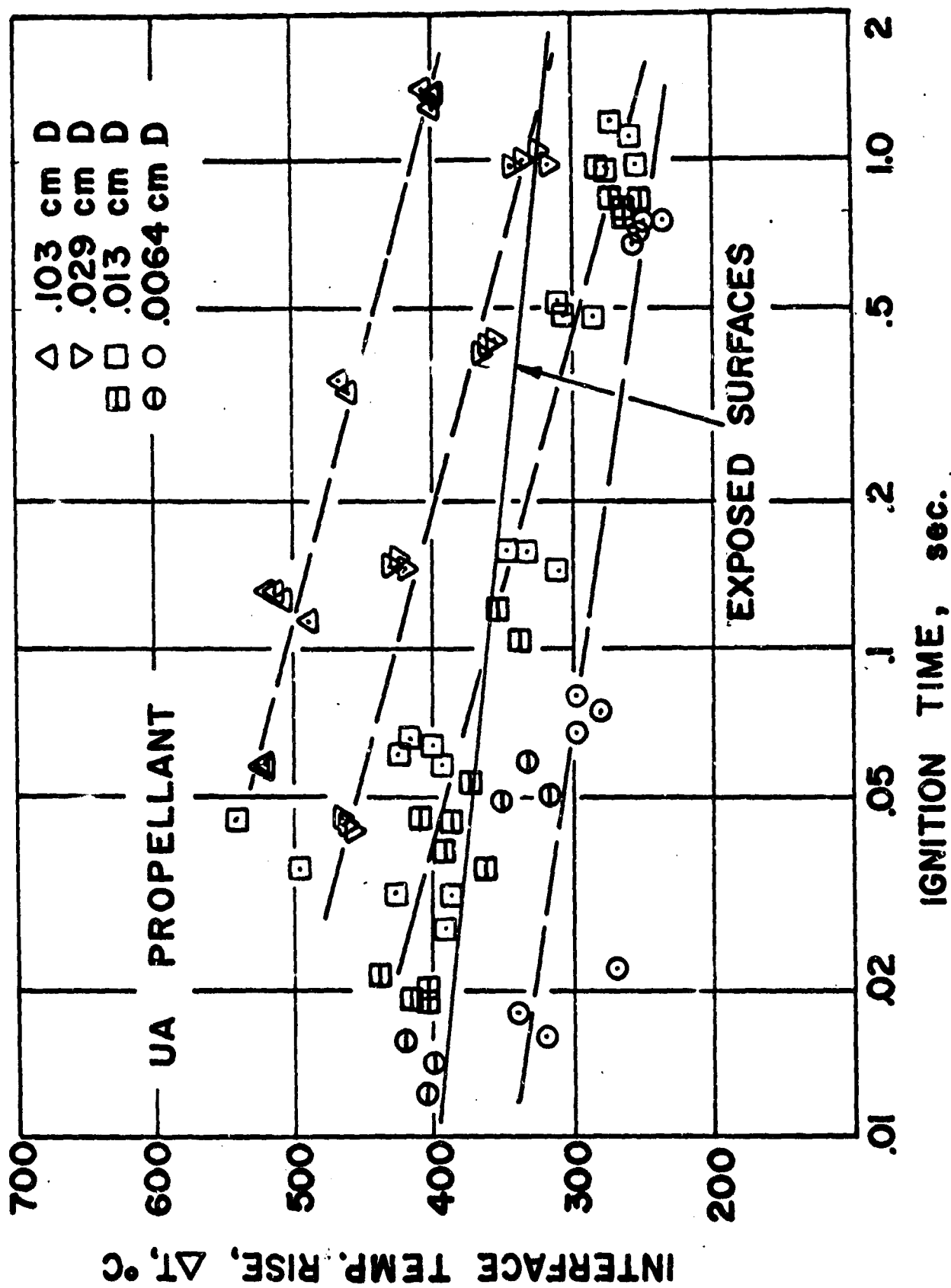
Figure 34. A summary of hot-wire ignition data for the UA propellant employing four different wire diameters. The normal wire length was 1/2 inch; points with horizontal bars denote 1/8-inch wire lengths. The line labeled exposed surfaces represents experimental radiation furnace and shock tube data.
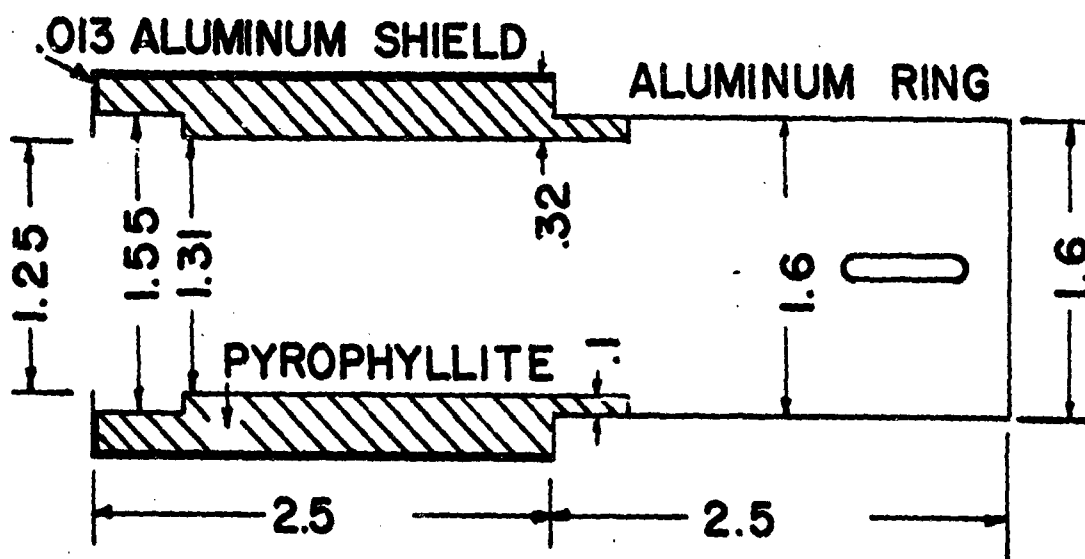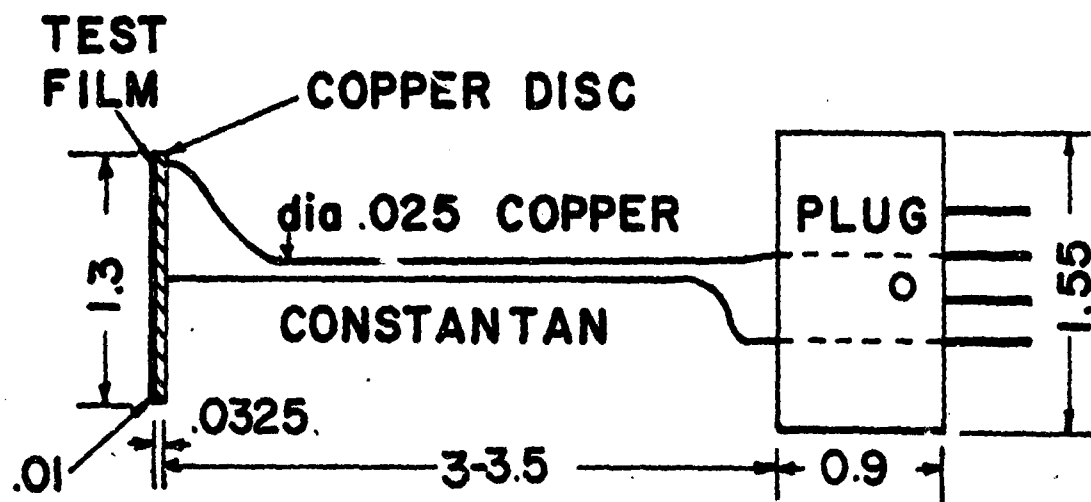
Figure 35. Sectional views of the apparatus used for measurement of the thermal effects of propellant component reactions. Dimensions are in centimeters. The upper assembly was placed inside cylindrical shield shown below.
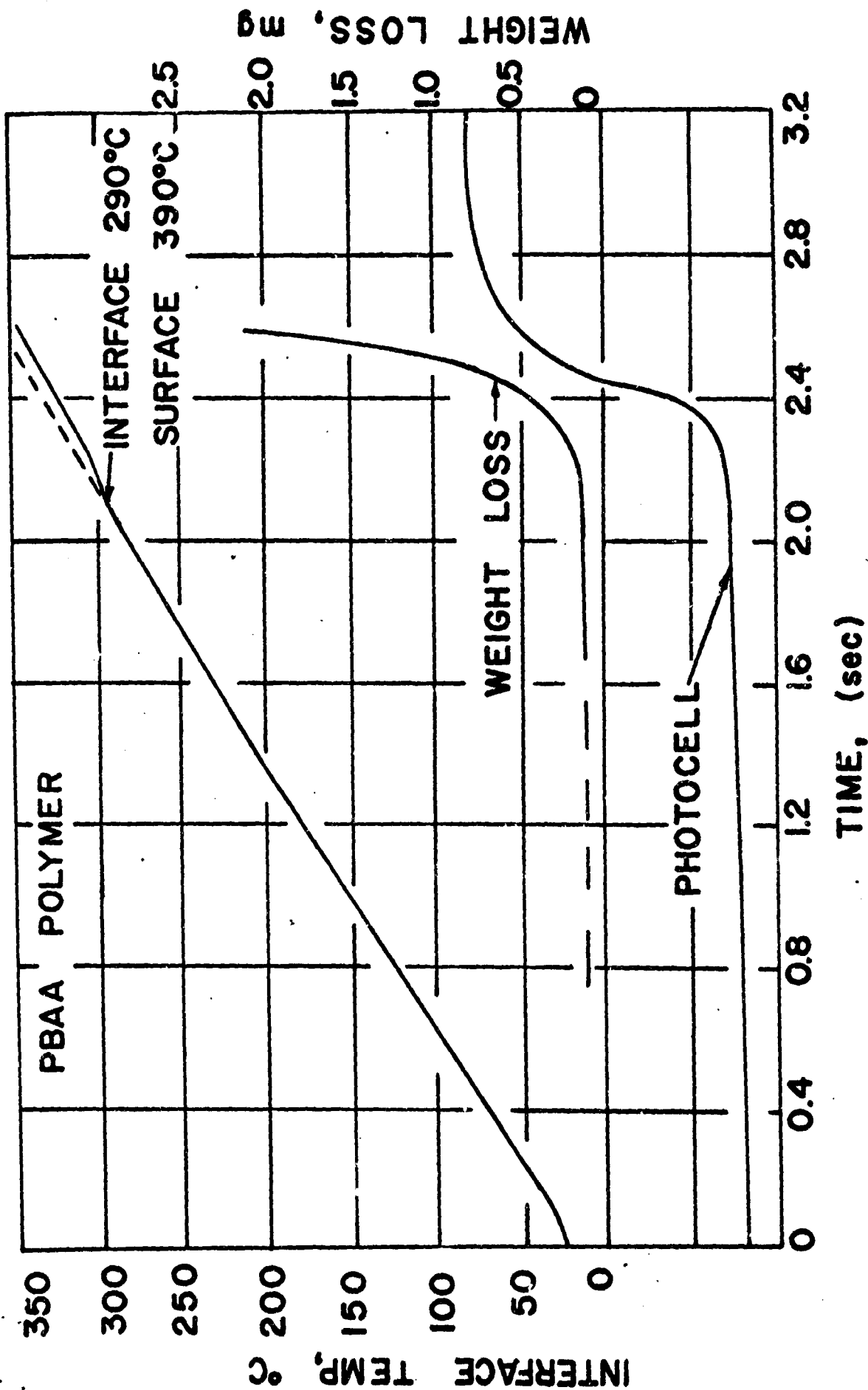
Figure 36. A typical record of the copper disc (interface) temperature history for a thin-polymer-film test. Also plotted is the output of a photocell which viewed the sample and the measured weight loss of samples removed from the furnace at the indicated times. The total film weight was 15 mg. The furnace temperature was 1100°C; the pressure was 0.85 atms of nitrogen.
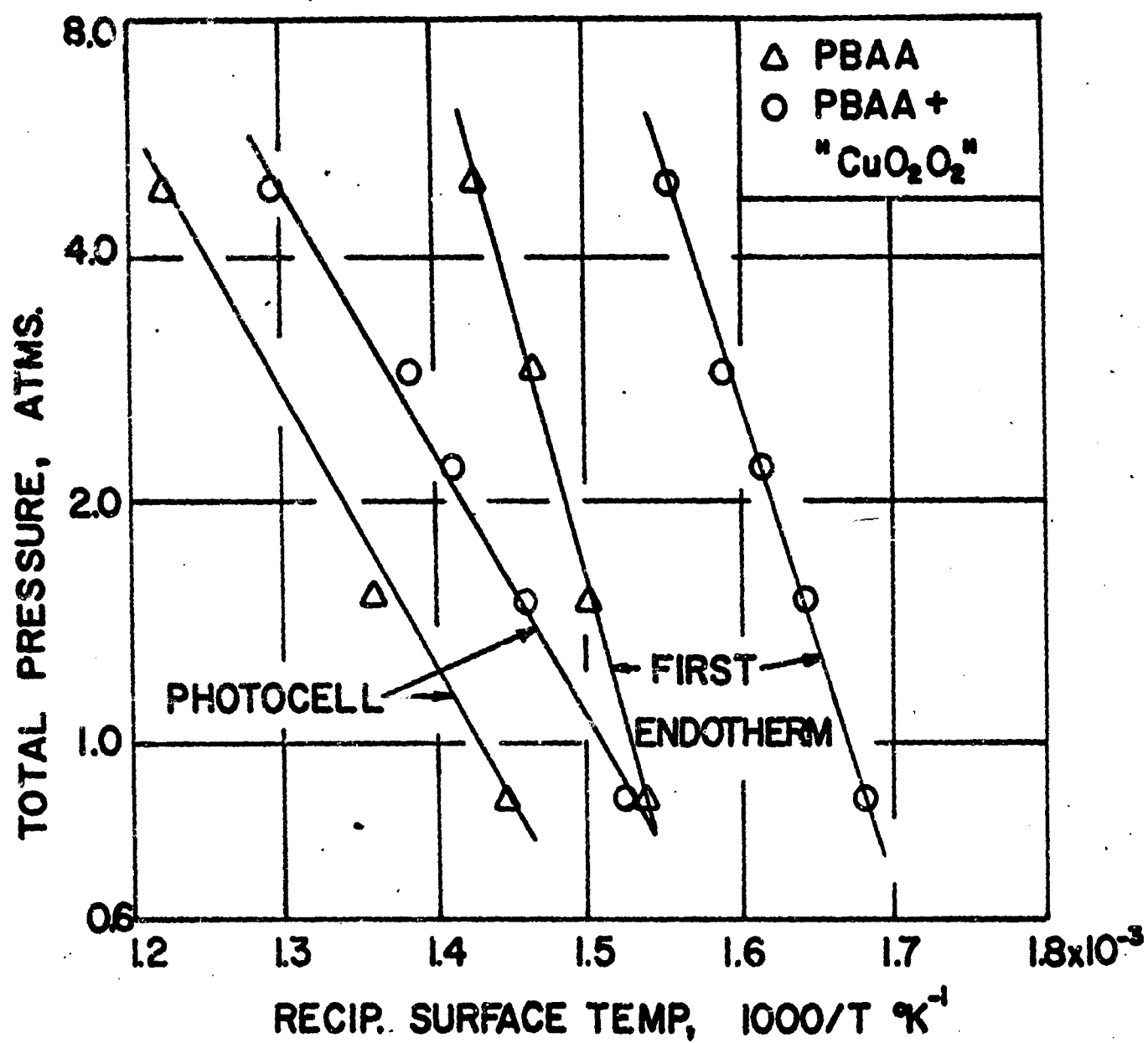
Figure 37. A summary of the data for decomposition of thin films of PBAA polymer. In all tests the furnace temperature was 1100°C and the gas in the furnace nitrogen.
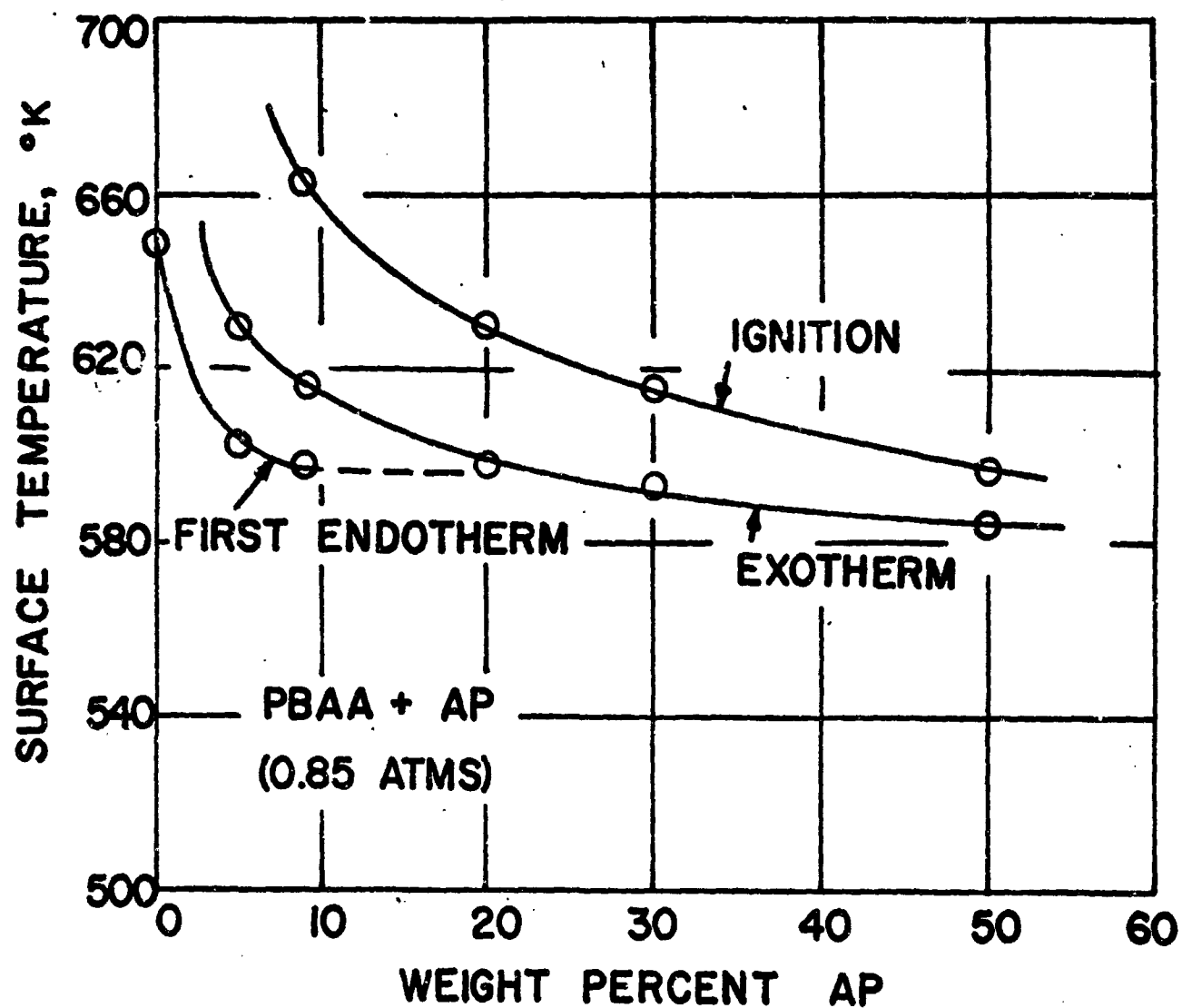
Figure 38. A summary of the data for reaction of thin films of PBAA polymer containing fine AP. All tests were at a furnace temperature of 1100°C and in 0.85 atms of nitrogen. The line labeled ignition was established by reference to the photocell signal.
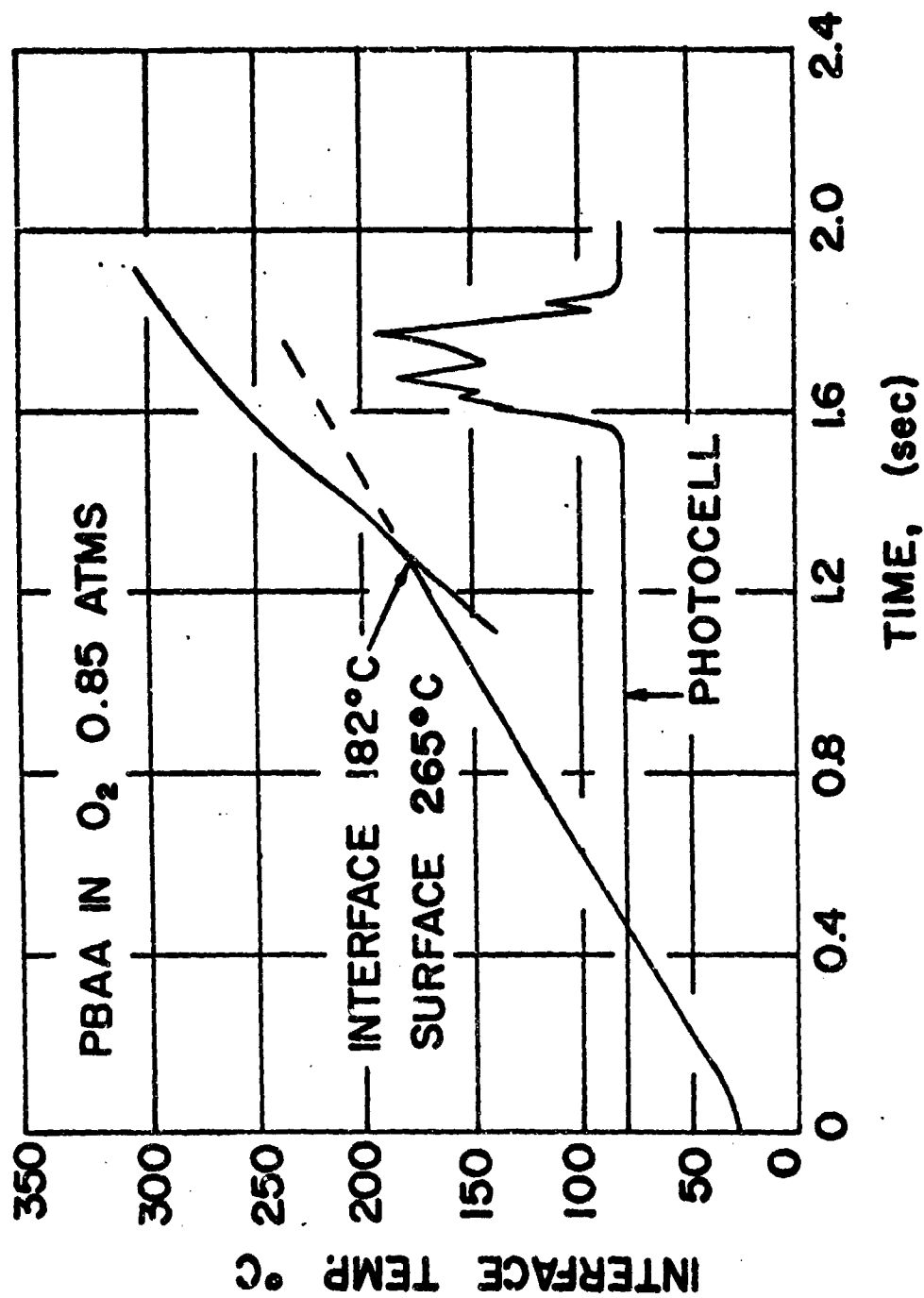
Figure 39. A record of the copper disc (interface) temperature history for a PBAA-film test in oxygen. The furnace temperature was 1100°C. Also shown is a reproduction of the signal from a photocell which viewed the sample surface.
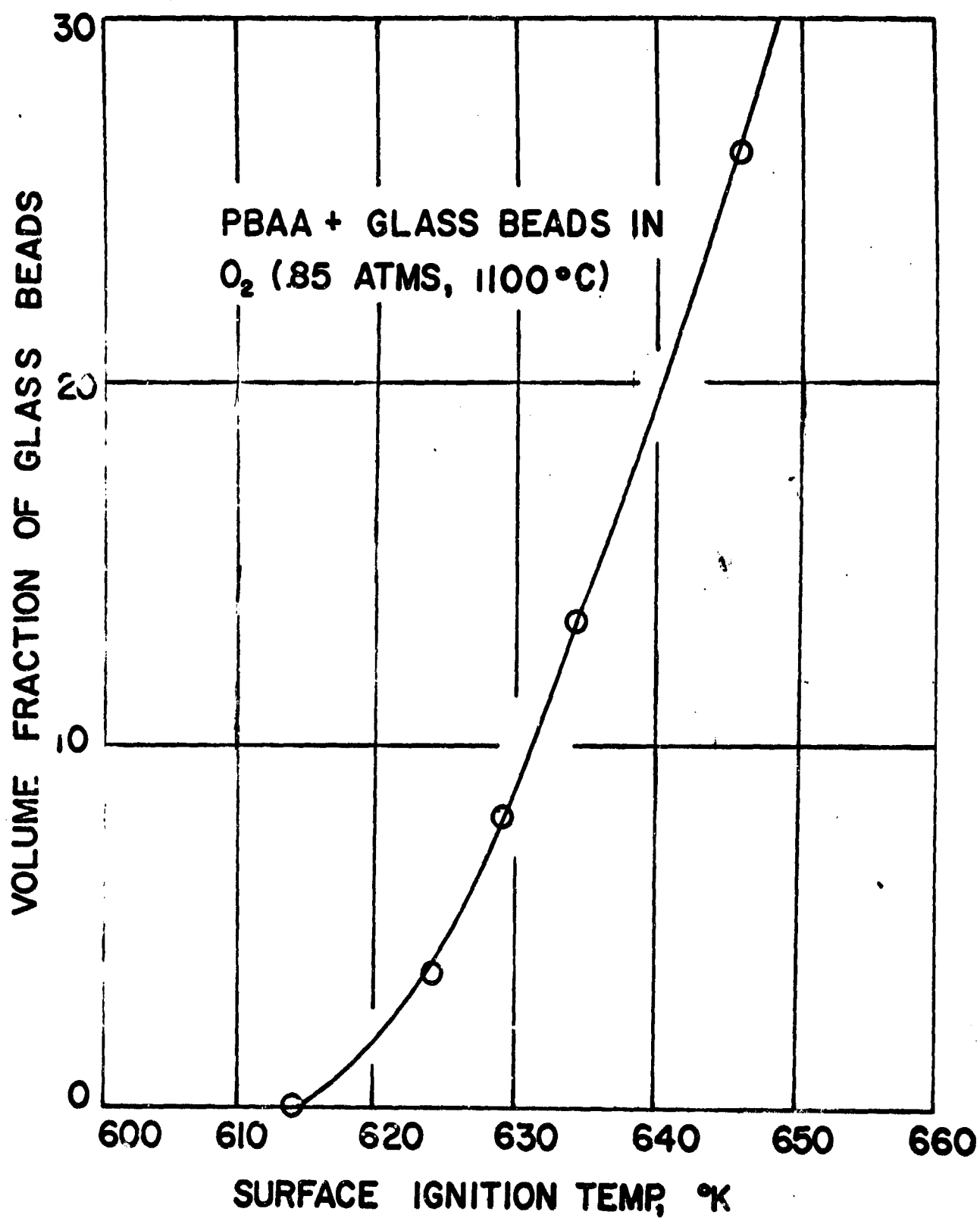
Figure 40. The effect of glass beads as a diluent on the surface temperature at ignition for thin PBAA films.
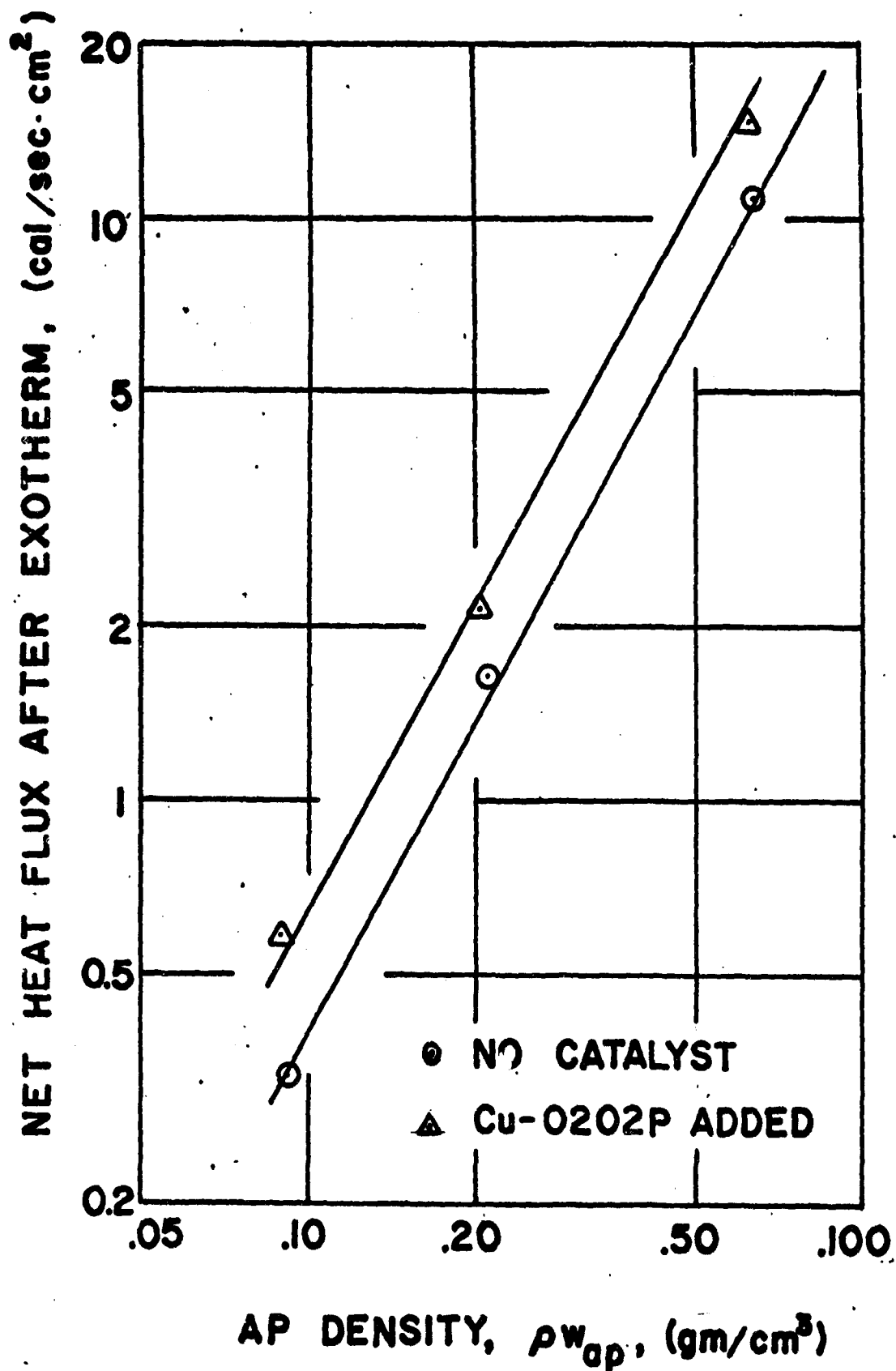
Figure 41. The net increase in heat flux, measured by the copper disc, after the first exotherm as a function of the AP density in films of mixtures of PBAA and AP.

$$\frac{d\ln p}{dt} = C$$
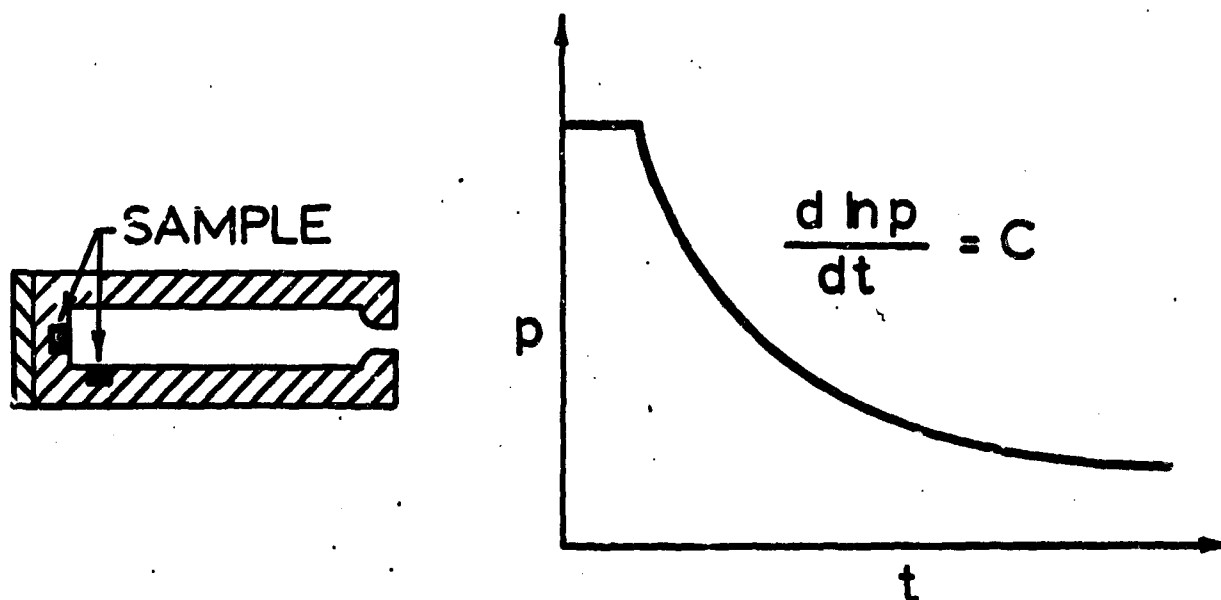
"BLOWDOWN" EXTINGUISHMENT
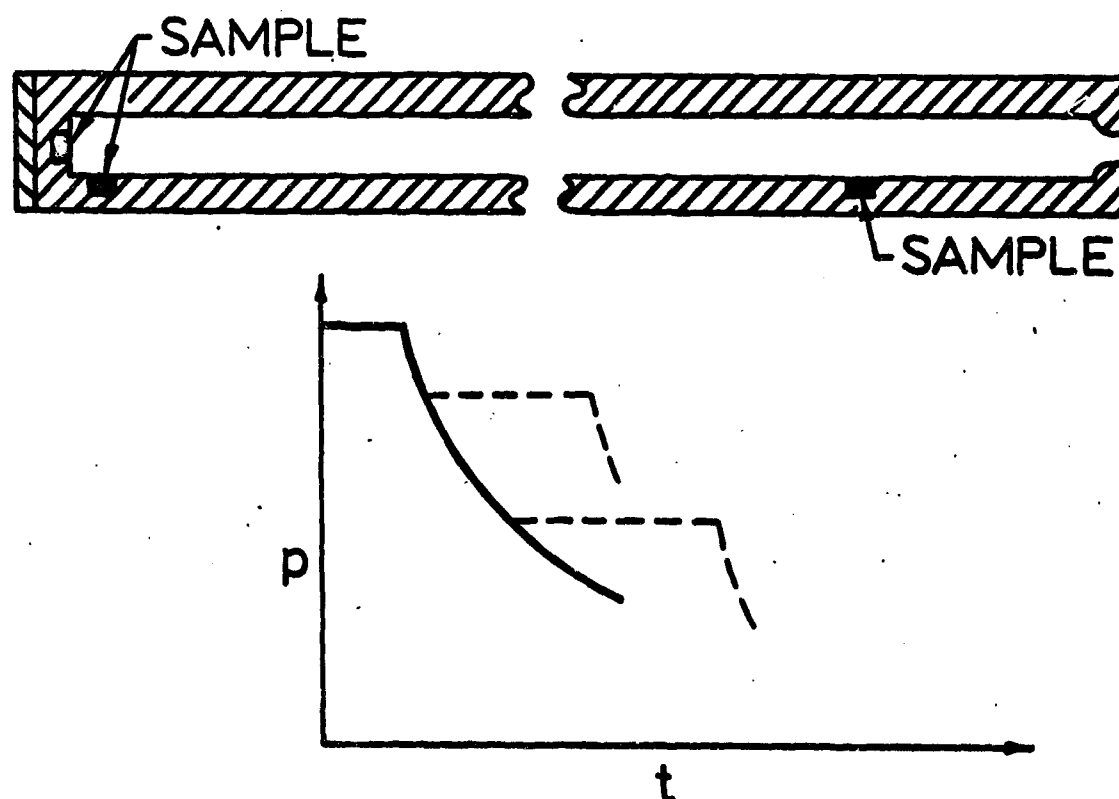
"FIRST RAREFACTION" EXTINGUISHMENT

Figure 42. An illustration of the two techniques for use of the cylindrical rarefaction tube to extinguish burning propellant samples. In the tests discussed here, samples were mounted only in the flat end of the rarefaction tube for the "blowdown" tests and only in the curved surface near the nozzle for the "first rarefaction" tests.
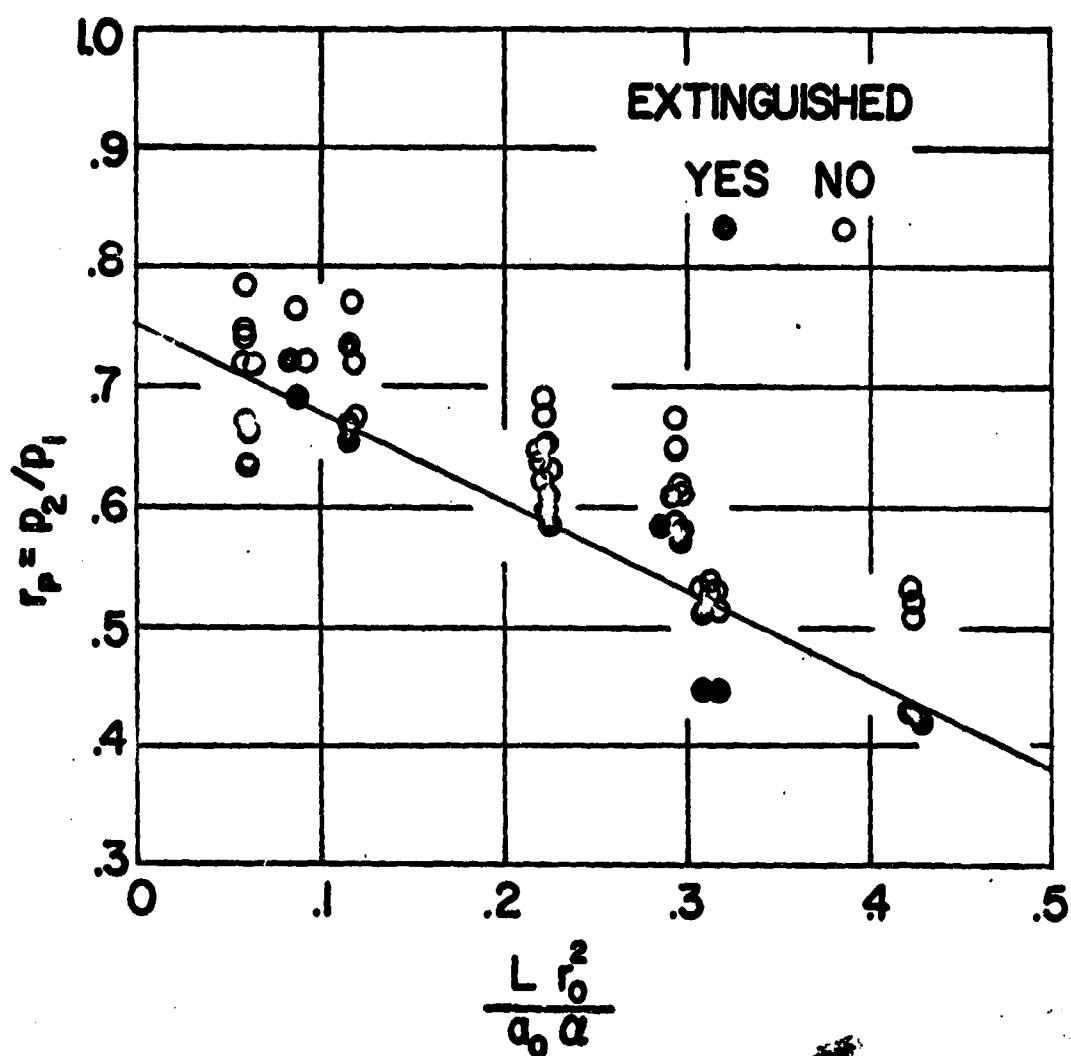
Figure 43. Critical pressure ratios for first rarefaction extinguishment of the G propellant as a function of the distance from the nozzle to the sample. The abscissa is actually the ratio of a characteristic time for the pressure drop to the characteristic time of the thermal wave in the solid.
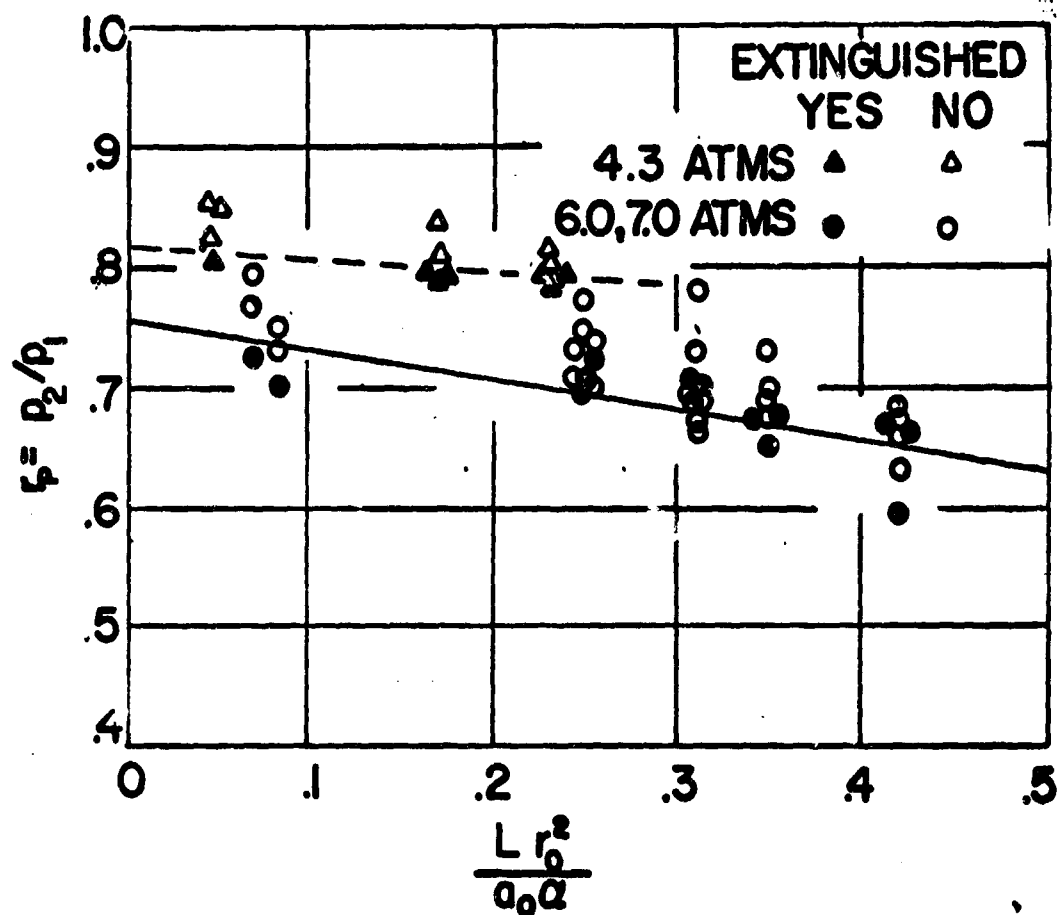
Figure 44. Critical pressure ratios for first rarefaction extinguishment of the UG propellant as a function of the distance from the nozzle to the sample.

APPENDIX B.   TABLES 1 THROUGH 13

TABLE 1.

SUMMARY OF THE PARAMETERS[1] FOR THE CASES OF HOMOGENEOUS IGNITION MODEL.

Parameter[2]	CASE									
	I	II	III	IV[3]	V	VI	VII	VIII	IX[3]	X
Dimensional Feedback Flux at 1 atms, $G_a \times 10^9$ cal/(sec)(cm²)	5	2	2	7.5	1	1	2	5	4.5	2
Dimensional Value	250	100	100	50	50	50	100	250	30	100
Dimensional Heat of Gasification, R_{nd} cal/(cm³)	0.125	0.05	.05	.05	.025	.05	.05	.125	.03	.05
Dimensional Value	1000	400	400	400	200	400	400	1000	240	400
Dimensional Heat of Vaporization, R_{se} kcal/(g-mole, gas)	1.94	1.94	1.94	1.94	1.94	1.94	0.775	1.94	1.94	1.38
Dimensional Value	28	28	28	28	28	28	11.2	28	28	20
Dimensional Surface Temperature at 1 atms, U_{sb} °K	.0515	.0515	.0545	.0545	.0545	.0545	.0545	.0545	.0545	.0545
Dimensional Value	773	773	818	818	818	818	818	818	818	818
Burning Rate at 1 atms, $R_{ex} \times 10^8$ cm/sec	3.14	2.5	2.37	8.9	1.68	1.18	2.37	3.14	7.0	2.37
Dimensional Value	0.20	0.16	0.15	.076	.105	.075	0.15	.20	.060	0.15

[1] A number of parameters were the same for all cases: Y = .02 [initial temperature 300°K and surface-reaction activation energy E_b/R = 15,000°K; n = 0.5 (the burning rate exponent); C_b = 34/p^.125 (parameter for converting surface-reaction flux to regression rate)].

[2] Dimensional parameters were calculated for the following assumed values of propellant properties: b = 5 × 10^10 cal/(sec)(cm²), Γ = .021 cal/(cm)(°K)(sec^1/2), ρc = 0.52 cal/(cm²), E_b/R = 15,000°K.

[3] For these cases, b was assumed equal to 6.7 × 10^9 cal/(sec)(cm²).

TABLE 2.

SUMMARY OF THE PARAMETERS FOR THE CASES OF THE TWO-LAMINA IGNITION MODEL.

Thermal Property	AP	Fuel Binder
Density, g/cm^3	1.95	1.11
Thermal Conductivity cal/(sec)(cm)(°C)	1.1×10^{-3}	0.47×10^{-3}
Heat Capacity cal/(g)(°C)	0.275	0.425

Case	F-1	F-2	F-3	F-4
Pre-exponential Constant for AP Surface Reaction cal/(cm^2)(sec)	4.75×10^{10}	4.5×10^{10}	4.75×10^{10}	$5. \times 10^{10}$
Pre-exponential Constant for Binder Surface Reaction cal/(cm^2)(sec)	-2.5×10^{10}	-2.5×10^{10}	-2.5×10^{10}	-2.5×10^{10}
Pre-exponential Constant for AP Body Reaction cal/(cm^2)(sec)	4.5×10^{10}	4.5×10^{10}	4.5×10^{10}	$5. \times 10^{10}$
Pre-exponential Constant for Binder Body Reaction cal/(cm^3)(sec)	-4.5×10^{10}	-4.5×10^{10}	-4.5×10^{10}	$-5. \times 10^{10}$
Pre-exponential Constant for Interface Reaction cal/(cm^2)(sec)	$2. \times 10^{10}$	$2. \times 10^{10}$	$2. \times 10^{10}$	$5. \times 10^{10}$
Activation Energy for All Exponentials E/R, °K	14.8×10^3	15.15×10^3	14.9×10^3	$15. \times 10^3$

TABLE 3.

SUMMARY OF PROPELLANT COMPOSITION.

Propellant Code	Ingredients (weight percent)		Ammonium Perchlorate	Ammonium-Perchlorate Particle Size[1]
	Fuel Binder	Catalyst		
AH	25.0 PBAA[2]	None	75.0	15 microns
AJ	25.0 PBAA	2.0 Ammonium Dichromate	73.0	15 microns
AK	22.8 PBAA	4.7 n-Butyl Ferrocene	72.5	15 microns
AL	25.0 PBAA	4.0 Cobalt Oxide[3]	71	15 microns
AR[4]	25.0 PBAA	2.0 Copper Chromite	70	15 microns
FM	18.0 PBAA	2.0 Copper Chromite[5]	40.0 40.0	15 microns 200 microns
G	18.0 PBAA	None	41.0 41.0	15 microns 200 microns
GM	18.0 PBAA	None	82.0	15 microns 200 microns
UA	25.0 PBAA	2.0 Copper Chromite	73.0	15 microns
UG	20.0 PU[6]	None	80.0	15 microns 200 microns
PP-E	4.5 Sterling VR Carbon Black[7]	2.5 Copper Chromite	46.5 46.5	15 microns 45 microns
PP-F	None	5.0 Copper Chromite	95.0	15 microns 200 microns

[1]Ammonium perchlorate of the designated particle size means that 50 weight percent of the particles have diameters less than the value indicated. For particle sizes greater than 35 microns, a screen analysis was used for measuring particle diameters. For particles less than 15 microns, particle sizes were determined microscopically. All ammonium perchlorate was obtained from American Potash and Chemical Corporation.

[2]The PBAA fuel binder was composed of 85 percent liquid polybutadiene-acrylic acid copolymer cured with 15 percent Epon 828 (manufactured by Shell Chemical Company).

[3]Cobalt-oxide powder from the J. T. Baker Chemical Company.

[4]Three percent of Phillips Petroleum Company Philblack-E added to fuel binder.

[5]Copper-chromite catalyst CuO_2O_2P from Harshaw Chemical Company.

[6]The PU (polyurethane) fuel binder was 93.75 w/o B. F. Goodrich Estane 5720X5 plus 6.25 w/o of a special curative agent supplied by Thiokol Chemical Corporation.

[7]Sterling VR carbon black was obtained from the Cabot Corporation.

TABLE 4

THERMOPHYSICAL PROPERTIES OF PROPELLANTS

Propellant	Test Temperature (°C)	Heat Capacity, Cal/(g)(°C)	Density g/cm³	Thermal Diffusivity (cm²)/(sec)	Thermal Responsivity Cal/(cm²)(sec)$^{1/2}$(°K)
AH	60	0.324	1.55	1.70×10^{-3}	0.0204 (1)
AJ	60				0.0202 (1)
AK	60	0.327	1.52		0.0200 (1)
AL	60				0.0200 (1)
FM	60	0.316	1.63	1.70×10^{-3}	0.0212
G	60	0.311	1.60	1.71×10^{-3}	0.0206
UA	60	0.322	1.56	1.63×10^{-3}	0.0203
UG	60	.311	1.61	1.73×10^{-3}	
PP-E	60		1.92		0.0244 (1)
PP-F	60		1.92		0.0244 (1)

Notes

(1) Values for thermal responsivity were estimated from experimental data on similar materials.

TABLE 5

IGNITION DATA FOR CAST PROPELLANT AH IN NITROGEN

Run No.	Shock Mach Number, M_E	Gas Temperature, T_g, °K	Gas Pressure, P_4, atms	Gas Velocity, u, m/sec	Ignition Time, t_1, msec	Mean Heat Flux, $\overline{F}$ cal/(sec)(cm²)	Linear Ignition Temperature, T_{si} °K
61-11-1	3.41	1713	20.8	55	18.3	60.9	751
61-11-2	3.07	1467	20.8	54	26.2	48.3	728
61-11-6	3.42	1771	19.9	111	9.0	93.8	788
61-11-7	3.30	1649	20.3	108	16.2	80.0	860
63-2-1	3.34	1641	17.7	107	15.1	74.4	795
63-2-2	3.47	1752	19.7	110	9.2	92.3	781
63-2-3	3.79	2028	19.6	119	6.7	111.6	797
63-2-4	3.19	1550	19.9	104	11.5	78.4	758
63-2-5	3.14	1533	22.8	104	13.4	82.2	820
63-2-9	3.46	1772	20.6	56	13.5	65.4	715
63-2-10	3.65	1906	19.4	58	12.8	68.6	724
63-3-1	3.27	1604	21.9	54	16.8	58.9	714
63-3-2	3.07	1456	21.3	51	26.6	48.4	729
63-3-5	3.37	1715	20.6	72	10.0	78.2	727
63-3-6	3.23	1565	20.6	69	15.9	66.1	755

Sample did not ignite; data given are those that correspond to time that test was terminated.

TABLE 6

IGNITION DATA FOR CAST PROPELLANT UA IN NITROGEN

Run No.	Shock Mach Number, M_E	Gas Temperature, T_g, °K	Gas Pressure, P_4, atms	Gas Velocity, u, m/sec	Ignition Time, t_i, msec	Mean Heat Flux, F cal/(sec)(cm²)	Linear Ignition Temperature, T_s °K
61-11-3*	3.04	1462	20.4	51	25	47.8	716
61-11-4	3.43	1751	20.6	56	12.5	64.8	698
61-11-5	3.45	1764	19.9	111	6.3	97.9	728
62-2-9*	2.79	1272	20.6	48	28	39.9	668
62-2-10	3.04	1428	20.1	51	25.3	46.0	703
62-2-11	3.26	1593	20.6	53	15.5	56.8	690
62-2-12	3.41	1729	20.1	106	11.7	63.5	678
62-2-13	3.04	1434	20.2	51	24.1	46.6	699
62-3-6	3.49	1813	21.4	112	5.9	106.9	752
62-3-7	3.23	1594	21.1	106	7.9	88.7	734
62-3-8	3.03	1427	19.4	100	14.6	67.4	749
62-3-9	2.84	1318	21.4	96	12.0	67.5	707
62-3-10	2.60	1072	21.2	91	24.0	50.2	729
62-3-11	3.42	1735	19.5	72	9.3	77.0	710
62-4-1	2.95	1388	18.6	65	19.5	52.6	700
62-4-2	3.20	1513	19.3	68	12.7	63.2	688
62-4-3	3.42	1698	19.9	71	8.6	77.3	692
62-4-4*	2.66	1157	20.8	59	27	42.1	678
62-4-5	3.06	1443	20.6	66	13.2	61.8	688

*Sample did not ignite; data given are those that correspond to time that test was terminated.

TABLE 7

IGNITION DATA FOR CAST PROPELLANT AJ IN NITROGEN

Run No.	Shock Mach Number, M_E	Gas Temperature, T_g, °K	Gas Pressure, P_4, atms	Gas Velocity, u, m/sec	Ignition Time, t_1, msec	Mean Heat Flux, $\bar{F}$ cal/(sec)(cm²)	Linear Ignition Temperature, T_s °K
510-26-1	2.94	1352	19.8	203	11.4	60.2	652
510-26-2	3.22	1606	21.7	220	8.8	80.1	714
510-26-3	3.38	1720	21.4	228	6.3	89.1	690
510-26-4	3.06	1476	21.4	211	8.4	72.6	667
510-26-5	3.05	1456	20.4	705	6.9	97.1	746
510-26-6	3.25	1618	20.6	740	4.5	117.9	738
510-26-7	3.42	1784	20.9	775	3.6	130.6	752
510-26-8	3.25	1617	22.0	107	16.5	49.9	653
510-27-1	3.52	1867	21.9	104	15.5	58.3	699
510-27-2	3.23	1607	21.3	106	22.1	46.5	681

TABLE 8

IGNITION DATA FOR CAST PROPELLANT AL IN NITROGEN

Run. No.	Shock Mach Number, M_E	Gas Temperature, T_g, °K	Gas Pressure, P_4, atms	Gas Velocity, u, m/sec	Ignition Time, t_1, msec	Mean Heat Flux, $\bar{F}$ cal/(sec)(cm²)	Linear Ignition Temperature, T_{s1} °K
61-8-1*	3.45	1785	19.7	230	10	82.8	759
61-8-2*	3.44	1768	19.7	111	16	51.1	659
61-8-3	3.04	1442	21.2	51	19.0	49.8	684
61-8-4	3.12	1470	19.2	51	24.1	46.6	704
62-2-14	3.45	1757	20.2	56	10.8	65.8	682
62-3-1	3.19	1522	19.8	52	26.9	48.6	742
62-3-2	3.39	1699	18.4	55	14.4	57.4	681
62-3-3	3.30	1642	18.6	107	8.6	82.9	727
62-3-4	3.15	1504	17.8	103	20.0	64.0	805
62-3-5	2.96	1395	18.8	112	21.2	59.8	787
62-4-6	3.24	1572	20.6	69	15.6	66.2	761
63-2-6	3.00	1393	20.7	99	15.9	66.9	770
63-2-7	3.19	1521	19.9	103	12.2	74.5	765
63-2-8	3.50	1795	21.2	112	7.6	101.4	794
63-3-3	3.45	1770	19.4	56	14.8	63.2	728
63-3-4	3.30	1631	21.3	54	21.0	56.9	760

*Sample did not ignite; data given are those that correspond to time that test was terminated.

TABLE 9

IGNITION DATA FOR CAST PROPELLANT AK IN NITROGEN

Run No.	Shock Mach Number, M_E	Gas Temperature, T_g, °K	Gas Pressure, P_4, atms	Gas Velocity, u, m/sec	Ignition Time, t_1, msec	Mean Heat Flux, F cal/(sec)(cm²)	Linear Ignition Temperature, T_{s1} °K
512-7-1	3.02	1436	20.6	209	9.0	68.2	658
512-7-2	2.85	1332	22.5	202	5.8	70.1	595
512-7-3	2.81	1308	21.5	200	10.5	61.4	649
512-7-4	3.25	1629	21.8	222	5.6	86.3	659
512-7-5	3.44	1820	20.6	741	2.4	144.3	694
512-7-6	3.42	1757	19.2	769	3.2	127.9	704
512-7-7	3.22	1595	19.7	734	2.5	120.8	637
512-7-8	3.05	1470	20.1	705	3.6	106.9	657
512-8-1	3.43	1758	21.6	111	6.0	61.3	561
512-8-2	3.19	1552	20.7	104	9.6	49.3	567
512-8-3*	2.88	1326	21.3	96	26	36.5	627
512-8-4	3.41	1753	20.8	111	16.2	52.2	669
512-8-5*	3.41	1718	20.1	96	17	49.8	661
512-8-6	3.38	1717	20.0	761	1.9	135.7	630
512-8-7	2.83	1316	20.8	668	3.6	96.2	622
512-8-8*	2.77	1288	20.6	661	8	82.4	712

TABLE 9 (continued)

IGNITION DATA FOR CAST PROPELLANT AK IN NITROGEN

Run No.	Shock Mach Number, M_E	Gas Temperature, T_g, °K	Gas Pressure, P_4, atms	Gas Velocity, u, m/sec	Ignition Time, t_1, msec	Mean Heat Flux, $\bar{F}$ cal/(sec)(cm²)	Linear Ignition Temperature, T_{s1} °K
512-8-9	2.80	1297	20.3	664	6.2	85.9	678
512-8-10	3.07	1491	20.6	710	3.8	109.7	678
512-9-1	3.27	1646	21.3	745	3.0	129.0	694
512-9-2	3.46	1795	21.2	777	2.65	143.2	711
512-9-3	3.44	1784	21.4	232	5.25	88.7	658
512-9-4	3.32	1704	21.7	226	5.1	91.0	664
512-9-5	3.08	1490	21.5	212	7.6	74.4	663
512-9-6	2.82	1296	21.6	198	8.4	62.9	621
512-9-7*	2.48	1055	13.4	179	14	33.4	518
512-9-8	2.99	1393	14.4	206	16.1	47.7	638
512-10-1	3.04	1439	17.3	209	10.0	59.8	634
512-10-2	3.19	1545	18.9	216	6.25	72.6	621
512-10-3	3.43	1797	18.9	229	5.05	87.3	648

*Sample did not ignite; data given are those that correspond to time that test was terminated.

TABLE 10

IGNITION DATA FOR CAST PROPELLANT FM-85 IN NITROGEN

Run No.	Shock Mach Number, M_E	Gas Temperature, T_g, °K	Gas Pressure, P_4, atms	Gas Velocity, u, m/sec	Ignition Time, t_1, msec	Mean Heat Flux, F cal/(sec)(cm²)	Linear Ignition Temperature, T_{si} °K
512-10-4	3.(	1445	20.8	209	6.8	.72.3	615
512-10-5	2.75	1255	20.0	195	10.2	56.8	602
512-10-6	2.57	1118	18.8	184	16.8	44.2	601
512-10-7(a)	2.05	797	21.1	156	20	26.6	542
512-10-8(b)	2.81	1292	20.1	198	8.4	77.6	630
512-11-1	2.56	1131	19.8	185	17.8	46.0	622
512-11-2(a)	2.18	861	20.7	162	30	29.6	569
512-11-3(b)	2.99	1423	19.4	207	5.6	69.9	576
512-11-4	3.44	1807	20.9	230	3.3	99.4	601
512-11-5(a)	2.20	879	21.2	164	30	30.8	581
512-11-6(b)	3.05	1463	20.4	210	4.9	74.8	575
512-11-7(a)	2.02	796	21.0	157	30	26.4	540
512-11-8(b)	2.76	1270	20.1	193	9.4	58.4	598
512-11-9	3.17	1503	18.9	210	6.0	71.7	592
512-11-10	3.25	1613	20.0	220	4.2	83.6	584

(a) Sample did not ignite; data given are those that correspond to time that test was terminated.

(b) For this run, the sample used in preceding run, which did not ignite, was used.

TABLE 11

IGNITION DATA FOR PRESSED PROPELLANTS IN NITROGEN

Run No.	Shock Mach Number, M_E	Gas Temperature, T_g, °K	Gas Pressure, P_4, atms	Gas Velocity, u, m/sec	Ignition Time, t_i, msec	Mean Heat Flux, $\bar{F}$ cal/(sec)(cm²)	Linear Ignition Temperature, T_{si} °K
63-4-1	3.46	1785	21.5	57	15.2	69.5	692
63-4-2	3.43	1763	20.9	56	19.0	65.5	713
63-5-1	3.43	1761	20.8	56	19.3	65.2	714
63-5-2	3.46	1781	21.0	112	10.0	101.4	764
63-5-3	3.22	1574	20.8	105	13.6	84.4	751
63-5-4	3.12	1523	23.0	103	13.5	87.1	764
63-5-5	2.90	1334	20.6	97	21.1	64.7	730
63-5-6	3.06	1458	19.9	50	30.0	48.3	683
63-5-7[2]	3.26	1609	20.2	54	22	57.0	687
63-5-8	3.25	1605	19.7	54	28.8	54.0	720
63-15-6	3.48	1804	19.2	113	8.9	98.0	725
64-12-4	3.43	1740	18.8	110	11.2	90.3	742
64-12-5	3.37	1719	18.4	110	17.0	82.9	799
66-13-1	3.39	1687	18.6	109	20.0	80.1	813
64-13-2	3.53	1806	19.2	112	11.2	95.8	758
64-13-3	3.27	1570	20.9	105	14.5	84.0	757
64-13-4	3.47	1767	21.8		20.0	67.3	729
64-13-5	3.41	1699	18.8		25.5	57.2	712

[1]Runs 63-4-1 through 63-5-8 employed propellant PP-E; runs 63-15-6 through 64-13-5 employed propellant PP-F.

[2]Sample did not ignite; data given are those that correspond to time that test was terminated.

TABLE 12.

SUMMARY OF BLOWDOWN-TYPE EXTINGUISHMENT DATA FOR VARIOUS PROPELLANTS.

The initial pressure range was 3.5 to 11 atms and the final pressure 0.85 atms.

Propellant[1]	Fuel Binder	Percent AP	AP Size microns	Additives	Burning Rate Exponent, n (1 - 5 atms)	Burning Rate at 1 atms, cm/sec	Low Pressure Limit, atms	Pressure Ratio for Rarefaction Wave, P/P_o	Extinction Requirement $-\dfrac{d \ln P}{dt}$, sec^{-1}
G	PBAA	82	200, 15	none	0.50	0.16	0.048	0.75	40 – 60
AH	PBAA	75	15	none	0.56	0.17	----	~0.82[2]	40 – 60
GB	PBAA	80	200, 15	2% carbon black	0.50	0.16	0.063	----	40 – 60
UA	PBAA	73	15	2% Cu-0202P	0.55	0.35	----	~0.4[2]	200 – 250
AF	PBAA	73	200, 15	2% Cu-0202P	----	----	----	----	500 – 700
P	PBAA	80	200, 15	2% Cu-0202P	0.58	0.25	0.033	<0.38	600 – 800
UG	PU	80	200, 15	none	0.78	0.097	0.15	0.75 – 0.82	9 – 13

[1] See Table 3 for details on fuel binders, AP particle size, and additives.

[2] These are values measured 34.5 cm from the nozzle and are not obtained by extrapolation to zero distance.

TABLE 13.

BLOWDOWN EXTINGUISHMENT DATA.

All tests were prepared in a 10.16-diameter tube, 50.8 cm long.

Propellant	Diameter of Sample, cm	Area Ratio A_N/A	Initial Pressure[1], atms	$-\dfrac{d \ln P}{dt}$, sec^{-1}	Extinguished?
UG	0.92	.0156	6.45	13.5	yes
UG	0.92	.0156	7.20	12.9	yes
UG	0.92	.0156	7.68	12.7	no
UG	0.92	.0156	7.44	13.5	yes
UG	0.92	.0156	5.61	13.7	yes
UG	0.92	.0088	6.60	9.06	no
UG	0.92	.0088	7.20	8.46	no
UG	0.92	.0088	7.85	8.43	no
UG	0.92	.0088	6.18	8.93	no
G	0.92	.0644	7.10	50.4	no
G	0.92	.0644	7.48	52.0	no
G	0.92	.0644	6.28	50.0	no
G	0.92	.0791	7.12	62.9	no
G	0.92	.0791	8.16	61.1	no
G	0.92	.1000	8.12	79.8	yes
G	0.92	.1000	----	83.2	yes
G	1.56	.0495	7.00	50.7	no
G	1.56	.0495	6.68	51.1	no
G	1.56	.0644	6.70	58.9	yes
G	1.56	.0644	6.67	60.3	no
G	1.56	.0644	7.48	61.1	no
G	1.56	.0644	8.18	63.3	no
G	1.56	.0644	9.52	64.5	no
G	1.56	.0644	7.48	66.5	no
G	1.56	.0791	7.88	78.0	yes
G	1.56	.0791	9.28	79.9	yes
G	1.56	.1000	6.98	95.0	yes

[1]This is the pressure in the tube at the time of diaphragm rupture. The pre-ignition pressure was about 0.6 and 0.25 and 0.35 of this value for 0.92- and 1.56-cm-diameter samples, respectively.

APPENDIX C. NOMENCLATURE

A	area; A, rarefaction tube cross-sectional area; A_N, nozzle cross-sectional area
a	feedback heat flux for P = 1 atms
a_o	speed of sound in a stagnent gas
b	coefficient of the Arrhenius expression for a surface reaction, also dimensionalizing factor for heat fluxes
C_b	ratio of R_{ex} to F_r
C	solid heat capacity
E	activation energy; Eb, for a surface reaction
F	dimensionless surface heat flux, f/b; F_r, reaction flux, see Eq. 2; F_e, igniter flux; F_{lim}, maximum flux for ignition
$\overline{F}_s$	mean surface heat flux for convective flux ignition tests
f	surface heat flux; f_1, feedback flux at P_1
G_a	dimensionless feedback flux for P = 1 atms, a/b, see Eq. 3
G_{aa}	dimensionless modified feedback flux for P = 1 atms, see Eq. 2
G_m	dimensionless heat flux at the solid surface, $(\partial U/\partial X)$ at X = 0
k	solid thermal conductivity
L	distance from burning sample to rarefaction tube nozzle
ℓ	total regression distance at surface vaporization temperature
M	Mach number; M_E, shock Mach number at end of driven section, M_{st}, gas flow Mach number past convectively-heated sample
n	exponent on pressure for regression rate
P	pressure; P_1, initial pressure; P_2, pressure after passage of rarefaction wave

99

APPENDIX C. NOMENCLATURE
(Continued)

P_ℓ pressure in shock tube test section

Q total energy transferred to a solid surface per unit area, $g_\tau \, b[R/E\Gamma]^2$

q net heat of gasification of a burning propellant per unit mass; q_v, per unit volume

q_{or} total energy transferred to a solid surface per unit area

R gas constant

R_{ex} dimensionless regression rate, $-(E_b/RB)(\rho cr)$

R_{nd} dimensionless volumetric net heat of gasification, $q_v R/\rho c E_b$

r regression rate; r_o or r_1, initial rate; r_2 final rate after passage of a rarefaction wave

T dimensionless time, $(kb/Eb\Gamma)\,t$

T_s surface temperature for ignition tests; T_{si}, surface temperature at ignition, T_{si}^L linear surface temperature at ignition

T_g gas temperature behind a reflected shock wave

t time, t_i, ignition time

U dimensionless temperature, Rv/E_b; U_2, surface temperature, U_{sb}, surface temperature for steady-state regression

u gas velocity at sample surface for convective ignition tests

v absolute temperature; v_s, surface temperature, v_o, initial uniform solid temperature

w_{ap} weight fraction AP in thin PBAA-AP films

X dimensionless distance from solid surface, $Rbx/E_b k)$

x distance from solid surface

APPENDIX C.   NOMENCLATURE
(Continued)

γ dimensionless initial temperature, R_{vo}/E_b

α solid thermal diffusivity, $k/\rho c$

Γ solid thermal responsivity, $(k\rho c)^{1/2}$

ρ solid density

APPENDIX D. REFERENCES

[1] Ryan, N. W., Baer, A. D., Keller, J. A., Cheng, J. T. and
    Bouck, L. S. "Ignition and Combustion of Solid Propellants,"
    Final Technical Report on Air Force Grant No. AFOSR 40-65 (1965).

[2] Inami, S. H., Rosser, W. A. and Wise, H. "Dissociation Pressure
    of Ammonium Perchlorate," *J. Phys. Chem., 67,* 1077 (1963).

[3] Powling, J., and Smith, W. A. W. "The Surface Temperature of
    Burning Ammonium Perchlorate," *Combustion and Flame, 7,*
    270 (1963).

[4] Keller, J. A., Baer, A. D. a d Ryan, N. W. "Ignition of Ammonium
    Perchlorate composite Propellants by Convective Heating,"
    AIAA J., 4, 1358 (1966).

[5] Baer, A. D. and Ryan, N. W. "Ignition of Composite Propellants
    by Low Radiant Fluxes," *AIAA J., 3,* 884 (1965).

[6] Powling, J. "Experiments Relating to the Combustion of Ammonium
    Perchlorate-Based Propellants," Paper 44, Eleventh Symposium
    (International) in Combustion, Berkeley, California, August
    14-20, 1966.

[7] Bouck, L. S. "A Model of the Ignition of a Heterogeneous Solid
    Rocked Propellant," M.S. Thesis, University of Utah (196).

[8] Keller, J. A. "Studies on Ignition of Ammonium Perchlorate-Based
    Propellants by Convective Heating," Ph.D. Thesis, University
    of Utah (1965).

[9] Beyer, R. B., McCulley, L. and Evans, Marjorie W. *Applied Optics,*
    3, 131 (1964).

[10] Hermoni, M., and Salmon, S. "The Catalytic Decomposition of
    Ammonium Perchlorate," *Eighth Symposium (International)*
    on Combustion, The Williams and Wilkins Company, Baltimore (1962).

[11] Baer, A. D. "Recent Results Concerning the Hot-Wire Ignition of
    Composite Propellants," *Pyrodynamics, 3,* 15 (1965).

DOCUMENT CONTROL DATA - R&D

(Security classification of title, body of abstract and indexing annotation must be entered when the overall report is classified)

1 ORIGINATING ACTIVITY *(Corporate author)*	2a REPORT SECURITY CLASSIFICATION
University of Utah	Unclassified
	2b GROUP

2 REPORT TITLE

Technical Report on Ignition and Combustion of Solid Propellants

4 DESCRIPTIVE NOTES *(Type of report and inclusive dates)*

Final Project Report, October 1, 1965 to September 30, 1966

5 AUTHOR(S) *(Last name, first name, initial)*

Baer, Alva D.; Ryan, Norman W.; Keller, John A.; Cheng, Jih-Tien;
Bouck, Larry S.; Mantyla, Robert G.

6 REPORT DATE	7a TOTAL NO. OF PAGES	7b. NO. OF REFS
May 15, 1967	102	11

8a CONTRACT OR GRANT NO.	9a. ORIGINATOR'S REPORT NUMBER(S)
Grant AFOSR 40-66	
b. PROJECT NO.	
c	9b. OTHER REPORT NO(S) *(Any other numbers that may be assigned this report)*
d	

10 AVAILABILITY/LIMITATION NOTICES

11 SUPPLEMENTARY NOTES	12. SPONSORING MILITARY ACTIVITY

13 ABSTRACT

The report discusses the progress and accomplishments of
several projects during the grant period. A model for the ignition
response of solid propellants is presented, which predicts ignition
behavior with respect to pressure and surface heat flux in quali-
tative agreement with experimental measurements. Surface regression
is treated and a steady-state burning model is employed, which assumes
equilibrium vaporization at the surface and a regression rate limited
by the feedback flux. A method is developed and discussed for the
determination of the net heat of gasification of a burning propel-
lant. The critical pressure ratio for extinction by instantaneous
depressurization, which is required for this method, is obtained by
use of a rarefaction tube. Summaries are presented of a study of
the PBAA and PBAA-AP decomposition reactions and of the results of
measurement of propellant surface temperature during the ignition
transient by detection of infrared emission from the surface.

DD FORM 1473
1 JAN 64

KEY WORDS	LINK A		LINK B		LINK C	
	ROLE	WT	ROLE	WT	ROLE	WT
Ignition						
Extinguishment						
Combustion						
Propellant						
Solid Propellant						

INSTRUCTIONS

1. **ORIGINATING ACTIVITY:** Enter the name and address of the contractor, subcontractor, grantee, Department of Defense activity or other organization (corporate author) issuing the report.

2a. **REPORT SECURITY CLASSIFICATION:** Enter the overall security classification of the report. Indicate whether "Restricted Data" is included. Marking is to be in accordance with appropriate security regulations.

2b. **GROUP:** Automatic downgrading is specified in DoD Directive 5200.10 and Armed Forces Industrial Manual. Enter the group number. Also, when applicable, show that optional markings have been used for Group 3 and Group 4 as authorized.

3. **REPORT TITLE:** Enter the complete report title in all capital letters. Titles in all cases should be unclassified. If a meaningful title cannot be selected without classification, show title classification in all capitals in parenthesis immediately following the title.

4. **DESCRIPTIVE NOTES:** If appropriate, enter the type of report, e.g., interim, progress, summary, annual, or final. Give the inclusive dates when a specific reporting period is covered.

5. **AUTHOR(S):** Enter the name(s) of author(s) as shown on or in the report. Enter last name, first name, middle initial. If military, show rank and branch of service. The name of the principal author is an absolute minimum requirement.

6. **REPORT DATE:** Enter the date of the report as day, month, year; or month, year. If more than one date appears on the report, use date of publication.

7a. **TOTAL NUMBER OF PAGES:** The total page count should follow normal pagination procedures, i.e., enter the number of pages containing information.

7b. **NUMBER OF REFERENCES:** Enter the total number of references cited in the report.

8a. **CONTRACT OR GRANT NUMBER:** If appropriate, enter the applicable number of the contract or grant under which the report was written.

8b, 8c, & 8d. **PROJECT NUMBER:** Enter the appropriate military department identification, such as project number, subproject number, system numbers, task number, etc.

9a. **ORIGINATOR'S REPORT NUMBER(S):** Enter the official report number by which the document will be identified and controlled by the originating activity. This number must be unique to this report.

9b. **OTHER REPORT NUMBER(S):** If the report has been assigned any other report numbers (either by the originator or by the sponsor), also enter this number(s).

10. **AVAILABILITY/LIMITATION NOTICES:** Enter any limitations on further dissemination of the report, other than those imposed by security classification, using standard statements such as:

(1) "Qualified requesters may obtain copies of this report from DDC."

(2) "Foreign announcement and dissemination of this report by DDC is not authorized."

(3) "U. S. Government agencies may obtain copies of this report directly from DDC. Other qualified DDC users shall request through

_____."

(4) "U. S. military agencies may obtain copies of this report directly from DDC. Other qualified users shall request through

_____."

(5) "All distribution of this report is controlled. Qualified DDC users shall request through

_____."

If the report has been furnished to the Office of Technical Services, Department of Commerce, for sale to the public, indicate this fact and enter the price, if known.

11. **SUPPLEMENTARY NOTES:** Use for additional explanatory notes.

12. **SPONSORING MILITARY ACTIVITY:** Enter the name of the departmental project office or laboratory sponsoring (paying for) the research and development. Include address.

13. **ABSTRACT:** Enter an abstract giving a brief and factual summary of the document indicative of the report, even though it may also appear elsewhere in the body of the technical report. If additional space is required, a continuation sheet shall be attached.

It is highly desirable that the abstract of classified reports be unclassified. Each paragraph of the abstract shall end with an indication of the military security classification of the information in the paragraph, represented as (TS), (S), (C), or (U).

There is no limitation on the length of the abstract. However, the suggested length is from 150 to 225 words.

14. **KEY WORDS:** Key words are technically meaningful terms or short phrases that characterize a report and may be used as index entries for cataloging the report. Key words must be selected so that no security classification is required. Identifiers, such as equipment model designation, trade name, military project code name, geographic location, may be used as key words but will be followed by an indication of technical context. The assignment of links, rules, and weights is optional.